IMPACT OF VARIOUS CHLORIDE SOLUTIONS ON THE LEACHING CAPACITY AND ADSORPTION/DESORPTION CHARACTERISTICS OF HEAVY METALS IN CEMENT-BASED MATERIALS

（各種塩化物溶液がセメント系材料中の重金属の溶出能力および吸脱着特性に与える影響）

March 2024

周　少軍

ABSTRACT

In light of growing environmental concerns, the construction industry, particularly in concrete production, has significantly contributed to global carbon dioxide emissions and resource depletion. Promoting sustainable development within the construction sector is crucial for mitigating its environmental footprint. In response, many cities are now using urban waste, industrial by-products, and construction and demolition waste (CDW) as alternative materials for concrete. For instance, granulated blast furnace slag, municipal solid waste incineration bottom ash, and fly ash are widely used as supplementary cementitious materials (SCMs). However, these additives often lead to substantial leaching of heavy metals. There is growing concern about the potential leaching of heavy metals from concrete structural components. Heavy metals typically leach through direct leaching from the surface phases and/or diffusion to the concrete surface through pore solutions, seeping into the water in contact with the concrete surface. Many past studies have shown that the leaching of heavy metals from cementitious materials depends on environmental conditions. Given that previous studies have not fully clarified how chlorides affect the fixation and leaching of heavy metals in cement hydrates, analyzing the behavior of heavy metals in concrete under different chloride environmental conditions is vital for ensuring the safety of this issue.

Limited prior research has addressed the leaching of heavy metals from concrete in chloride environments, particularly regarding how chloride influences the immobilization and leaching of heavy metals from cement hydrates. Although the effect of contact solutions has been discussed, the systematic compilation of data on the leaching of heavy metals from hardened cements with immobilized heavy metals is lacking. When the contact solution is a chloride, previous studies focused on sodium chloride. Consequently, the comprehensive understanding of the effects of various chlorides is still limited. The aim of this study was to comprehensively assess the long-term leaching of copper (Cu), zinc (Zn), and lead (Pb) from mortars exposed to sodium chloride (NaCl), potassium chloride (KCl), magnesium chloride ($MgCl_2$), and calcium chloride ($CaCl_2$), as well as to investigate the adsorption behavior of Pb

on cement hydrate and calcium silicate hydrate (CSH) under these conditions. Additionally, the study aims to explore how variations in pH, influenced by different nitric acid additions or liquid-solid ratios, impact Pb's adsorption characteristics in these chloride environments.

To achieve the aforementioned objectives, the structure of this thesis is arranged as follows:

Chapter 1 introduces the background, objectives, and methodology of this study.

Chapter 2 presents a literature review on the content of heavy metals in cement and SCMs. This chapter explores the mechanisms of heavy metal fixation and examines the impact of environmental factors, such as pH and chlorides, on heavy metal leaching. Additionally, it discusses various leaching tests used for assessing the safety of heavy metals in cement-based materials.

Chapter 3 provides a description of the experimental program, including detailing the experiments conducted to study the leaching and adsorption behavior of heavy metals in cement-based materials under various chloride environments. The experiments start by preparing sand mortar specimens using Ordinary Portland Cement (OPC) that conforms to Japanese Industrial Standards, combined with quartz sand and deionized water. The focus is on three heavy metals: Cu, Zn, and Pb, chosen due to their prevalence in supplementary cementitious materials (SCMs) and recycled aggregates. These metals are introduced into the cement mixtures in nitrate form, at a 1% ratio by mass relative to the cement, to ensure uniform distribution within the cement matrix. The specimens are prepared with two different water-to-cement ratios (0.40 and 0.55) and are subjected to a tank leaching test. This test involves placing the cured mortar specimens in polyethylene tanks filled with different chloride solutions (10 mass% concentration of NaCl, KCl, $MgCl_2$, $CaCl_2$) and deionized water, simulating various environmental conditions. The leaching behavior of heavy metals from these specimens is monitored over time, with periodic renewal of the leaching solutions and measurement of their pH values. The concentration of the leached heavy metals is quantitatively analyzed using flame atomic absorption spectrophotometry.

Additionally, the porosity of the mortar specimens is assessed both before and after their exposure to the chloride solutions using mercury intrusion porosimetry. This analysis helps understand the effect

of environmental exposure on the pore structure of cement-based materials.

Furthermore, the study extends to the X-ray diffraction (XRD) analysis of the mortar samples, aiming to identify any changes in the crystalline phases of the specimens before and after immersion in the tank leaching tests. This analysis provides insights into the structural alterations within the mortar specimens and the state of the heavy metals post-exposure. To identify the reasons for the differences in the varying effects of different chlorides on Pb leaching, the study examined the penetration of chloride ions from KCl and $CaCl_2$ solutions into the mortar, as well as the distribution of Pb and Ca in the specimens post-exposure, using electron probe microanalysis (EPMA).

The chapter also delves into the adsorption characteristics of Pb, on cement paste and CSH. This analysis is achieved through adsorption tests using various chloride solutions and a nitric acid solution for pH adjustment. The study examines the impact of pH on lead adsorption by altering the liquid-to-solid ratio and using nitric acid. These tests aim to understand the interaction between lead and the cementitious materials under different environmental conditions. The synthesized CSH samples are then analyzed using XRD and energy dispersive X-ray spectroscopy (EDX) to investigate the adsorption properties and determine the Ca/Si ratios after exposure to different solutions.

Chapter 4 delves into the impact of chloride-based salts on the leaching and immobilization of heavy metals like Cu, Zn, and Pb in cement hydrates. The chapter meticulously examines how different chloride solutions affect the leaching behavior of these metals over a prolonged duration of 625 days. Observations indicated that leaching was highest in the presence of $CaCl_2$, significantly exceeding the leaching levels observed with other chloride solutions such as NaCl, KCl, and $MgCl_2$, as well as in deionized water. This finding underscores the unique role of $CaCl_2$ in enhancing heavy metal leaching from cement-based materials.

The chapter also explores how these chloride solutions influence the internal crystalline structure of the cement hydrates. Through XRD analysis, it was found that exposure to $MgCl_2$ led to the transformation of portlandite into brucite, resulting in a reduction in pH and consequently in the leachate quantities of Cu, Zn, and Pb. This transformation was not observed with other chloride solutions.

Additionally, EPMA results revealed that in the case of KCl solutions, the weaker binding capacity of chloride ions compared to $CaCl_2$ may explain the lower leaching of Pb. These findings underscore the significant and varied influences of different chloride solutions on the long-term leaching behavior of heavy metals from cement-based materials.

Chapter 5 centers on the influence of various chloride solutions on the adsorption and desorption properties of Pb in hardened cement and CSH. Key findings reveal that the adsorption behavior of Pb is significantly impacted by the type of chloride solution used. Among the tested solutions, $MgCl_2$ showed the highest Pb adsorption, while $CaCl_2$ resulted in the lowest. This indicates that different chloride solutions can alter the adsorption capacity of cement hydrates for heavy metals.

The study further highlights the effect of pH on Pb adsorption, noting an increase in adsorption as the pH shifts from alkaline towards neutral. This trend, however, is not evident in the presence of chlorides, suggesting other influencing factors beyond pH. Furthermore, XRD analysis did not definitively identify Pb compounds in any samples, indicating the complexity of these interactions.

In the case of CSH, the adsorption characteristics differed based on the Ca/Si ratio and the chloride solution used. The study confirms that lower Pb adsorption on CSH correlates with higher leachate quantities in chloride solutions. It was also found that $CaCl_2$ plays a role in retaining calcium in CSH, which in turn affects Pb adsorption.

Chapter 6 describes the conclusions of this study and makes recommendations for future work.

ACKNOWLEDGEMENTS

First and foremost, I would like to express my deepest gratitude to my supervisor, Professor KENJI KAWAI, for his unwavering guidance, mentorship, and encouragement throughout my research journey. His extensive knowledge and professional skills have set the direction for my study, and I am immensely thankful for his patience and dedication.

I would also like to sincerely thank Professor KENICHIRO NAKARAI for his profound understanding of the subject matter and constructive comments, which have greatly benefited my research.

Special thanks go to Assistant Professor YUKO OGAWA, for providing valuable insights and constructive feedback on my work, which has been crucial in refining my project. Whenever I needed her assistance during my Ph.D. studies, she was always ready to lend a helping hand.

I appreciate the support and guidance from my co-supervisor, Associate Professor ATSUSHI TERAMOTO and Professor TAKASHI TSUCHIDA's assistance and advice.

I appreciate the encouragement from Honorary Professor RYOUICHI SATO.

I wish to thank Assistant Professor Dr. RIYA CATHERINE GEORGE and ex-Assistant Professor Dr. BUI PHUONG TRINH, for their support and help.

Special appreciation goes to my lab mates, Mr. SHINYA TANAKA, Mr. MASAHARU YAMASAKI, Mr. TAKUMI NISHIWAKI, and all the members of Structure Materials and Concrete Structures laboratory of Hiroshima University for their various kinds of help during my Ph.D. studies.

Last, I would like to express my gratitude to my husband, Dr. YUE ZHOU, my beloved daughter, Niina, and my parents for their consistent support and love.

Hiroshima, December 2023
Shaojun Zhou

CONTENTS

LIST OF FIGURES

LIST OF TABLES

CHAPTER 1. INTRODUCTION

1.1 Background

The construction industry is frequently praised for its ability to generate employment opportunities and make a significant impact on the global economy. Nevertheless, it is widely acknowledged as a primary industry that has adverse impacts on the environment[1]. Concrete, as the most widely used building material in the construction and infrastructure industries for buildings, bridges, roads, and many other forms, is second only to water in global consumption[2,3]. Approximately 30 billion tons of concrete products are consumed annually[2], accounting for about 40% of global greenhouse gas emissions[4] and roughly 9-10% of global energy-related CO_2 emissions[2,5]. According to the latest data released by Statista Research Department in 2023, global cement production reached 4.1 billion tons[6]. The construction industry's large-scale exploitation has led to severe resource wastage and environmental pollution.

Promoting sustainable development in the construction sector is crucial in reducing its environmental impact. Recently, more cities are utilizing urban waste, industrial by-products, and construction and demolition wastes (CDW) as concrete materials. For example, granulated blast furnace slag, fly ash, silica fume, crushed waste cathode ray tubes (CRT), glass powder, and municipal solid waste incineration bottom ash are used as supplementary cementitious materials (SCMs)[7–14]. CDW are employed as recycled aggregates (RA) to replace coarse/fine aggregates[15–18], and materials like blast furnace slag and CRT glass are utilized as artificial aggregates[19,20].

However, these by-products and wastes may contain heavy metals (especially Cu, Zn, Pb, Cr (VI), V, Fe, Co, As, and Cd), whose presence is not systematic and can vary significantly depending on the source and processing methods[14,20–22].

Stabilization/solidification (s/s) technology, as recognized by the United States Environmental Protection Agency, is a highly effective method for converting materials that may pose potential hazards into substances that are either less hazardous or non-hazardous[23]. Cement is one of the most suitable binders for heavy metal s/s, often used in the disposal of heavy metal waste, as heavy metals (HMs) typically cannot leach easily once the cement has hardened[24–27]. Nevertheless, the leaching of HMs remains a major aspect of the environmental compatibility of cement-based materials.

Studies by Belebchouche et al.[28], Moussaceb et al.[29], and others have clearly demonstrated the efficiency of the s/s process in capturing HMs and reducing waste pollution characteristics. On the other hand, it has been noted that HMs can easily desorb from hardened cement when in contact with calcium chloride solutions[30]. Researchers like Ledesm et al.[31] and van der Sloot et al.[32] have noted that pH variations in solutions interacting with cement affect the leaching of HMs. Hartwich et al.[33] indicated that the availability of bicarbonates and the concentration of calcium in the contact solution significantly impact the heavy metal leaching rate. The generation of bicarbonates through material carbonation suggests that carbonation is an important leaching condition. Moreover, carbonation plays a crucial role in controlling heavy metal leachability by affecting factors like system pH, heavy metal precipitation, the formation of stable phases, and reducing the porosity of the cementitious materials[34–36]. Consequently, environmental conditions play a crucial role in the leaching of HMs from cement in practical applications. Since concrete is a widely used building material in modern construction and is cost-effective for harsh usage environments[18,37], studying the immobilization and leaching behavior of HMs in adverse environments is essential. In chloride environments, excessive use of concrete containing HMs in by-products and wastes may lead to leaching of HMs, posing significant risks to human health, the environment, and the ecosystem[38–41]. Cu, Zn, and Pb are widely distributed HMs, and their potential hazards have garnered significant

attention. Excessive Cu accumulation in the body can lead to general weakness and damage to vital organs such as the kidneys and brain[42,43]. Excess Zn has been associated with a reduction in lymphocyte stimulation and cholesterol metabolism[42]. Furthermore, excessive Pb intake can result in neurotoxic damage, skeletal alterations, hypertension, renal and blood disorders, and even the potential development of cancer[42,44]. This underlines the critical importance of monitoring and managing the presence of these HMs in environmental and construction contexts to mitigate their adverse health impacts.

Since previous studies have not clarified how chlorides affect the fixation and leaching of HMs in cement hydrates, analyzing the behavior of HMs in concrete under different chloride environmental conditions is vital for ensuring the safety of this issue.

1.2 Objectives

There are few previous studies on the leaching of HMs from concrete immersed in chloride environments such as marine environments or de-icing salts, and previous studies have not elucidated how chloride affects the immobilization and leaching of HMs from cement hydrates. Although the effect of contact solutions has been discussed, the leaching of HMs from hardened cements with immobilized HMs has not been systematically compiled. When the contact solution is a chloride, previous studies focused on sodium chloride. Therefore, we are not yet able to comprehensively understand the effects of various chlorides.

The main objectives of this study are as follows:

- To investigate the long-term leaching behaviors of Cu, Zn, and Pb from mortars under continuous exposure to environments containing NaCl, KCl, $MgCl_2$, and $CaCl_2$.
- To study the adsorption characteristics of Pb on cement pastes when exposed to NaCl, KCl, $MgCl_2$, and $CaCl_2$.

- To analyze how these chlorides impact the adsorption properties of Pb in cement pastes, with a focus on the similarities and differences in these properties across various pH environments, altered by the addition of chloride, nitric acid, or changes in the liquid-to-solid ratio (L/S).
- To study the adsorption characteristics of Pb on CSH when exposed to NaCl, KCl, $MgCl_2$, and $CaCl_2$.

1.3 Methodology

Currently, leaching tests are useful for determining the efficacy of the s/s method for HMs[45]. In the Netherlands, NEN7345 is positioned as a test to understand the elution behavior governed by diffusion phenomena. The test conditions for the tank leaching test in this study were determined with reference to NEN7345, an official leaching test in the Netherlands. In this study, a 625-day tank leaching test was performed using NEN7345 to analyze the leachability of Cu, Zn, and Pb from cement mortar over time. The leaching solutions were periodically renewed at specific intervals: 0.25, 1, 4, 9, 16, 25, 36, 64, 100, 225, 400, and 625 days. The pH values of the leaching solutions were measured by a pH meter before the renewal of each leaching solution to observe the effect of pH on the behavior of Cu, Zn and Pb. Concentrations of Cu, Zn and Pb ions in these leachate solutions were quantified using flame atomic adsorption spectrophotometer (FAAS). To explain the effects of different contact solutions on the leaching of Cu, Zn, and Pb, the pore structure, crystalline phases, and distribution of element content of the mortar samples post-contact with 10 mass% NaCl, 10 mass% KCl, 10 mass% $MgCl_2$, 10 mass% $CaCl_2$ and deionized water were assessed using mercury intrusion porosimetry (MIP), X-ray diffraction (XRD) and electron probe microanalysis (EPMA).

According to prior studies, chlorides also accelerate the dissolution of silicates and

the leaching of calcium from calcium silicate hydrate (CSH), resulting in the leaching of calcium ions from the cement matrix[46,47]. Both mechanisms have an impact on transport parameters, such as apparent diffusivity. This study undertook adsorption tests of Pb on synthetic CSH. Two types of synthesized CSH with Ca/Si ratios of 0.83 and 1.40 were used for the experiment. To evaluate the effects of various chlorides on the Pb adsorption in CSH, XRD analysis and energy dispersive X-ray spectroscopy (EDX) analysis were performed on synthetic CSH post-contact with 10 mass% NaCl, 10 mass% KCl, 10 mass% $MgCl_2$, 10 mass% $CaCl_2$, and the pore solution of cement paste, analyzing the crystalline phases and the Ca/Si ratio in CSH.

To understand the effect of various chlorides on the adsorption characteristics of Pb in cement hydrates and their intrinsic mechanisms, Pb adsorption tests on cement pastes were also carried out in this study. Adsorption experiments of cement slurry on Pb were conducted in two distinct environments: 1. In a chloride environment, and 2. In varying pH conditions created either by altering the liquid-to-solid ratio (L/S) or by adding nitric acid. For the chloride environment, the contact solutions consisted of 10 mass% NaCl, 10 mass% KCl, 10 mass% $MgCl_2$, 10 mass% $CaCl_2$, and the pore solution. In the second type of environment, the pH value was modified either through the change in L/S ratio or by the addition of nitric acid, to study the Pb adsorption behavior under different pH conditions.

The concentration of Pb in the filtrate was measured using FAAS to determine both the equilibrium concentration and the adsorbed amount of Pb. The pH value was monitored at each stage of the experiment, and powder XRD was used to qualitatively analyze the composition of the cement slurry before and after the adsorption test.

1.4 Thesis outline

This thesis has six chapters, and the arrangement of the thesis is outlined in detail as

follows:

Chapter 1 provides a background of the context, objectives, and methodology employed in this research.

Chapter 2 provides an overview of several topics pertinent to this research, along with a review of existing literature. This includes investigations into the content of HMs in cement and supplementary cementitious materials (SCMs), the mechanisms of HM fixation within the cement matrix, and the influence of various environmental factors such as pH, chlorides, sulfates, and time on HM leaching. Additionally, the chapter discusses various leaching tests employed to assess the safety and stability of HMs in cement-based materials.

Chapter 3 outlines the research methodology, including the materials used and their mixture proportions, as well as the curing conditions. It also describes the experimental methods and procedures, along with the instrumental analysis involved.

Chapter 4 discusses how chloride-based salts affect the immobilization and leaching of Cu, Zn, and Pb from cement hydrates and analyzes the associated internal changes in crystalline phase.

Chapter 5 investigates the Pb adsorption characteristics of hardened cement under different chloride environments and different pH values through adsorption experiments. The effect of various chlorides on the Ca/Si of synthesized CSH was also investigated.

Chapter 6 presents the findings and outcomes of this study, together with suggestions for future works.

CHAPTER 2. LITERATURE REVIEW

This chapter provides a comprehensive review of the existing literature pertaining to the heavy metals (HMs) content in cement and SCMs. It examines in-depth the mechanisms governing the fixation of HMs within the cement matrix and various factors influencing the leaching of HMs from cement-based materials subjected to solidification/stabilization (s/s) treatment. These factors encompass carbonation, chlorides, sulfates, pH levels, and time. Furthermore, this section introduces the leaching tests used to assess the safety of HMs in cement-based materials, with a specific focus on tank leaching tests. The primary aim of this chapter is to offer a holistic perspective that aids in developing safer and more effective cement-based materials for containing HMs.

2.1 Trace element leaching from concrete

Ordinary Portland cement (OPC) contains trace amounts of HMs such as Cu, Zn, Pb, Cr (VI), Mn, As, and Cd, ranging from a few milligrams to several hundred milligrams per kilogram of cement[48,49]. These amounts are considered minute when compared to the cement's major chemical components. Similarly, the cement industry is an important example of venous industry, an industry that collects the unwanted and discarded products, and recycles them into the material circulation processes of society and nature. The use of by-products and wastes such as ground granulated blast furnace slag (GGBS), copper slag, fly ash, silica fume, and municipal solid waste incineration (MSWI)bottom ash as SCMs, which occurs already to a certain extent in the making of cement, has received growing attention as a potential route toward 'eco-concrete'[8–13,50,51]. However, HMs (notably Cu, Zn, Pb, V, Cr (VI), Co, Fe, As, and Cd) also may be present in such by-products and wastes[21,52]. As shown in Fig. 2.1[49], it is suggested that during the various stages of

concrete's life cycle: production, construction, operation, maintenance, demolition, and disposal, there is a potential for these substances to leach out.

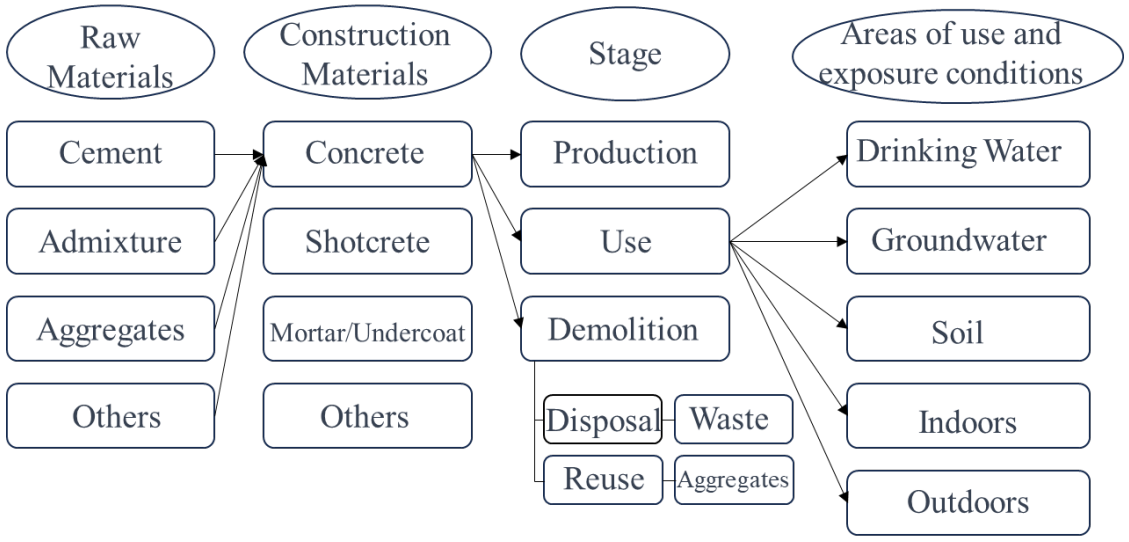

Figure 2.1 Impact range of cementitious materials on trace element leaching into the environment.

2.1.1 Origins of HMs in Hardened Portland cement (PC)

HMs of diverse origins may be present in varying levels in hardened Portland cement (PC) pastes.

HMs originate from materials used in the production of clinker, including:

(i) Primary raw materials

Cement's primary raw materials, limestone and clay, inherently possess varying levels of trace elements and potentially dangerous HMs[48,53].

(ii) Industrial slag used as a raw material substitute, usually steel slag[54,55].

(iii) Alternative[56] (e g. Municipal Solid Waste, MSW) and primary fuels[57].

Table 2.1 summarizes the median trace element and HMs compositions of raw materials and several illustrative fuels.

Table 2.1 Median concentrations of trace elements and HMs in the raw materials and fuels utilized in cement manufacturing.

Trace elements/HMs	Raw materials[48]			Fuels[8]		
	Limestone mg/kg	Clay mg/kg	Marl mg/kg	Hard coal mg/kg	Petroleum coke mg/kg	Used tires mg/kg
Cu	13	29	24	18	2.4	68
Zn	13	78	48	63	16	6100
Pb	<10	27	14	27	13	125
As	<5	15	5	9	0.5	1.6
Cr	7	105	53	14	4.3	137
V	14	128	90	39	758	19
Sb	10	7	8	1	0.6	136
Ni	<7	43	28	23	263	90
Mo	<5	<5	<5	-	-	-

2.1.2 Origins of HMs in SCMs

(i) GGBS

GGBS is a by-product derived from the iron-making process and is extensively utilized in the cement and concrete sectors because of its remarkable hydration characteristics[58]. This by-product can act as a viable substitute for conventional cement on a one-to-one weight basis. The replacement rates for this material can vary significantly, ranging from 30% to as high as 85%[59].

GGBS consists mainly of SiO_2, CaO, Fe_2O_3 and Al_2O_3. The trace elements are sourced from natural raw materials such as iron ore and limestone. HMs in GGBS may include, but are not limited to, Pb, Cd, Cr, As, Hg, Ni, Co, Cu, and Zn, and the types and amounts of these elements usually depend on the composition of the feedstock as well as the conditions under which the blast furnace is operating. Different manufacturers, different geographic locations of raw materials and different production processes have an impact on

the HMs content in GGBS. Typically, the HMs content in GGBS is relatively low and, as they are mostly present in a stable oxidized state, their bioavailability and mobility are also low.

Table 2.2[49] shows examples of GGBS determinations. Compared to ordinary silicate cement, blast furnace slag is characterized in this respect by a very low content of hexavalent chromium.

Table 2.2 Example of trace element content measurement of GGBS[49].

Trace elements/HMs	Range mg/kg	Average mg/kg
Cu	1.0-18	7
Zn	2.0-10	7
Pb	<0.1-40	6
As	<0.1-0.5	0.1
Cr	<0.1	<0.1
Se	<0.1-2.0	0.8
Cd	<0.1-3.0	0.1

(ii) fly ash

Fly ash is the fine particulate ash emitted from coal-fired power stations. Fly ash is frequently utilized as a partial substitute for OPC in the manufacturing of concrete due to its pozzolanic activity and spherical shape[60,61]. Numerous businesses and power generation facilities rely on coal as a primary source, resulting in the production of substantial quantities of coal ash. The environmental concern associated with coal power plants is in the copious amounts of byproducts they generate, which have the potential to include hazardous compounds and HMs capable of causing harm to the ecosystem[62]. The chemical composition and qualities of fly ash are contingent upon various factors, including the specific type of coal utilized, the method of combustion employed, and the effectiveness of

emission control mechanisms[62,63]. Table 2.3 shows examples of testing of HMs element concentrations in fly ash by Spain, Japan, China, UK, Greece, India, Germany.

Table 2.3 Examples of tests for HMs element concentrations in fly ash from some countries.

HMs	Location						
	Spain[64] (mg/Kg)	Japan[49] (mg/Kg)	China[65] (mg/Kg)	UK[65] (mg/Kg)	Greece[66] (mg/Kg)	India[66] (mg/Kg)	Germany[33] (mg/Kg)
Cr	134.2	83.11	n/r	n/r	110-160	103	15.7
Co	29.2	n/r	n/r	n/r	n/r	18	15.7
Cu	71.8	n/r	n/r	n/r	31.8-62.8	83	55.3
Pb	52	51.7	843-847	17-176	123-143	56	21.4
Mn	324.6	n/r	n/r	n/r	213-330	62	n/r
Ni	87.9	n/r	n/r	n/r	n/r	63	40.9
Zn	221.3	n/r	n/r	n/r	59.6	124	70.8

n/r: Not reported

(iii) MSWI bottom ash and MSWI fly ash

Municipal solid waste encompasses various forms of discarded materials, often called trash or garbage. These materials comprise everyday goods that are disposed of after use, such as metals, paints, glass, batteries, appliances, food scraps, packaging, newspapers, bottles, grass clippings, and clothing[67,68]. Globally, refuse production rates are increasing in tandem with the acceleration of urbanization. Global solid waste production was projected to reach 2.24 billion tons in 2020, representing an individual daily footprint of 0.79 kilograms. An anticipated 73% surge in annual waste production is a result of urbanization and accelerated population expansion, which is projected to reach 3.88 billion tons by 2050[69,70].

The use of a practical waste management approach for municipal solid waste incineration can significantly enhance the practicality of achieving a 90% decrease in MSW volume[71,72]. Ashes refer to the solid residue produced during the burning of various materials, and they can be categorized into two distinct types: MSWI bottom ash and MSWI fly ash. The quantity of bottom ash is significant due to the fact that 80% -95% of the overall solid residue produced by MSWI is obtained from the incinerator bed[73–75]. MSWI bottom ash and MSWI fly ash are characterized by being rich in many metals, including Cu, Zn, Pb, Cr, Co, Cd, Ni, Mn, Cr, Ba and Sn. Table 2.4 shows the range of HMs content in MSW bottom ash and MSW fly ash. Moreover, Hjelmar et al. found that most of the HMs elements were present in the form of oxides[75].

Table 2.4 Ranges of composition of MSWI residues[75].

HMs	MSWI Bottom ash (mg/kg)	MSWI Fly ash (mg/kg)
Cu	900-4800	860-1400
Zn	1800-6200	19000-41000
Pb	1300-5400	7400-19000
Mn	<700-1700	800-1700
Co	<10-40	29-69
Se	0.6-8	6.1-31
Mo	2.5-40	15-49
Cr	230-600	140-530
As	19-80	49-320
Ag	4.1-14	31-95
Ni	60-190	92-240
Ba	900-2700	920-1800
Sn	<100-1300	1400-1900
Hg	<0.01-3	0.8-7

2.2 Mechanism of HMs fixation by cement matrix

Cement is one of the most suitable binders for HMs s/s, often used as a solidifying material when HMs waste is discarded, because HMs cannot normally be leached from cement with ease once it has hardened[24–27]. There are several main mechanisms for the immobilization

of HMs contaminants via the s/s process. These mechanisms include physical fixation and adsorption to the cement hydration reaction products, oxidation/reduction precipitation, pH-dependent precipitation, and isomorphic replacement with the cement matrix[76–78]. The mechanism of fixation of HMs in the s/s process is simplified as Eq. (2.1)[79]:

$$A + B + H_2O \rightarrow H(M)OH_2 \quad (2.1)$$

where,

A: anhydrous binder, e.g., cement.

B: waste that contains metal.

M: HMs to be trapped.

$H(M)OH_2$: hydrated compound that traps M in its structure which is produced by the hydration reaction of A and B.

2.2.1 Encapsulation of HMs through densification of hydrate structures

During the hydration process of cement hydrates, substances like calcium silicate hydrate (CSH) are formed, which are gel-like in nature. These substances fill up spaces during the cement hardening process, resulting in a more compact structure. This compaction reduces the number of pores, thereby physically limiting the migration of HMs ions through these pore systems[80].

Typically, the cement paste is composed of cement hydrates like CSH and calcium hydroxide (CH), unhydrated cement particles, and voids. The particle size of CSH is approximately 0.1 to 1.5 μm, and according to previous studies, its interlayer distance is about 1.0 to 2.6 nm. Considering that the size of water molecules is approximately 0.245 to 0.3 nm, the dissolution of HMs ions in water and their movement within the gel pores of CSH becomes more challenging, even if they desorb, dissolve, or are initially present in a

free state.

Therefore, the compaction of the cement hardened body during the hydration process can be regarded as an important mechanism for restricting and immobilizing HMs ions.

2.2.2 Binding capacity of CSH for HMs

The primary outcome of silicate phase hydration in Portland cement is the formation of CSH gel, comprising amorphous particles with diverse morphologies. Analyzing and evaluating these hydrates presents significant challenges due to their amorphous nature, variable composition, and easily altered structure. Additionally, isolating a single phase of CSH is nearly impossible, as it is homogeneously mixed with other phases, further complicating analysis.

In previous studies, CSH produced from Portland cement has been considered to be similar in composition and structure to natural crystalline calcium silicate hydrates such as 14Å tobermorite (plombierite) and jennite[81,82]. The two known highly crystalline synthetic CSHs are CSH(I) with Ca/Si<1.4 and CSH(II) with Ca/Si>1.4. CSH(I) is considered to be 14Å tobermorite (plombierite) with an incomplete crystal structure, and CSH(II) is considered to be jennite with an incomplete crystal structure[83]. The main differences in the crystal structures between natural tobermorite and CSH(I) lie in their chain structures. Fig. 2.2 (a) shows the crystal structure of double-chain tobermorite and Fig. 2.2 (b) shows the crystal structure of single-chain tobermorite. Natural tobermorite is only known to have the double-chain structure shown in Fig. 2.2 (a), while CSH(I) is thought to have the single-chain structure shown in Fig. 2.2 (b)[84].

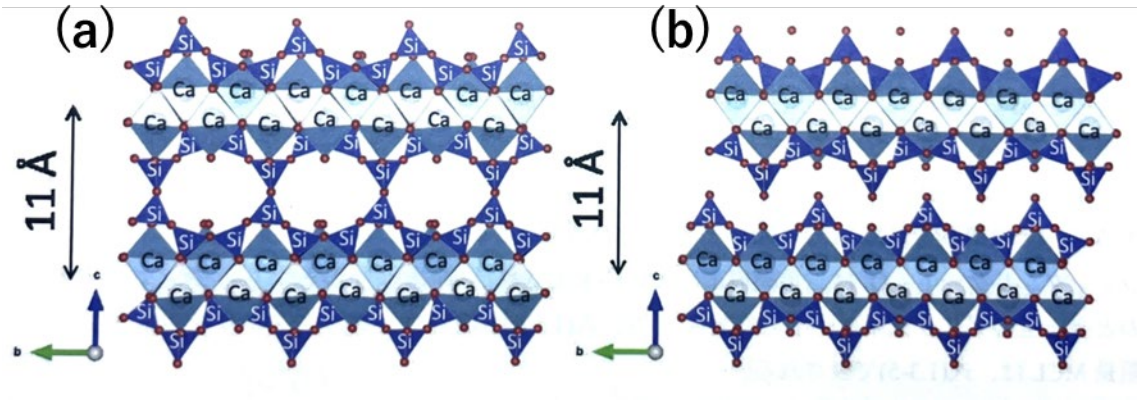

Fig.2.2 (a) Crystal structure of double-chain tobermorite, (b) Crystal structure of single-chain tobermorite[84].

The CSH gel is primarily composed of micro-porosity. The presence of gel pores results in a significant increase in surface area and plays a major role in determining the sorption capabilities. The study conducted by Hong and Glasser provided empirical evidence supporting the assertion that CSH gel possesses a robust ability to effectively bind metallic elements[85]. In addition, HMs may become incorporated into the crystal structures of hydration products or become adsorbed into the CSH gel[86]. The adsorption occurring at the surface of CSH is responsible for determining the proportion of free ions to adsorbed ions. During the phase of intensified cement hydration, the co-precipitation of HMs ions with hydration products (CSH) has been observed[87,88]. Recent research has indicated that HMs possess the ability to substitute various locations within CSH or hydrated calcium silicate aluminate (C–A–S–H) structures (see Fig. 2.3):

(1) Surface Adsorption: HMs adsorb on the surface of hydrated calcium silicate particles[89–91].

(2) Interlayer Substitution: HMs replace calcium in the interlayer positions of the CSH or CASH structures[92–95].

(3) Tetrahedral Substitution: HMs substitute for silicon in the silicon chains[89–91].

(4) Octahedral Substitution: HMs substitute in the calcium-oxygen layers, typically in an octahedral coordination[95,96].

Compared to the other two alternatives, it is significantly easier for metal ions to be deposited in the surface and interlayer regions, which are recognized as the primary types of substitutions[97].

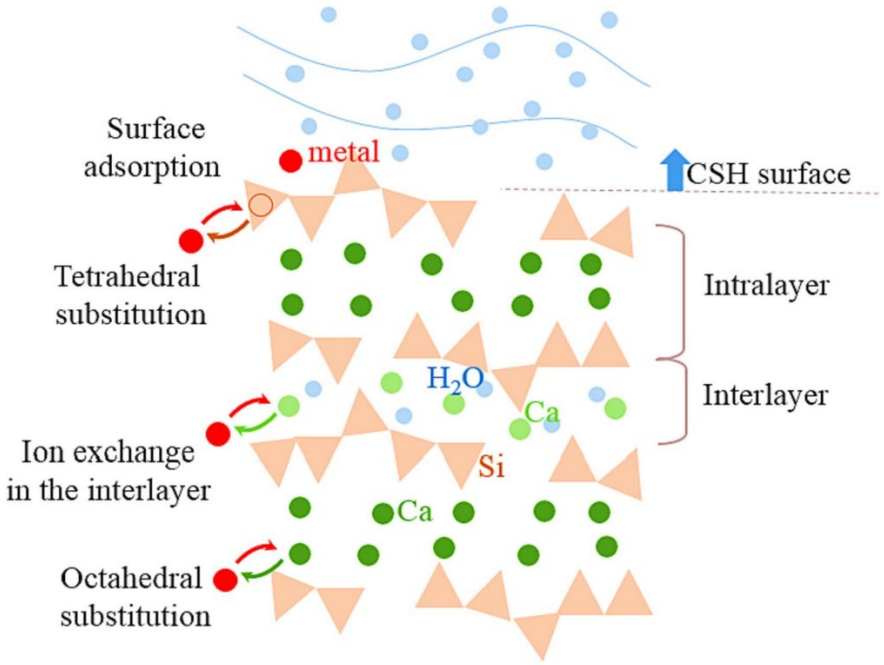

Fig.2.3 The dynamic processes and chemical bonding of HMs adsorbed on the CSH surface and the effect of HMs on the pore structure[62].

The simulation conducted by Qiao et al. illustrates that the bonding capability between CSH and HMs (e.g., Cu, Zn, Pb) is contingent upon the exchangeability of calcium with these metals. During the binding of CSH to HMs, the stability of the hydrated shell layer of the metal ions affects their ability to exchange with calcium (Ca) ions in CSH[97].

2.2.3 Trapping of HMs by formation of insoluble compounds

In general, the solubility of metal hydroxides, carbonates, sulfates and silicates in water decreases on the alkaline side, and insoluble compounds are formed in alkaline regions of the system where the pH and redox potential are appropriate[98].

The equilibrium of hydroxide (M(OH)n) in water is shown in Eq. (2.2). If the solubility of hydroxide is Ksp, the solubility product of water is Kw, and the concentration of metal ions is expressed as $[M^{n+}]$, Eq. (2.3) is obtained. In other words, the relationship is as shown in Eq. (2.4).

$$M(OH)n \rightleftarrows M^{n+} + nOH^- \quad (2.2)$$

$$[M^{n+}] = Ksp/[OH^-]^n = Ksp \cdot [H^+]^n / Kw^n \quad (2.3)$$

$$\log[M^{n+}] = \log Ksp - n\log Kw - npH \quad (2.4)$$

Ksp : Solubility Product

Precipitation of metal hydroxides occurs when the pH of a solution containing dissolved metal ions is increased, reaching a level where these hydroxides become insoluble. This optimal pH level varies depending on the specific metal and its valence state[99]. In some cases, the precipitation of metal carbonates may be more favorable than that of metal hydroxides, especially in scenarios where metal carbonates have a lower solubility compared to their corresponding hydroxides[100]. Fig. 2.4 shows the relationship between pH and the solubility of each dissociated species of Cu, Zn, Pb, Cr and Cd[101].

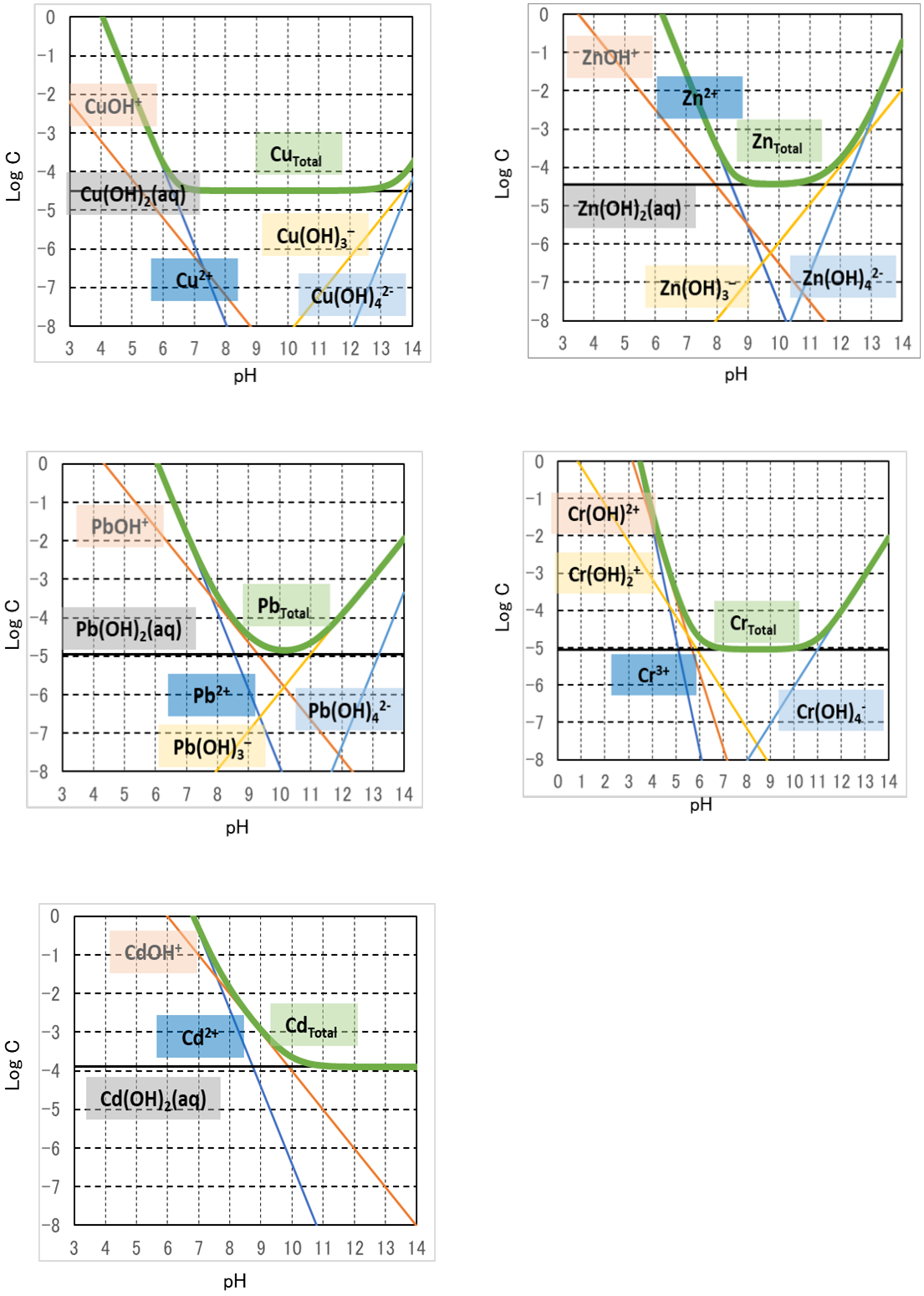

Figure 2.4 Relationship between solubility of Cu, Zn, Pb, Cr, Cd and pH[101].

Metallic compounds with high density tend to form precipitates on the surface of a solid material more rapidly compared to their formation from a larger volume of

solution[102,103]. As shown in Table 2.5, Komarneni et al. highlight the differing solubility behaviors of metal hydroxides in various environments and note that HMs such as Pb^{2+}, Zn^{2+}, and Cu^{2+} tend to form hydroxides and deposit on calcium silicate minerals[104].

Table 2.5 The solubility of metal hydroxides[104].

Metal ions	logKsp (in solution)	logKsp (on the surface of silica)
Cu^{2+}	-19.32	-20.91
Zn^{2+}	-16.6	-18.17
Pb^{2+}	-15.1	-16.52
Cr^{3+}	-29.8	-32.19
Ca^{2+}	-5.19	-6.67
Mg^{2+}	-11.15	-12.75
Al^{3+}	-33.5	-35.97
Fe^{3+}	-38.8	-41.2

2.2.4 Fixation mechanism by ettringite

Ettringite ($3CaO{\cdot}Al_2O_3{\cdot}3CaSO_4{\cdot}32H_2O$, AFt) is a primary hydration product in cement materials. It constitutes about 7% by weight of the total hydration products in Portland cement and between 22% to 25% in sulfoaluminate cements. As shown in Fig. 2.5, the ettringite structural units are composed of $\{Ca_6[Al(OH)_6]_2{\cdot}24H_2O\}^{6+}$ and $\{(SO_4)_3{\cdot}2H_2O\}^{6-}$. The repetitive central column structure of ettringite is composed of alternating $[Al(OH)_6]^{3-}$ octahedra and three electrically charged calcium-oxygen polyhedra, a configuration that imparts distinctive physical and chemical properties to the mineral[105].

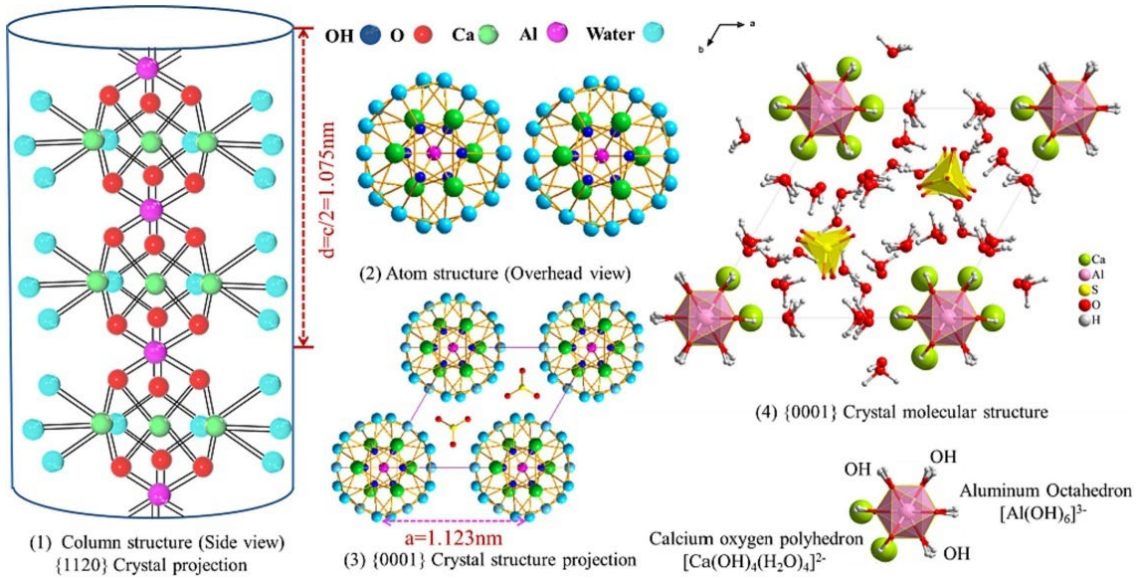

Figure 2.5 Ettringite crystal structure unit: simulated illustration[106,107].

Ettringite crystals have excellent adsorption qualities and ion-exchange capabilities, a large specific surface area, and are rich in diverse linked pore architectures[108]. Table 2.6 lists the various substitutions of Ca^{2+} sites, Al^{3+} sites, and SO_4^{2-} sites in AFt that have been confirmed in previous studies[87,105,109–115].

Table 2.6 Ion substitution in ettringite.

Ca^{2+} sites	**Zn^{2+}**	**Pb^{2+}**	**Ni^{2+}**	**Cd^{2+}**	**Co^{2+}**	**Ba^{2+}**	**Sr^{2+}**
Al^{3+} sites	Cr^{3+}	Si^{4+}	Fe^{3+}	Mn^{3+}	Ni^{3+}	Co^{3+}	Ti^{3+}
SO_4^{2-} sites	CO_3^{2-}	Cl^-	OH^-	CrO_4^{2-}	AsO_4^{3-}	NO_3^-	SO_3^{2-}

2.3 Factors influencing the leaching of HMs from s/s treated cement-based materials

As the primary binder in the S/S process, Portland cement's ability to immobilize a wide

range of hazardous metals through precipitation and adsorption reactions is attributed to its high pH value. However, cementitious materials that have undergone solidification and stabilization are susceptible to both physical and chemical breakdown mechanisms. When exposed to atmospheric conditions, they can be attacked by chlorides, carbon dioxide, water, organic degradation products, and sulfates. These environmental erosions may subsequently impact the immobilization of HMs within the cementitious matrix[116]. Fig. 2.6 illustrates that the leaching behavior of HMs in the environment falls into three categories: gas corrosion, microbiological leaching, and liquid corrosion. Following this, Fig. 2.7 details the factors influencing the release of contaminants. It distinguishes between material-specific factors in monolithic materials such as concrete, blocks, and bricks, as well as in granular materials like sand, fine sand, gravel, and steel slag, and also highlights the external chemical and physical factors affecting leaching. Table 2.7 provides a comprehensive overview of the various aspects that influence the process of release. It is important to note that the relevance of these factors may vary depending on the specific scenario being considered.

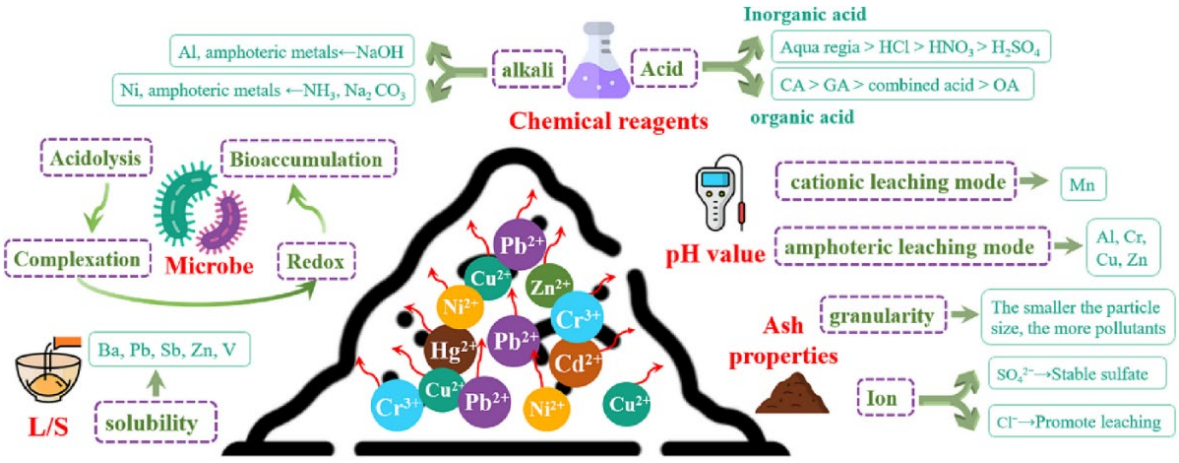

Figure 2.6 Factors influencing HMs leaching from cement-based products[117].

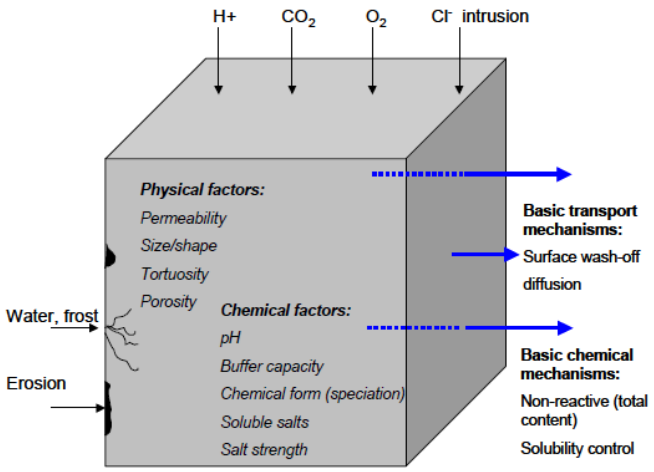

Figure 2.7 Influences on contaminant release: material-specific and external chemical and physical factors in monolithic (concrete, blocks, bricks) and granular (sand, sinters, gravel, steel slag) materials[32].

Table 2.7 Summary of key factor affecting substance release[32].

Chemical processes	Physical factors	External factors
- Dissolution - pH - Chemical form -Total composition/ availability - Redox. - Acid-base buffering - DOC - Composition water phase/ionic strength - Temperature - Time	- Percolation - Diffusion - Surface wash off - Granular/monolithic - Size (particles or monoliths) - Porosity - Permeability - Tortuosity - Erosion	- Amount of water, - Contact time - pH of environment - Temperature - Redox of environment - DOC / Adsorption

2.3.1 Effect of carbonation on the leaching of HMs

Environmental carbon dioxide (CO_2) attack, commonly known as carbonation, is a well-documented process associated with cement-based products[118–120]. Extensive research has reported on the impact of carbonation on the hydration chemistry, permeability, and porosity of structural concrete in ambient environments[118,119,121,122].

The chemical processes that mostly occur during the carbonation process of cement-based materials are illustrated in Eq. (2.5) and Eq. (2.6).

$$Ca(OH)_2 + CO_2 \rightarrow CaCO_3 + H_2O \quad (2.5)$$

$$CSH + CO_2 \rightarrow CaCO_3 + SiO_2 \cdot n\,H_2O \quad (2.6)$$

The typical pH range of the pore water within the cement matrix is 12–13. The potential reduction in pH to 8.3 by the reaction of portlandite and CSH to calcite is contingent upon the extent of carbonation.

The initial stage of the carbonation process in a cement matrix involves the permeation of CO_2 into the cement paste, followed by the dissolution of CO_2 in the pore water. This results in the formation of a relatively mild carbonic acid (H_2CO_3), which then dissociates, forming carbonate and hydrogen ions. These ions react with hydroxide compounds to produce carbonates with lower solubility. Owing to the limited solubility of calcium carbonate in the pore solution, $CaCO_3$ typically precipitates within the pore structure. Consequently, the carbonation process in cementitious materials generally leads to an increase in strength and a decrease in permeability. These characteristics are advantageous for matrices used in the containment of hazardous substances[118,123]. However, in certain instances, the chemical immobilization of HMs in cementitious materials may be compromised due to a decrease in the pH of the hydrated cement paste caused by carbonation, which leads to increased solubility of these HMs. In summary, CO_2 attack, or carbonation, is arguably the most common form of environmental attack on concrete. It induces changes in the chemical composition and physical properties of cement, which can affect the long-term preservation and immobilization of HMs.

Carbonation can play a crucial role in controlling the leachability of HMs by influencing various factors such as the pH of the system, the precipitation of HMs, the formation of stable phases, and the reduction of porosity in cementitious materials[34–36]. In recent years, reports on the leaching results from carbonated specimens have been inconsistent, leading to confusion and uncertainty. The research on carbonation in

cementitious materials reveals a dichotomy in its effects on leaching rates: certain substances, such as chromium, calcium, lead, cobalt, cadmium, copper, zinc, arsenic, molybdenum, and various anions, show increased leaching post-carbonation, as indicated in several studies[34,124–126]. Conversely, other studies have noted a significant reduction in the leaching of metals like Cu, Zn, Pb, Ni, Cr, As, Mo, Ca, Hg, along with elements such as lead, calcium, sodium, potassium, and fluoride. This highlights the complex and variable impacts of carbonation on different substances within cementitious materials[36,127,128].

According to Zha et al.[34], the leaching rate of copper in carbonated cement-solidified fly ash is typically higher compared to that in uncarbonated samples (see Fig. 2.8). One contributing factor to this outcome is the effect of carbonation on the pH level of cement-cured fly ash. In high pH environments, the chemical stability of elemental copper, present in forms such as hydroxide or carbonate, is compromised. This degradation facilitates the dissolution of elemental copper, leading to higher levels of leachable copper and an increased leaching rate. Another potential contributing factor is that excessive carbonation may lead to the formation of microcracks, which, in turn, enhances the leaching process. This occurs despite the formation of calcium carbonate during carbonation, which typically acts to inhibit the leaching of HMs.

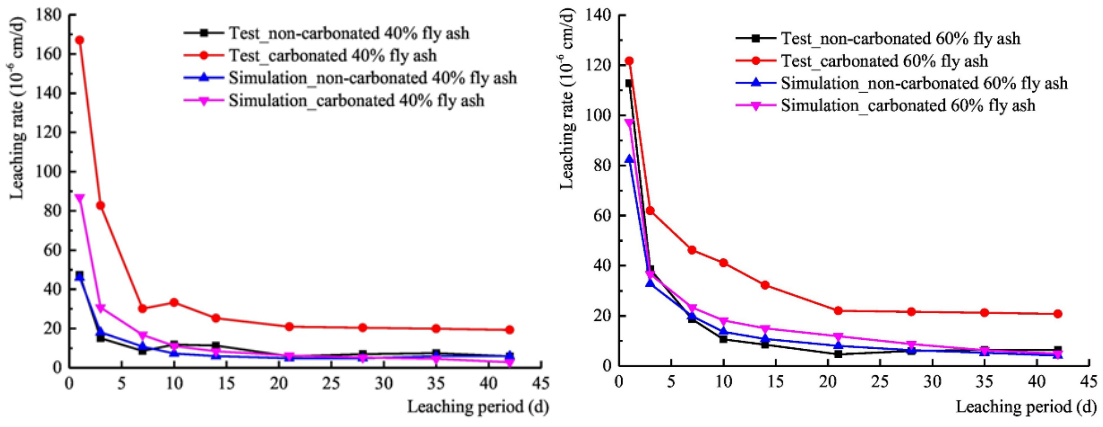

Figure 2.8 Leaching rates of Cu in 40% and 60% cement-solidified fly ash.

Valls et al.[129] reported that carbonation leads to increased levels of nickel, copper, and zinc in leachates due to three factors (see Table 2.8). First, there is a slight increase in the solubility of the metal compounds as a result of the decreased pH within the stabilization system. Second, the decomposition of ettringite hydrate, which incorporates zinc into its crystalline structure, contributes to this increase. Lastly, the polymerization of the CSH leads to the release of metal cations previously bound to the Si–O groups.

Table 2.8 HMs concentration in uncarbonated and carbonated mortars (mg-HM/m²-mortar specimen).

	Cd	Cu	Mn	Ni	Pb	Cr	Zn	Ba
Mixed	Uncarbonated/carbonated							
CM25A	< 0.19/< 0.29	11.07/16.13	< 0.19/< 0.29	12.97/23.48	< 1.93/< 2.91	< 0.40/< 0.58	3.01/10.71	72.51/0.75
CM25A + ad	< 0.19/< 0.29	9.63/10.58	< 0.19/< 0.29	9.64/6.10	< 1.95/< 2.89	< 0.40/< 0.58	3.16/5.86	77.30/1.80
CM25B	< 0.20/< 0.28	12.37/11.01	< 0.20/< 0.28	12.50/10.24	< 2/< 2.83	< 0.40/< 0.56	1.71/6.31	89.12/< 0.28
CM25B + ad	< 0.20/< 0.29	11.43/11.61	< 0.20/< 0.29	12.47/76.85	< 2.02/< 2.94	< 0.40/< 0.58	11.12/2.3	71.52/2.22
CM35A	< 0.20/< 0.23	20.32/24.4	< 0.20/0.73	22.85/17.14	< 2.03/< 2.28	< 0.41/< 0.45	2.68/3.41	195.03/1.28
CM35A + ad	< 0.20/< 0.23	22.94/19.38	< 0.20/1.96	15.87/12.71	< 2/< 2.25	< 0.40 7< 0.45	< 0.40/4.11	119.54/1.54
CM35B	< 0.18/< 0.27	10.34/11.78	< 0.18/< 0.27	9.92/9.96	< 1.87/< 2.69	< 0.37/< 0.54	14.03/4	84.46/0.63
CM35B + ad	< 0.20/< 0.25	11.05/12.8	< 0.20/< 0.25	10.04/11.19	< 2.02/< 2.56	< 0.40/< 0.51	25.44/3.76	68.80/2.80
25L5CV	< 0.20/< 0.3	14.47/15.51	< 0.20/< 0.31	8.45/16.86	< 2.01/< 3.10	< 0.40/< 0.62	< 0.40/2.86	121.12/0.87
25L10CV	< 0.20/< 0.29	15.08/18	< 0.20/0.63	11.97/18.75	< 1.97/< 2.91	< 0.40/< 0.58	< 0.40/5.58	94.34/0.91
25L15CV	< 0.20/< 0.29	12.7/18.39	< 0.20/< 0.29	7/15.66	< 2/< 2.94	< 0.52/< 0.59	< 0.40/6.77	54.09/0.82
25L25CV	< 0.20/< 0.29	14.25/22.91	< 0.20/0.42	9.36/18.6	< 2/< 2.91	0.47/< 0.58	4/6.85	77.50/0.84
35L5CV	< 0.19/< 0.26	17.8/17.10	< 0.19/< 0.26	9.20/10.24	< 1.97/< 2.60	< 0.40/3.96	< 0.40/1.31	137.10/3.59
35L10CV	< 0.21/< 0.25	17.61/16.65	< 0.21/< 0.26	10.91/20.83	< 2.1/< 2.50	< 0.42/< 0.50	0.8/3.5	126.16/0.90
35L15CV	< 0.20/< 0.25	15.05/12.45	< 0.20/< 0.25	7.11/12.45	< 2/< 2.50	< 0.4/< 0.51	0.67/2.04	78.77/1.46
35L25CV	< 0.19/< 0.26	19.86/10.77	< 0.19/< 0.26	13.47/15.11	< 1.94/< 2.66	< 0.38/< 0.53	5/3.72	155.69/0.67
U_1	1	50	–	50	100	150	200	600

U: limit of NEN7345 standard.

2.3.2 Effect of chlorides and sulphates on the leaching of HMs

Müllauer et al.[130] observed a significant increase in the release of Cr when concretes were exposed to chloride or sulphate solutions, as depicted in Fig. 2.9. The reason behind the heightened dissolution of Cr in concrete, when it comes into contact with a NaCl solution, can be attributed to the dissolution of CrO_4^{2-} present in the compounds known as AFt and AFm. This dissolution occurs due to the formation of Friedel's salt ($3CaO{\cdot}A_2O_3{\cdot}CaCl_2{\cdot}10H2O$) in the pore solution. The process by which Friedel's salt is formed can be elucidated by Eqs. (2.7) and (2.8). Furthermore, the chromium dissolution is facilitated by the decreased pH of the NaCl elution solution. In contact with a high

concentration of sulfate, the solubility equilibrium of AFt and AFm, which have incorporated CrO_4^{2-}, is disrupted. This process leads to the replacement of CrO_4^{2-} by SO_4^{2-}-ions, resulting in the release of CrO_4^{2-} into the pore solution of the cement.

$$Ca(OH)_2 + 2NaCl \rightarrow CaCl_2 + 2NaOH \quad (2.7)$$

$$3CaO \cdot Al_2O_3 \cdot 3CaSO_4 \cdot 32H_2O + CaCl_2 \rightarrow 3CaO \cdot Al_2O_3 \cdot CaCl_2 \cdot 10H_2O + 3(CaSO_4 \cdot 2H_2O) + 16H_2O \quad (2.8)$$

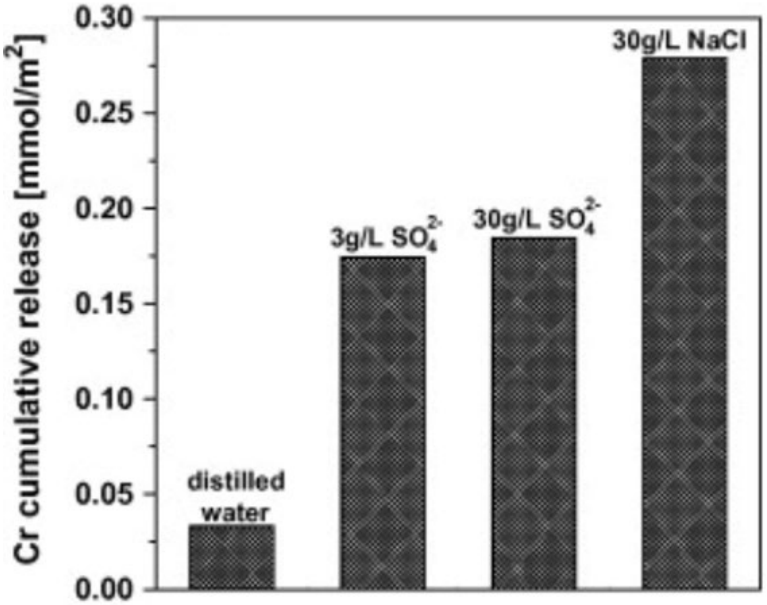

Figure 2.9 Cumulative release of Cr from concrete exposed to chloride and sulphate solutions.

The study conducted by Ebert and Kirkelund[131] investigated the influence of NaCl and Na_2SO_4 solutions on the leaching process of HMs (see Fig. 2.10). This research found notable variability in leaching yields, which depended on the specific metal and sample under consideration. One significant observation was that the variations in leaching concentrations could be influenced by the pH levels (see Table 2.9). Generally, solutions containing NaCl and Na_2SO_4 showed a higher leaching capacity for HMs like Cd and Cr, compared to those adjusted to a pH of 4. This outcome might be attributed to the introduction of additional chloride and sulfate ions. These ions can form both soluble

complexes, such as metal-chloride complexes, and insoluble complexes, like $PbSO_4$. As a result, the presence of these ions can lead to either an increase or decrease in the leaching yield, underscoring the complexity and variability of the leaching process in the presence of these solutions.

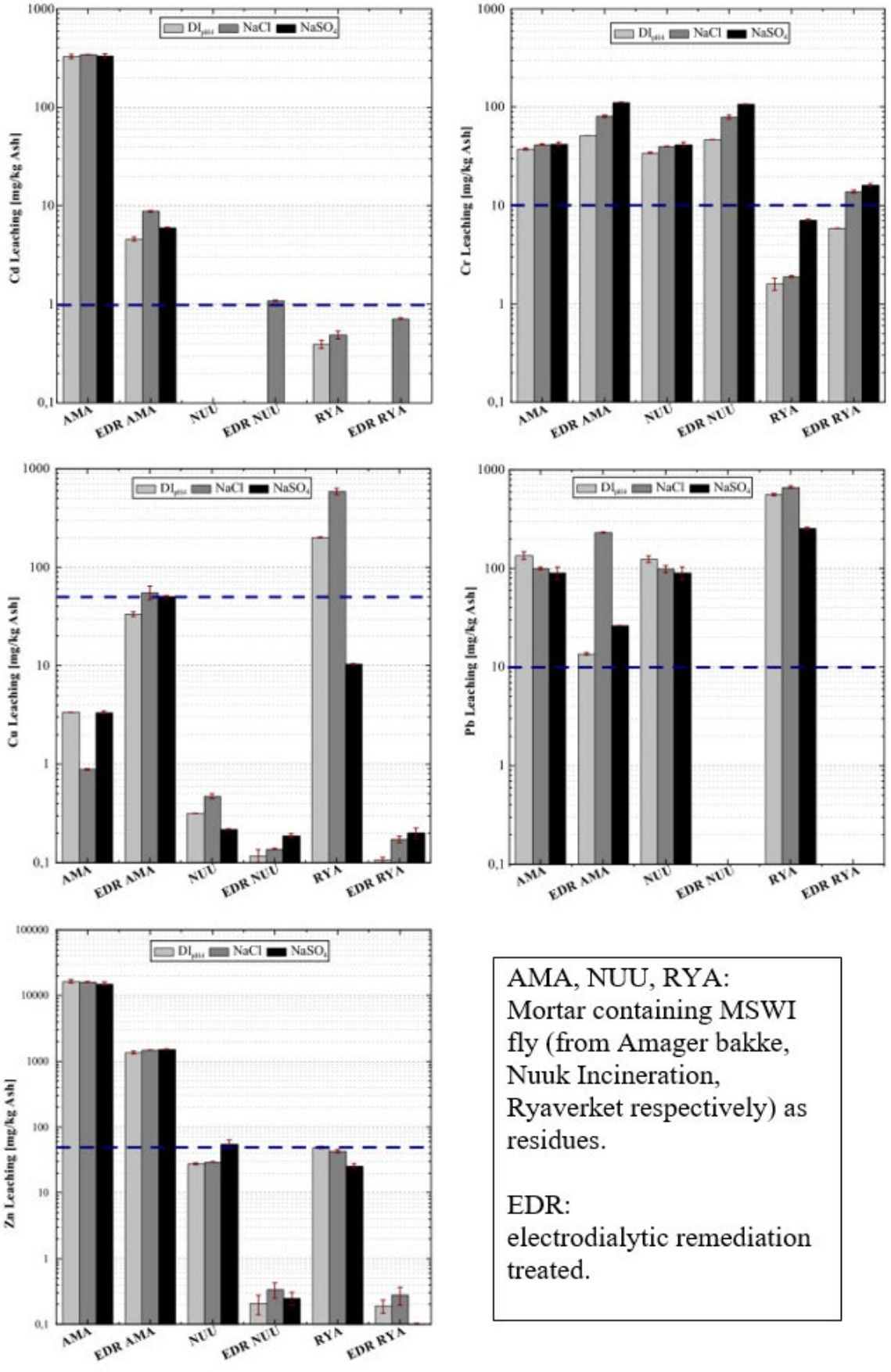

Figure 2.10 Leachate analysis from residues in distilled water at pH 4 adjusted with HNO_3, and 30 g/L NaCl solution[131].

Table 2.9 Resulting pH in the raw and EDR treated residue batch leaching experiments[131].

	AMA	EDR AMA	RYA	EDR RYA	NUU	EDR NUU
$DI_{pH\ 4}$	6.6	5.1	11.5	8.3	11.9	9.1
NaCl	6.4	4.9	11.6	8.3	11.8	9.1
Na_2SO_4	6.6	5.3	11.5	8.8	12	9.9

2.3.3 Effect of pH on the leaching of HMs

In recent years, there has been notable growth in the examination of leaching behavior by testing materials under controlled pH conditions. This increased interest is motivated by the understanding that pH plays a pivotal role in determining the extent to which components are released from the solid phase into the solution. Numerous researchers have shown the significance of pH levels in relation to the release of elements in monolithic or granular materials[31,32,132–137]. Specifically, the pH of the material itself, the pH of its surrounding environment, and the pH of the leaching liquid have been identified as critical factors in this determination. While the release curves of elements in relation to pH exhibit notable similarities, it is important to note that each substance possesses its own unique release curve that is influenced by pH[31]. For example, ledesma et al.[31] demonstrated that elevated emissions of Pb and Mo were observed when pH values exceeded 12 (see Fig. 2.11 (a) and Fig. 2.11 (b)) . Conversely, the release of Cd was significantly higher when pH levels were below 10 (see Fig. 2.11 (c)), while the release of Se was not observed to be affected by changes in pH (see Fig. 2.11 (d)).

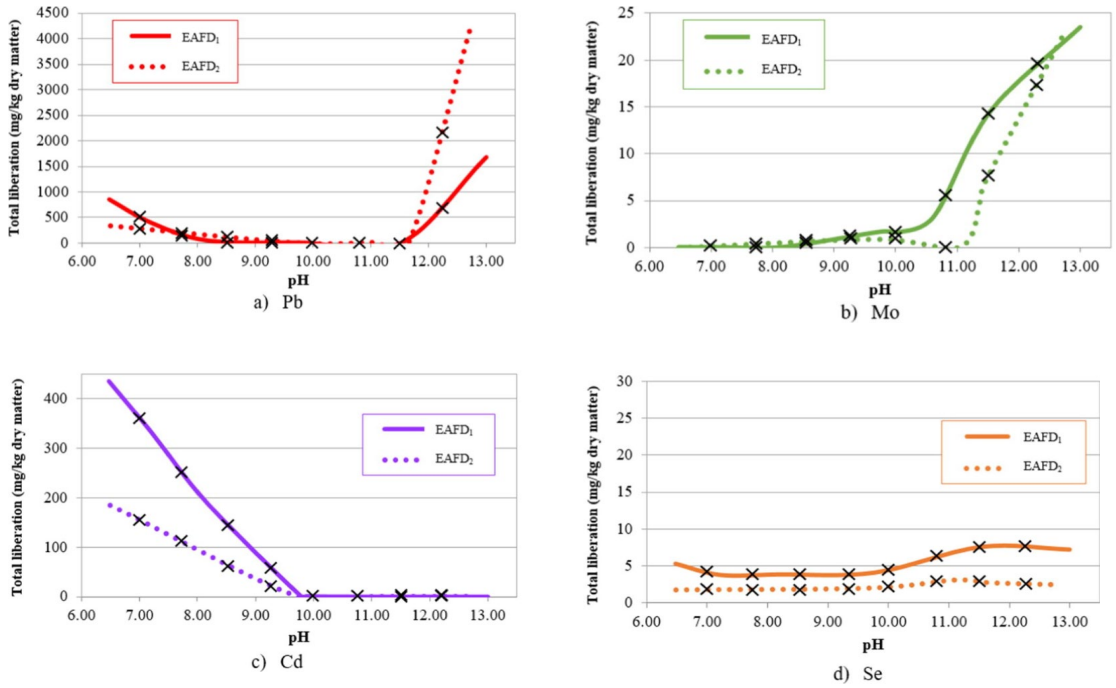

Figure 2.11 The impact of pH on the release rates of Pb, Mo, Cd, and Se[31] ($EAFD_1$ and $EAFD_2$ are electric arc furnace dust from two steel companies located in Olaberría and Zumárraga).

van de Sloot[137] found that the leachability of Ba is seemingly regulated by the solubility of $BaSrSO_4$ in all matrices, as depicted in Fig. 2.12. Moreover, the leachability of oxyanions, specifically CrO_4^{2-}, MoO_4^{-}, and VO_4^{2-}, exhibits a shared characteristic wherein leachability demonstrates a peak value within the pH range of neutral to mildly alkaline conditions. Leachability is often reduced at low pH (5) and high pH (>11) (see Fig. 2.13).

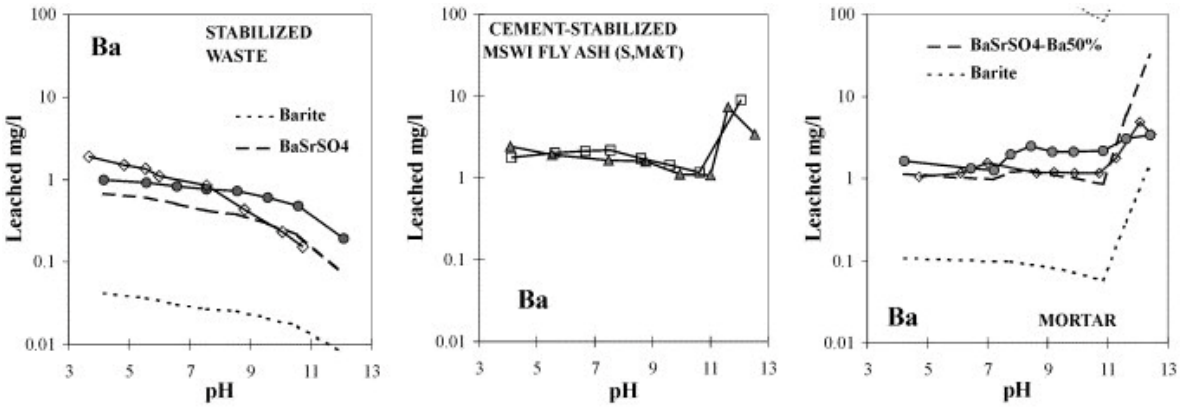

Figure 2.12 Ba release analysis in size-reduced cement mortar and varied load cement-stabilized waste, correlated with pH levels and illustrated by geochemical modeling[137].

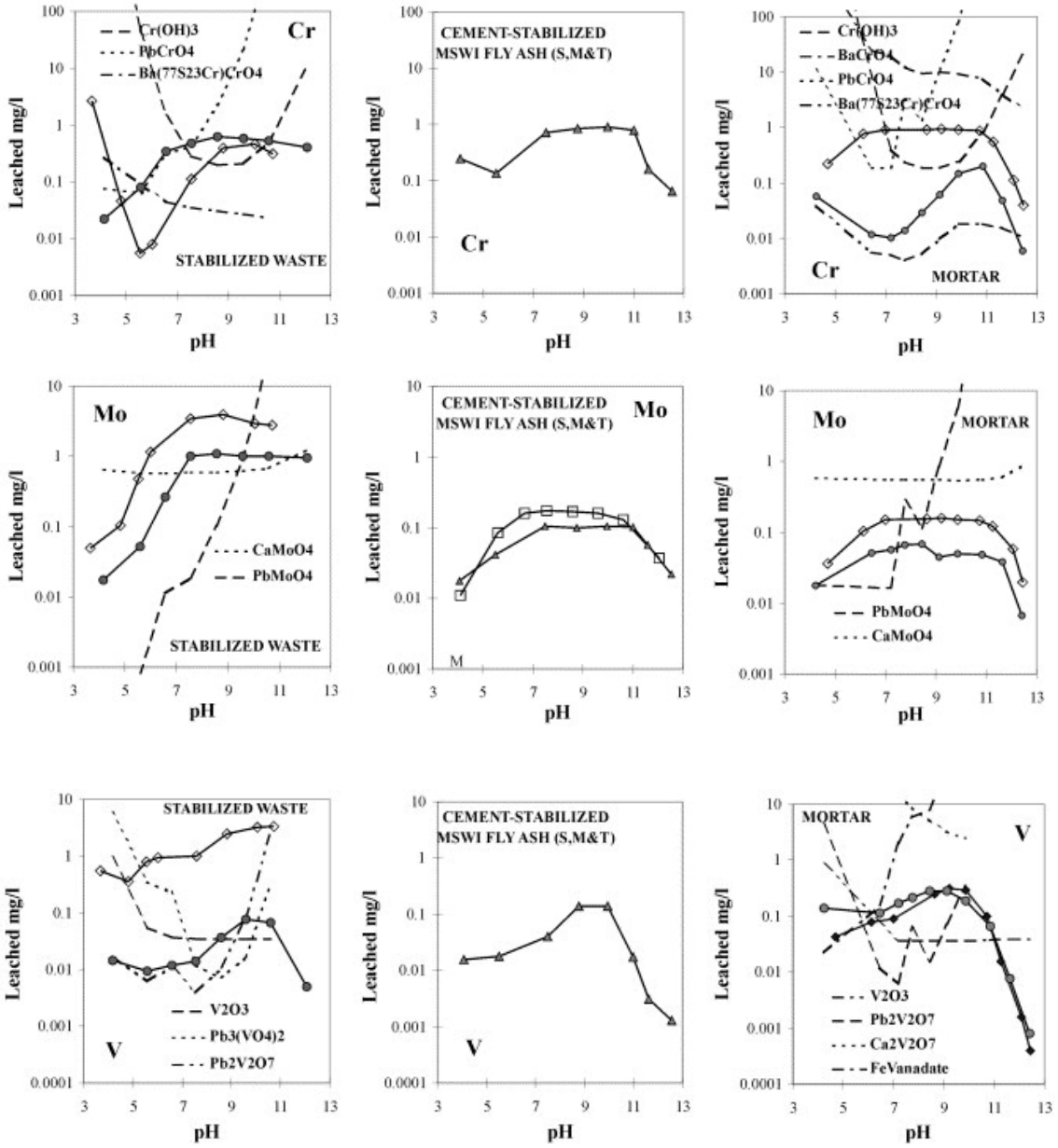

Figure 2.13 Cr, Mo and V release analysis in size-reduced cement mortar and varied load cement-stabilized waste, correlated with pH Levels and illustrated by geochemical modeling[137].

Fig. 2.14 presents the results of leaching tests on Pb- and Zn-enhanced mortars, conducted by Marcello et al.[138], under varying L/S and pH levels relative to the solution. The data indicate that elution increases in acidic environments and at higher L/S ratios. Notably, a marked change in elution is observed between pH 4 and 6, and a slight increase in elution occurs at pH 10 or above. This suggests that the solubility of HMs, as shown in Fig. 2.4, is pertinent. This study also performed continuous leaching tests on monolithic

mortar samples, maintaining constant leachate pH conditions (either pH 4 or 6). The results showed a significant increase in the release of both metals when the pH of the leaching solution was lowered from 6 to 4 (see Fig. 2.15). Overall, it is evident that pH exerts a significant influence on the elution of HMs.

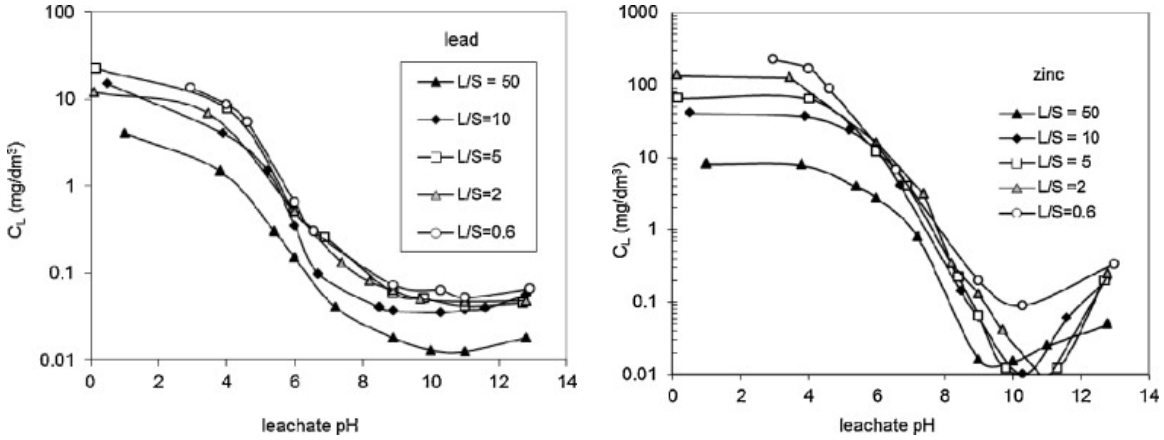

Figure 2.14 Relationship between the leached amounts of HMs (Pb, Zn) and pH and liquid-solid ratio[138].

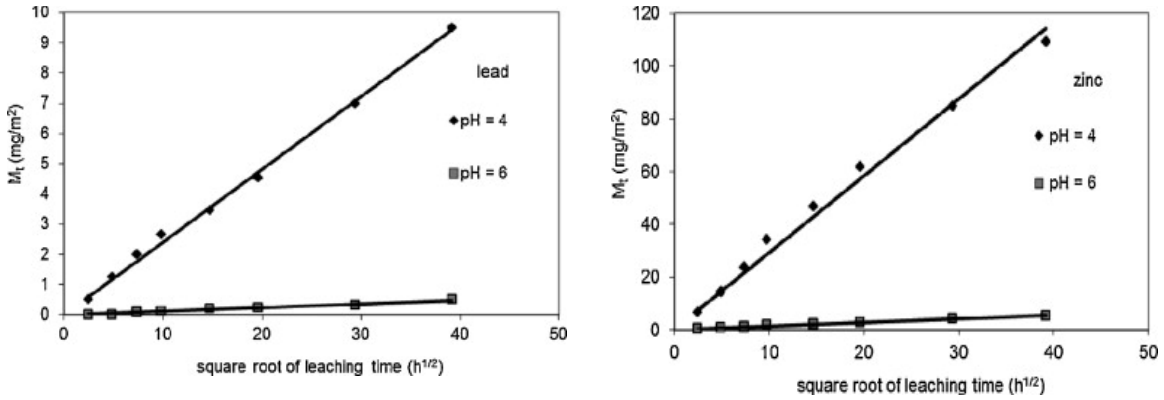

Figure 2.15 Relationship between the leached amounts of HMs (Pb, Zn) and pH and liquid-solid ratio[138].

2.3.4 Effect of time on the leaching of HMs

Time significantly influences the amount of material released through several factors:

a) The intended duration of a material's use in a specific application can affect its release over time.

b) The rate of underlying processes, such as slow mineral dissolution or diffusion, can limit release. If these reactions are too slow to reach completion within a practical timeframe, their long-term impact on overall release must be estimated.

c) Material properties and environmental conditions evolve over time, impacting release. For instance, the carbonation of alkaline products can change their release properties, and erosion can increase the surface area of a monolith, altering its leaching behavior.

It is reported[45,133,139,140] that the leaching of HMs from solid waste blocks is a dynamic process exhibiting temporal variability. Fig. 2.16[133] illustrates the leaching properties of HMs in cement-stabilized municipal solid waste incineration fly ash (MSWIFA) blocks. Under acid rain conditions, the leaching rates of Cu, Cr, Ni, As, and Pb initially peak and then gradually decrease over time. The leaching trends of Cu, Cr, and Ni exhibit similarities, as their cumulative leaching rates experience a quick increase within the initial 16-day period, reaching a maximum by day 36. In contrast, As attains equilibrium faster due to its comparatively lower available leaching rate and distinct leaching control processes. The leaching pattern observed for Pb is notably different, peaking within the initial 16-day period and maintaining an elevated rate until day 64, suggesting that equilibrium was not attained within the experimental timeframe. The experimental group, employing a mixture of nitric acid (HNO_3) and sulfuric acid (H_2SO_4) with a pH of 3.2 ± 0.05, exhibited higher leaching levels compared to the control group using deionized water, attributable to increased stimulation of HMs release in acid rain conditions. Over a 64-day period, the cumulative leaching of copper, chromium, lead, arsenic, and nickel from the acid rain resulted in only 2.5% to 22.0% of their respective total leachable quantities, indicating that the leaching of these metals extends beyond the designated experimental timeframe.

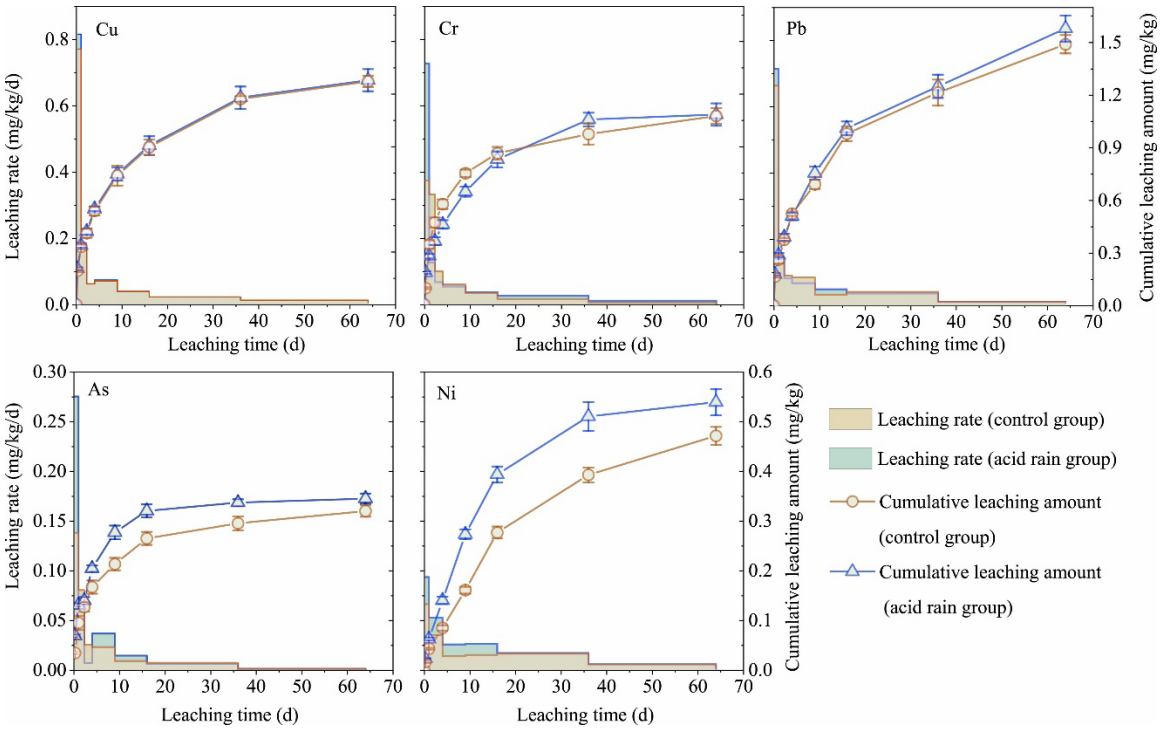

Figure 2.16 Leaching analysis of Cu, Cr, Pb, As, and Ni in cement-stabilized MSWIFA blocks: cumulative amounts and rates[133].

Song et al.[140] determined that regardless of the specific mortar and HMs being investigated, each curve exhibited two different linear segments. These segments were shown to demonstrate a linear relationship between the cumulative fraction, CFR, and the square root of time (see Fig. 2.17). Following the initial stages of leaching, which were marked by elevated leaching rates, the subsequent release of HMs exhibited a significantly reduced pace. The link between the plot of CFR vs the square root of time demonstrated a strong linear correlation in both segments, indicating a diffusion-based leaching process for the specific HMs (Cu, Ni, Zn, and Pb) present in the sewage sludge. This aligns with the finding reached by Cinquepalmi Cinquepalmi[141] et al (see Fig. 2.18).

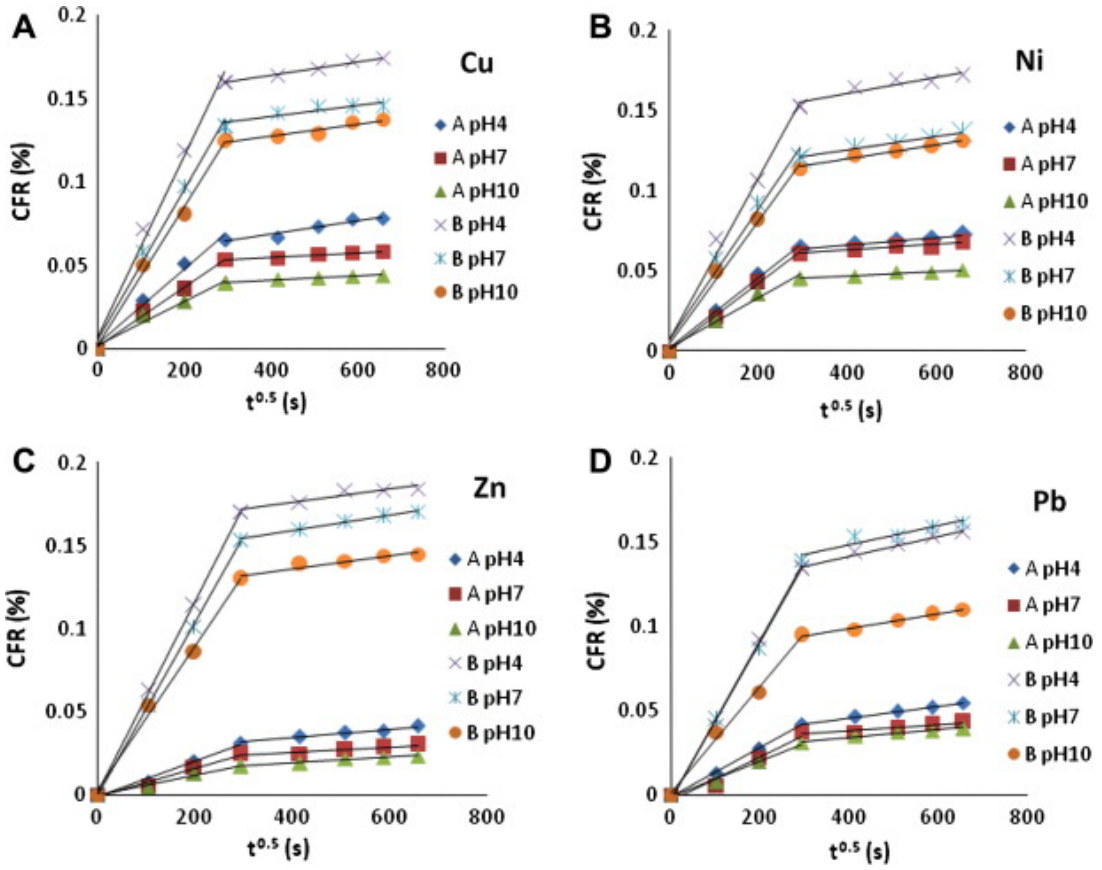

Figure 2.17 Release dynamics of Cu, Ni, Zn, Pb from s/ s sewage sludge: A semi-dynamic leach test analyzing cumulative fractions over leach time √(t) at constant pH levels (4, 7, 10) [140].

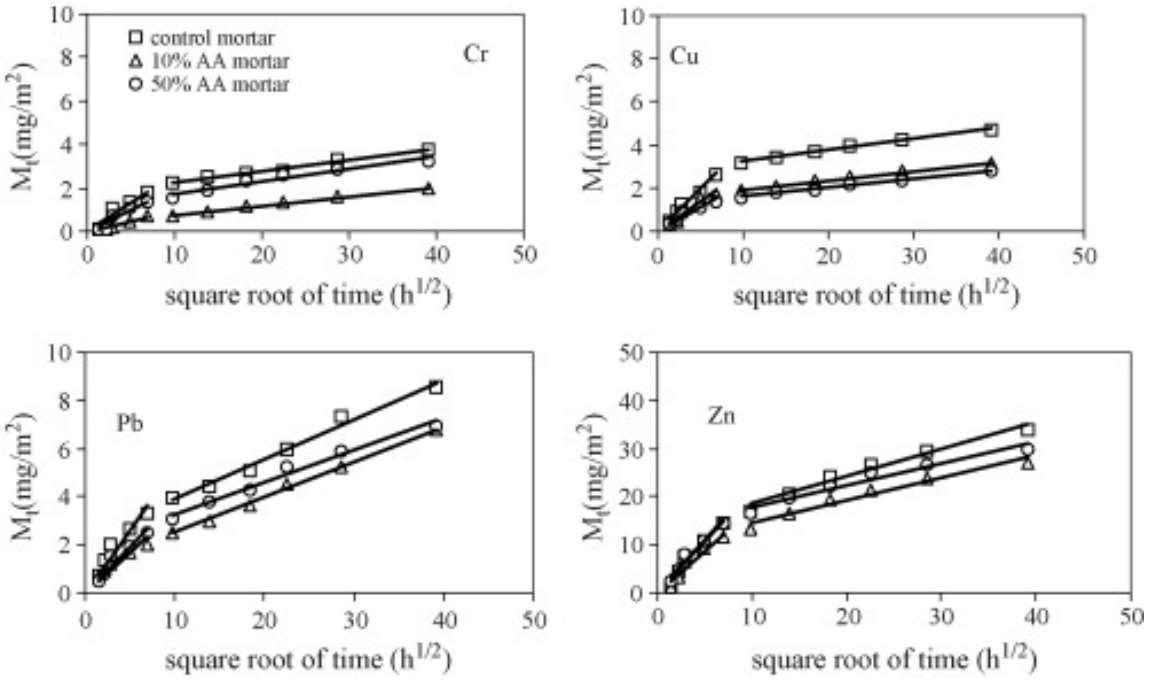

Figure 2.18 Release in different mortar types: sequential monolith leach test results[141].

2.4 Current Elution Evaluation Status for Effective Waste Utilization in Construction

The potential release and migration of hazardous substances from construction materials into the environment is widely acknowledged as a significant environmental danger. The release phenomenon can occur at various stages, including the initial utilization of materials, subsequent use following recycling, and, ultimately, during the final disposal process. Contaminants released upon contact with water and then transported by water can potentially harm the quality of many environmental components, including groundwater, surface water, and soil. Within many technical committees, there is a consensus that the assessment of a material's environmental performance should prioritize the evaluation of its release of potentially hazardous elements, rather than concentrating only on the overall content of such constituents. The foundation of this should be rooted in the fundamental mechanisms that govern the process of release.

While considering the behavior of product releases, it is necessary to differentiate between two distinct types of products. These materials can be classified as either monolithic or granular. Granular materials typically demonstrate release mechanisms dominated by percolation, wherein the release of constituents occurs due to water percolating through the product. On the other hand, monolithic materials often demonstrate diffusion-controlled release mechanisms. In such cases, the release of constituents from the materials primarily occurs through diffusion. The number of substances released depends on the diffusion of elements from the materials into the aqueous phase over time. Monolithic products encompass cementitious materials like concrete, bricks, and coated materials.

2.4.1 Basic transport mechanisms[32]

Advection: This transport mechanism involves the movement of substances due to the

infiltration of water, such as rainwater, through or alongside a material. Advection is particularly notable during precipitation events, contributing significantly to the discharge of constituents and their subsequent impact on soil and groundwater. This process is more evident in materials that allow water to pass through or alongside them.

Percolation: Percolation is a process specific to materials with porosity, such as granular substances. It refers to the movement of water or other fluids through the porous spaces within these materials. This movement facilitates the transportation of soluble components within the substance, affecting the distribution and eventual release of these constituents.

Diffusion: In this process, the transport of constituents occurs solely through molecular movement, without any external flow aiding their movement. This is common in compacted materials with very low permeability and porosity, where water stagnates within the pores. In such materials, diffusion becomes the primary mechanism for the release and transport of substances. The rate of diffusion depends on the concentration gradient between the material and the aqueous phase it contacts and can vary over time.

Surface Wash-Off: This term describes the initial removal of soluble substances from the surface of monolithic materials. Surface wash-off, akin to advection, involves the movement of constituents due to water flow over the surface. After the initial rinsing, diffusion typically becomes the dominant transport mechanism within these materials, dictating the further movement of constituents.

In the case of monolithic materials, the process of initial surface wash-off might have a notable impact. Under such circumstances, soluble salts present on the surface undergo fast dissolution, resulting in an initial increase in release.

2.4.2 Leaching test

Leaching tests are now recognized as valuable for evaluating the effectiveness of the s/s

approach for HMs[45]. As indicated in Fig. 2.19, three primary categories of tests are considered most prevalent: the single-batch extraction test, the tank leaching test, and the column test. Bone et al.[142] have summarized the major benefits and drawbacks of these tests as outlined in Table 2.10. It is noted in Table 2.10 that due to the limitations of each test, reproducing the leaching mechanism under natural conditions with a single test may not be feasible. However, by considering the advantages and disadvantages of each test, alongside the specific objectives of the research, one or more tests can be selected to fulfill the requirements of the study.

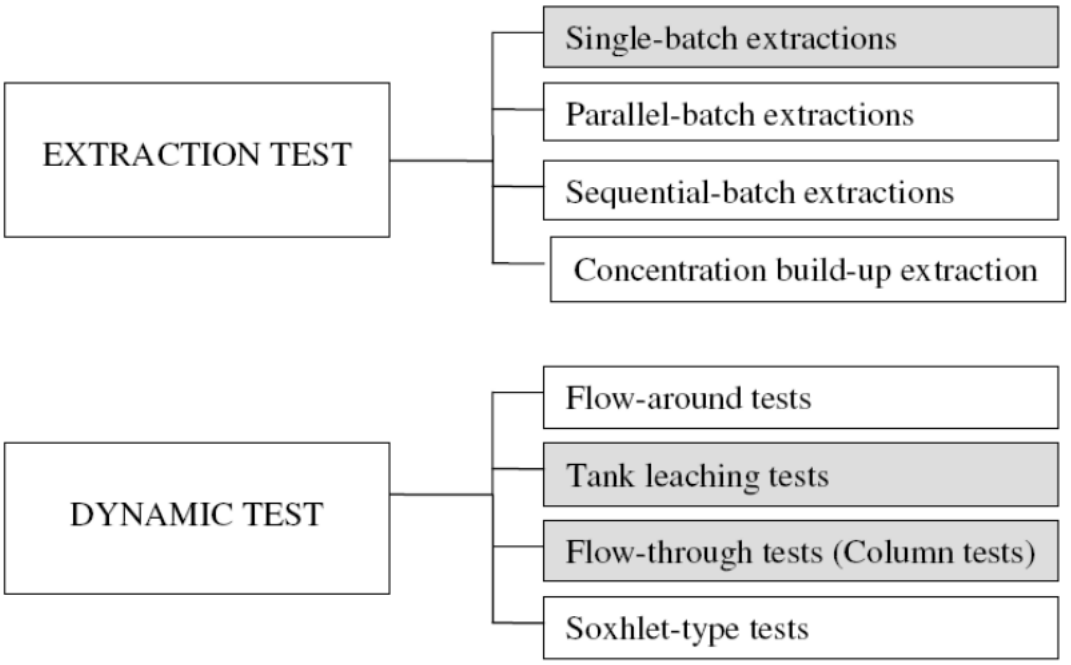

Figure 2.19 Categories of leaching tests and key group classifications.

Table 2.10 Benefits and drawbacks of key leaching test methods[142].

TEST CATEGORY/ OPERATING PARAMETER	ADVANTAGES	DISADVANTAGES
Agitated extraction tests (Batch tests)	• Tests are simple to set up and perform. • Tests can be of short duration (hours) in controlled conditions and if performed at various times can highlight the mechanisms of contaminant retention. • Disturbed samples can be tested easily. • Drying material makes it easier to crush samples if desired and achieve required solid to liquid ratios. • Deionised water is an easily controllable substance that does not affect the stabilization and solidification contaminant retention mechanism in the same way as an acid. • Once equilibrium is achieved leachate can be removed and replaced with 'fresh' leachant as many times as required. • Synthetic or real leachants, representing leachants *in-situ* can provide a more representative leaching model.	• Does not represent environmental leaching conditions and is therefore inherently qualitative. • Drying can affect the species of contaminants present and remove volatile organics. • Neither drying nor crushing represent environmental conditions. • Distilled water does not necessarily represent site-leaching conditions. • Synthetic or *in-situ* leachants require characterization to obtain leaching results by subtraction. • There is no account of time dependent changes in leachant composition. Some minerals do not separate easily from the liquid fraction. • Filter medium can affect chemical determination by element release or attenuation from or onto filter membranes respectively. • Centrifugation can affect results.
Flow-around tests (Diffusion tests)	• Easy to control leachant, solution temperature. • Contaminated samples can be tested as monoliths without pretreatment. • Diffusion mechanisms are investigated, which are important in low leachate flow conditions. • Solid and liquid separation is not necessarily required.	• Difficult to interpret the results and may not represent the diffusion conditions of a particular disposal site. Results are therefore qualitative, similar to the extraction tests.
Flow-through tests (Column leach tests)	• Can represent environmental leaching conditions. • Conditions can be controlled and changed throughout the test. • Unlike the other tests the sample can be subjected to varying physical stress conditions to represent individual sites. • Monolithic samples can be tested without pre-treatment. • Leachate can be passed through samples under pressure to accelerate leaching.	• The tests are not considered suitable for regulatory purposes due to the poor reproducibility and long duration. • Tests can last a number of months depending on material permeability and are difficult to set up and perform. • It is difficult to obtain representative undisturbed *in-situ* samples. • Data from this process are inherently qualitative.

Tank leaching tests, classified as 'semi-dynamic' mass transport rate tests, function as serial-batch extractions with extensive leaching. These tests, which involve repeated leaching to maintain a robust diffusive driving force, yield more consistent substance release concentrations than dynamic flow-around tests. This consistency benefits analytical procedures by simplifying the detection and quantification of released substances, thereby reducing variability and enhancing measurement accuracy. Additionally, tank leaching tests are straightforward to execute as they do not require pumps. Standard protocols for these tests include ANSI/ANS-16.1-2003[143] and the Dutch standard NEN 7345.

Specifically, the NEN 7345[144] is a semi-dynamic test designed to assess surface area-related release from monolithic waste, building materials, and stabilized waste materials. It entails immersing a geometrically regular monolith, with a known surface area, in a set volume of contact solution. The leaching fluid either intermittently or continuously diffuses into this solution, with regular refreshing of the contact solution. Periodic sampling and analysis of the leachate provide insights into the leachability of inorganic constituents over time.

The results of tank tests on monolithic materials are typically presented as milligrams per square meter (cumulative) plotted against time (in days). This representation is due to the release process, which is diffusion-controlled and influenced by the product's surface area and exposure duration. Fig. 2.20 illustrates a schematic of the outcomes obtained from the tank test, offering insights into various release processes observed in this context. A release mechanism driven solely by diffusion results in a slope of 1:0.5 on the curve. An initial surface wash-off step involves the rapid dissolution of soluble salts present on the surface of the product. The cumulative release curve may exhibit a plateau when a diffusion-controlled constituent becomes depleted over time, depending on the size of the test specimen. This phenomenon is particularly relevant for materials that are more permeable and have relatively small thickness[32].

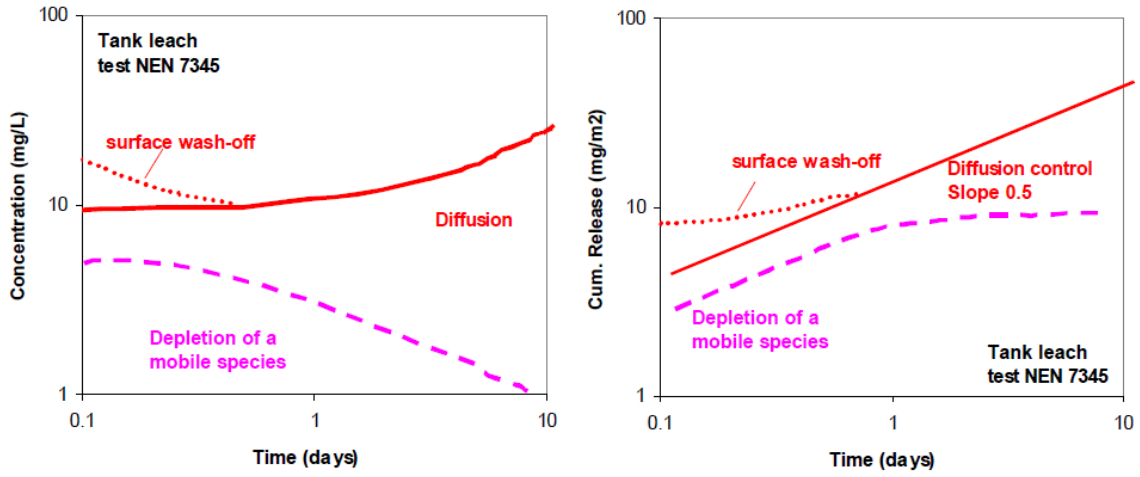

Figure 2.20 NEN 7345 tank leaching test results: standard analysis. Left: concentrations (mg/L), Right: cumulative leachate (mg/m^2)[32].

The effective diffusion coefficients (De, measured in m²/s) can be determined by analyzing the release curve of the tank test. These coefficients are then utilized to extrapolate the test results to real-world application scenarios or to make long-term predictions[145]. The NEN 7345 standard offers detailed information and context regarding the calculations involved in these applications. The phenomenon of pollutants leaching from materials subjected to s/s treatment can be broadly characterized by Eq. (2.9)[45,145–147].

$$\frac{M_t}{M_0} = \frac{4Dobst^{0.5}}{\pi L^2} \qquad (2.9)$$

where,

M_t: the mass of leachable contaminant leached by time 't'.

M_0: the initial mass of leachable contaminant in the solid.

Dobs: the observed diffusivity.

t: leaching duration in seconds.

L: the waste volume to surface area ratio for leaching exposure.

CHAPTER 3. MATERIALS AND METHODS

This chapter presents a detailed and methodical approach to studying HMs' leaching and adsorption behaviors in cement-based materials, employing a range of analytical techniques to understand these complex interactions under various environmental conditions.

3.1 Tank leaching test

3.1.1 Materials

Sand mortar specimens were prepared using ordinary Portland cement (OPC) conforming to the Japanese Industrial Standard (JIS) R 5210[148], sourced from Taiheiyo Cement Corporation, combined with quartz sand (with a density of 2.62 g/cm³ and water absorption of 0.16%) and deionized water. The chemical composition of the OPC is detailed in Table 3.1. The mortar's water-to-cement ratios (W/C) were set at 0.40 and 0.55, as indicated in Table 3.2. In this study, Cu, Zn, and Pb were chosen as representative HMs, given their higher likelihood of presence in SCMs[33,49,64–66,75] and recycled aggregates[149,150]. In the preparation of cement mixtures, 1% of Cu, Zn, and Pb, by mass relative to the cement mass, was incorporated as their respective nitrates: $Cu(NO_3)_2 \cdot 3H_2O$, $Zn(NO_3)_2$, and $Pb(NO_3)_2$.The added amount in this context was determined by considering the amount of HMs present in waste materials like fly ash, and by forecasting the maximum quantity that could potentially be included in concrete in the future. HMs are added as nitrates for two key reasons. First, the exceptional aqueous solubility of these nitrate compounds ensures their complete dissolution in the mixing water, providing uniform distribution of the HMs in the cement matrix. Second, their relative inertness during the cement hydration process minimizes the impact of the nitrates on the chemical and physical properties of the cement.

This is an advantage over other soluble heavy metal salts which might actively participate in hydration reactions, potentially altering the characteristics of the cement. This approach ensures that the HMs are evenly distributed without significantly affecting the hydration dynamics or the final properties of the cement. Chloride media, comprising NaCl, KCl, $MgCl_2$, $CaCl_2$, and deionized water at predetermined concentrations, were employed to replicate saline intrusion and establish a hostile testing environment.

Table 3.1 Chemical composition of the Portland cement.

Chemical composition (%)									
LOI	SiO_2	Al_2O_3	Fe_2O_3	CaO	MgO	SO_3	Na_2O	K_2O	Cl
2.25	20.8	5.15	2.92	64.6	1.13	2.29	0.2	0.38	0.014

Table 3.2 Mix proportion of mortar.

Name of specimen	W/C	Unit content (kg/m³)			Addition (kg/m³)	
		W	C	S	HMs	Nitrates
Cu40	0.40	329	823	1074	8.2	30.43
Cu55	0.55	375	681	1074	6.8	25.16
Zn40	0.40	329	823	1074	8.2	38.55
Zn55	0.55	375	681	1074	6.8	31.87
Pb40	0.40	329	823	1074	8.2	13.16
Pb55	0.55	375	681	1074	6.8	10.89

3.1.2 Casting and curing of specimens

Mortar was prepared using a Hobart mixer (see Fig. 3.1), and then cast into monolithic cubes measuring 40 × 40 × 40 mm via the following steps. At first, blend cement and quartz sand in a defined ratio at a low speed for 30 seconds. Subsequently, the predetermined amount of mixing water was incorporated and mixed for an additional 30 seconds. This mixture was then homogenized at high speed for 120 seconds to ensure uniform consistency. Manual homogenization was employed to ensure complete absorption of water into the mortar paste. After thorough mixing, the mortar was cast into

a standard 40 x 40 x 160 mm three-gang beam mold conforming to JIS R5201 specifications for structural formation. After the mortar had adequately set, it was carefully demolded. To mitigate the risks of heavy metal ion leaching and carbonation, the surfaces of all specimens were sealed with adhesive aluminum tape. For optimal curing, the specimens were placed in a controlled environment at 20°C and allowed to mature undisturbed for a period of 28 days.

Figure 3.1 Hobart mortar mixer.

3.1.3 Tank leaching test procedure

A tank leaching test was conducted to analyze the leaching behavior of HMs from mortars, with the setup illustrated in Fig. 3.2. Cubic specimens of 40mm x 40mm x 40mm were positioned in a polyethylene tank, using a plastic net at the bottom to ensure full contact of all surfaces with the solution. The test conditions for the tank leaching test in this study were determined with reference to NEN7345[144], an official leaching test in the Netherlands. In the Netherlands, NEN7345 is positioned as a test to understand the elution behavior governed by diffusion phenomena. Mortar specimens, cured for 28 days, were placed in tanks that were filled with five different types of contact medium: namely, NaCl, KCl, $MgCl_2$, and $CaCl_2$ solutions in addition to deionized water. The concentrations of the

chloride solutions used were all 10 mass %; a concentration that was selected to prevent precipitation of chloride crystals. The deionized water served as a control. The volume of the solution was 480 mL per specimen. This corresponds to the ratio of the surface area of the specimen to the volume of contact solution (20 mm^2/mL) specified in the Japan Society of Civil Engineers Standards (JSCE-G 575)[151].

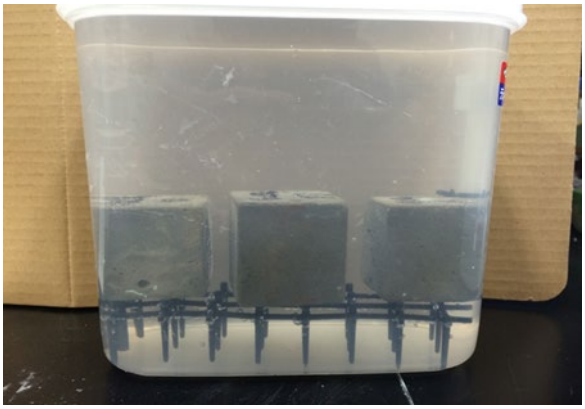

Figure 3.2 Tank leaching test.

The leaching solutions were periodically renewed at specific intervals: 0.25, 1, 4, 9, 16, 25, 36, 64, 100, 225, 400, and 625 days. The pH values of the leaching solutions were measured by a pH meter before the renewal of each leaching solutions. Concentrations of HMs ions in these solutions were quantified using FAAS (see Fig. 3.3) to determine the cumulative leaching rates of the metals. Significantly, on the 64^{th} day, one out of three specimens were permanently extracted for pore structure measurement. Additionally, at the culmination of the tank leaching test on the 625^{th} day, another specimen was subjected to XRD analysis to assess its crystalline phases. Post-removal of specimens on the 64th day, adjustments were made to the volume of the contact solutions to maintain a consistent surface area-to-volume ratio of the specimen (20 mm^2/mL). To halt further aqueous reactions before measuring pore volume, conducting EPMA and XRD analysis, a solvent extraction method was employed. This involved crushing the mortar specimens to less than

5 mm in size and immersing them in acetone within a beaker. To expel air bubbles, the beaker was placed in a vacuum desiccator. The acetone was periodically refreshed throughout the procedure, ensuring continuous specimen saturation to prevent air re-entry. To inhibit further carbonation and hydration, the specimens were preserved in acetone until measurement.

This methodical approach to specimen preparation and analysis ensures precise and reliable data on the leaching behavior and structural changes in cement-based materials, providing valuable insights into their long-term environmental impact. The pH of the leachate is detected by pH meter.

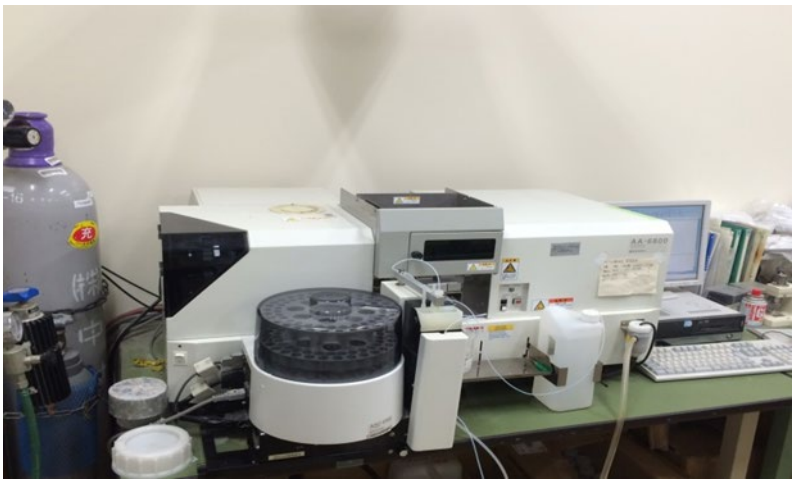

Figure 3.3 FAAS apparatus.

3.1.4 MIP analysis

As depicted in Figure 3.4, the study conducted a comprehensive evaluation of the pore size distribution in mortar specimens using MIP. This analysis included both pre-experimental mortar specimens and those that had been submerged for 64 days in various chloride solutions or deionized water, providing insights into the effects of environmental exposure on the pore structure.

For accurate measurement of the pore structure, a precise sample preparation

procedure was followed. Initially, the surface layer of each mortar specimen was removed to a depth of 5 mm mm using an oil cutter. Following this, the specimens were meticulously cut into smaller fragments, with sizes ranging from 2.5 to 5.0 mm.

To arrest further hydration processes, which could potentially alter the pore structure, the samples were then immersed in acetone. Prior to the porosity measurement, the samples were placed in a vacuum desiccator for 24 hours to remove any residual moisture. The mass of the sample used for the MIP analysis was about 1.5 g.

The pore volume assessment of the mortar specimens was carried out using a high-precision mercury intrusion porosimeter instrument (Poresizer 9310, Micromeritics). This instrument facilitated the measurement of pore diameters spanning from 6.5 nm to 200 μm, applying a maximum pressure of 228 N/mm².

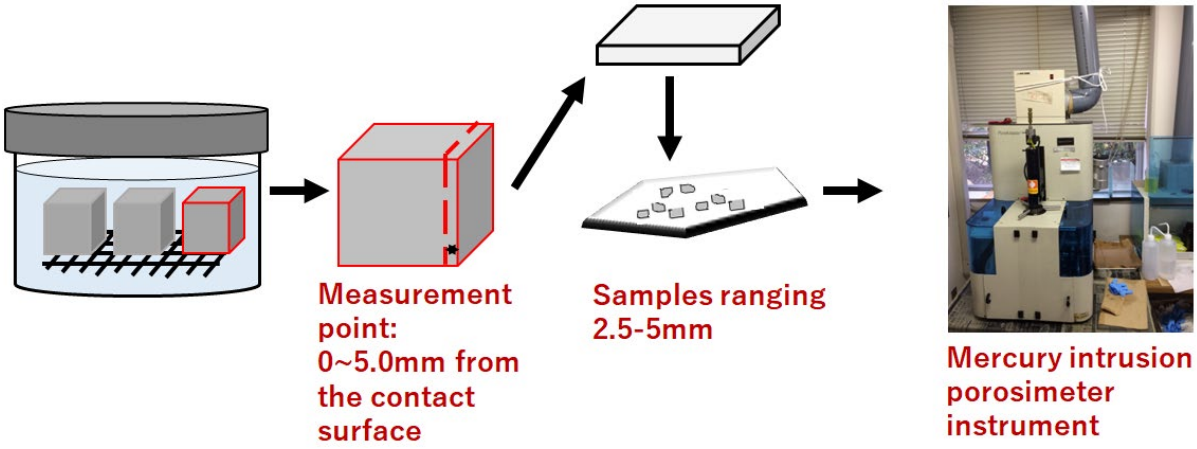

Figure 3.4 Pore size distribution measurement.

3.1.5 XRD analysis

The crystalline phases of mortar samples, both before and after immersion in tank leaching tests, were identified using XRD with an AXS D2 Phaser X-ray diffractometer (Bruker Corporation), as shown in Fig. 3.5. This analysis was conducted to investigate the alterations in the specimens and the state of HMs within the mortars. It included both pre-

experimental specimens and those submerged for 625 days in various chloride solutions or deionized water. Samples were collected from both the outermost layer and the interior of the specimens.

To halt any further chemical reactions, the samples were immersed in acetone. Prior to the XRD measurement, the samples were placed in a vacuum desiccator for 24 hours to remove any residual moisture. The samples were then pulverized to particle sizes smaller than 150 μm before the measurement. The XRD test was performed over a Bragg angle (2 theta) ranging from 5° to 65°, using a Cu Kα X-ray source. Data from these tests were analyzed with the EVA software tool.

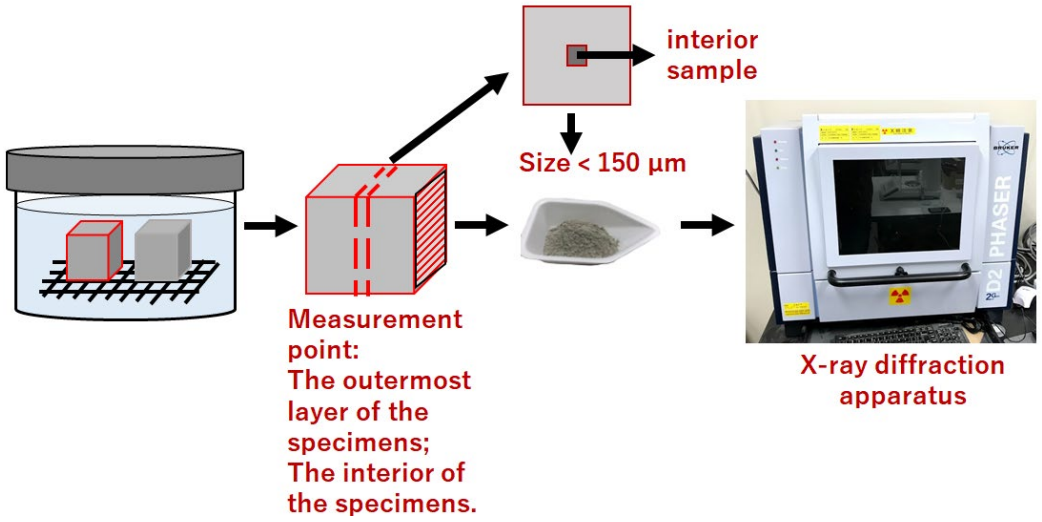

Figure 3.5 X-ray diffraction analysis.

3.1.6 EPMA analysis

EPMA analysis was carried out using a JEOL JXA-8200 electron probe microanalyzer and the steps are shown in Fig. 3.6. The objective was to find out the penetration of chloride from KCl and $CaCl_2$ solutions into the mortar and the distribution of lead and calcium in the specimens after contact with KCl and $CaCl_2$ solutions. The specimens tested were those immersed for 625 days in KCl, $CaCl_2$ solutions or deionized water. The analyses were

performed from the immersion surface to the interior.

After 625 days of immersion in the tank leaching test, the samples were cut into 40 x 40 mm plate specimens with a thickness of 5 mm. To halt any further chemical reactions, the samples were immersed in acetone. Prior to the EPMA measurement, the samples were placed in a vacuum desiccator for 24 hours to remove any residual moisture. The provided samples were then encapsulated in epoxy resin, and after the resin was cured at room temperature, dry grinding was performed on the sample. Carbon was then deposited on the surface to provide conductivity, and this was used as the analysis sample. The measurement conditions and elements analyzed are outlined as follows:

- Acceleration Voltage: 15 kV
- Sample Current: 1×10^{-7} A
- Measurement Time: 40 msec/pixel
- Analyzed Elements: For H_2O: Pb, Ca, Si; For $CaCl_2$ and KCl Solutions: Cl, Pb, Ca, Si
- Standard Samples: Wollastonite for Ca, Si (CaO = 48.3 mass%, SiO_2 = 51.7 mass%), Halite for Cl (Cl = 60.7 mass%), PbF for Pb (Pb = 91.7 mass%), Anhydrite for S (SO_3 = 58.8 mass%)
- Probe Diameter: 5 μm
- Pixel Size: 10×10 μm
- Number of Pixels: For H_2O Samples: 1000 (width) × 1000 (depth) for an analysis area of 10.0×10.0 mm; For $CaCl_2$ and KCl Solutions:1000 (width) × 2000 (depth) for an analysis area of 10.0×20.0 mm.

Furthermore, the average contents of various elements at the same depth in the horizontal direction of the sample was calculated. By correlating this with the depth measured from the immersion surface, the concentration distribution curves for each element were obtained.

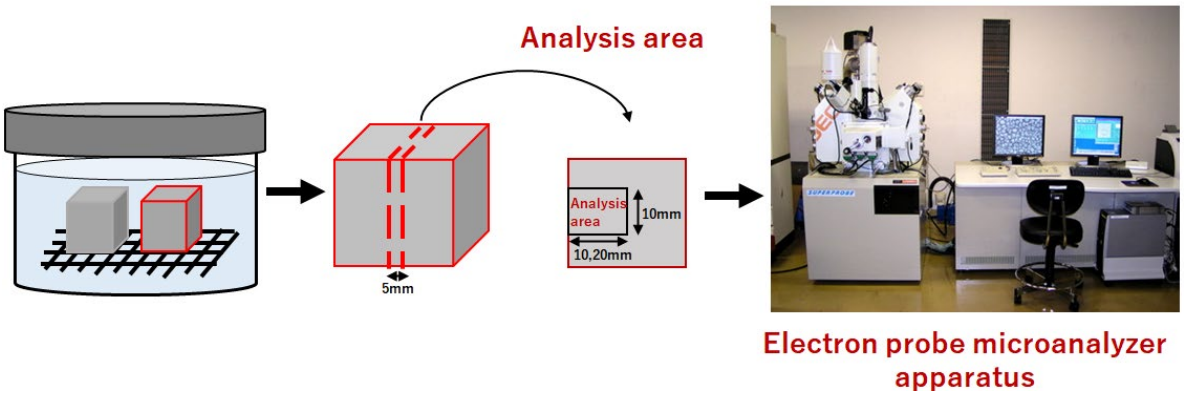

Figure 3.6 Electron probe microanalysis.

3.2 Adsorption test

Since the adsorption phenomenon is closely related to the migration of HMs in concrete, the adsorption characteristics of HMs on cement paste and CSH were investigated in this study. Based on previous research[152] in our laboratory, the adsorption experimental results for Cu and Zn (the relationship between equilibrium concentration and adsorption amount) showed dispersed values, and the impact of pH variation on the adsorption amount was also minimal. For Cu and Zn, under conditions that suppress precipitation, the maximum permissible concentration of HMs that can be added is very low, 25 g/L for Pb, while Cu and Zn are 150 mg/L. The target heavy metal for the adsorption experiments in this study was identified as Pb.

3.2.1 Materials and adsorption test procedure

In this research, Pb (II) nitrate ($Pb(NO_3)_2$) solution was employed to introduce lead into hardened cement paste and CSH powders. The primary objective was to elucidate the adsorption and desorption behavior of lead in these materials when exposed to various aqueous solution environments. This approach facilitated a detailed understanding of the

interaction between lead and cementitious materials under different conditions.

3.2.1.1 Adsorption test of Pb by hardened cement paste

Cement paste made of OPC and deionized water was used as a specimen for the purpose of obtaining basic information. The same cement was used as for the tank leaching tests. The cement paste was sealed and cured in a thermostatic chamber at 20°C for 28 days, and the water-cement ratio was 0.40; the hydrated cement pastes then were pulverized to obtain a powder finer than 150μm. $Pb(NO_3)_2$ was used as heavy metal.

(1) Adsorption test using chloride solution

In this test, various chlorides (NaCl, KCl, LiCl, $MgCl_2$, $CaCl_2 \cdot 2H_2O$) were used as reagents. Due to $CaCl_2$ being a deliquescent salt, the dihydrate form is used. The concentration is determined by taking into account the solubility of the solution and the expected concentration in the actual environment. Considering the very high immobilization capability of HMs in cement hydrates, it is important to ensure a sufficient concentration of chloride to observe leaching effects without exceeding the saturated solubility of the solution. The concentrations of 10 mass% NaCl, KCl, LiCl, $MgCl_2$, and $CaCl_2$ were chosen for this experiment.

The test method is shown in Fig. 3.7. The adsorption test was conducted assuming an environment in which the structure is exposed to chloride. First, 1 g of cement paste powder was added to 20 mL of deionized water, NaCl solution, KCl solution, LiCl solution, $MgCl_2$ solution, and $CaCl_2$ solution, stirred for 10 hours, and then 1 mL of $Pb(NO_3)_2$ solution with different concentrations was added and stirred for another 6 hours. The $Pb(NO_3)_2$ solution added had Pb concentrations of 4000, 10,000,

16,000, and 25,000 mg/L. The solution was then suction filtered through a 0.45-μm membrane filter and adjusted to the acidic side by adding 2 mL of 2 mol/L nitric acid solution to the filtrate. The filtrate was then fixed volume to 50 mL and its concentration was measured by FAAS, from which the adsorbed amounts were calculated by Eq. (3.1).

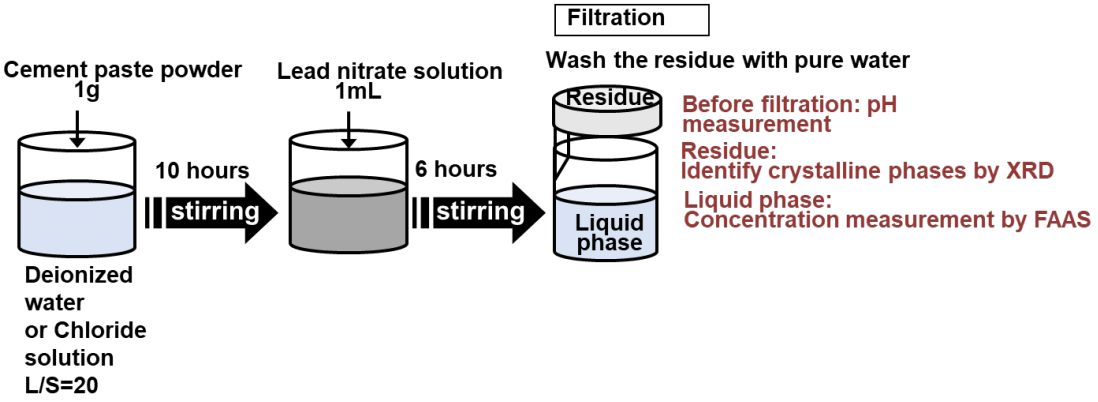

Figure 3.7 Adsorption test in contact with various chlorides.

$$V = (S/1000)\ \{(C-P)/m\} \qquad (3.1)$$

where,

V: Degree of Pb adsorption (mg per gram of cement paste).

S: Volume of solution (mL).

C: Concentration of Pb in initial $Pb(NO_3)_2$ solution (mg/L).

P: Equilibrium concentration of Pb after the adsorption test (mg/L).

m: Mass of cement paste powder (g).

(2) Adsorption tests under different pH environments

Assuming a scenario where the pH value of the pore solution decreases, as in the case of neutralization or dissolution in hardened cement, this study examines the impact of pH

value on the Pb adsorption characteristics on hardened cement. Furthermore, these adsorption results are compared with those obtained under pH variations caused by the addition of various chlorides. Two methods were employed to adjust the pH value of the contact solution: one is by altering the liquid-to-solid ratio (L/S), and the other involves using nitric acid to regulate the pH value, aiming to study environments with lower pH values.

The first method, as illustrated in Table 3.3, involves adjusting the pH by varying the L/S between 20 and 30,000, using deionized water as the contact solution. The L/S ratios were set at 20, 50, 200, 1000, and 3000 (mL/g), with the pH values just before the addition of HMs being 12.80, 12.73, 12.52, 12.13, and 10.88, respectively. The experimental steps are shown in Fig. 3.8. Following established research protocols, the adsorption test procedure began with adding cement paste ground to a particle size of 150μm or less to deionized water. Then, 5mL of $Pb(NO_3)_2$ solution was added, followed by stirring for 6 hours. The post-stirring solution was filtered using a 0.45μm membrane filter, and the concentration of Pb in the filtrate was measured using an FAAS. This process determined the equilibrium concentration and the amount of adsorbed Pb. The pH of the solution was measured at each stage of the procedure.

Table 3.3 pH adjustment by L/S change.

L/S	Mass of cement paste (g)	pH
20	5.0	12.80
50	2.0	12.73
200	0.5	12.52
1000	0.1	12.13
30000	0.1	10.88

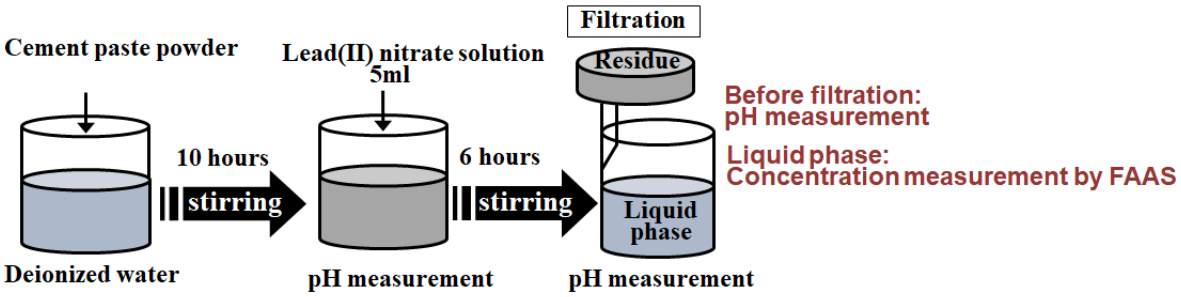

Figure 3.8 Adsorption test (pH adjustment by L/S).

The second method, as depicted in Table 3.4, involves adjusting the pH by adding a nitric acid solution to the contact solution. The experimental steps are shown in Fig. 3.9. Initially, the cement paste sample was stirred with deionized water alone. Subsequently, a predetermined amount of nitric acid solution was added and stirred thoroughly to stabilize the pH. First, 5g of cement paste was added to deionized water and stirred for 10 hours. Then, a predetermined amount of nitric acid solution was added, and the mixture was further stirred for 6 hours to stabilize the pH. Afterwards, 5mL of various concentrations of $Pb(NO_3)_2$ solution were added and stirred for an additional 4 hours. The concentrations of the Pb in the added $Pb(NO_3)_2$ solution were set to 4000, 10000, 16000, and 25000mg/L. Notably, the stirring time after the addition of the $Pb(NO_3)_2$ solution differs from the first method, but was set to 4 hours based on preliminary tests that showed almost no change in adsorption amount after this duration. The post-stirring solution was then filtered through a 0.45μm membrane filter, and the concentration of Pb in the filtrate was measured using an FAAS to determine the equilibrium concentration and the amount of adsorbed Pb. The total volume of the contact solution, comprising the deionized water and nitric acid solution, was maintained at 100mL, with an L/S ratio of 2 (mL/g) for all solutions. The pH was measured at each stage. The composition of the cement paste before the adsorption test and the residue after the test were qualitatively analyzed using powder XRD.

Table 3.4 pH adjustment by nitric acid solution.

Deionized water (mL)	Nitric acid solution (mL)	pH (after 6 hours of stirring)
59	41	8.35
63	37	9.14
67	33	10.02
75	25	11.24

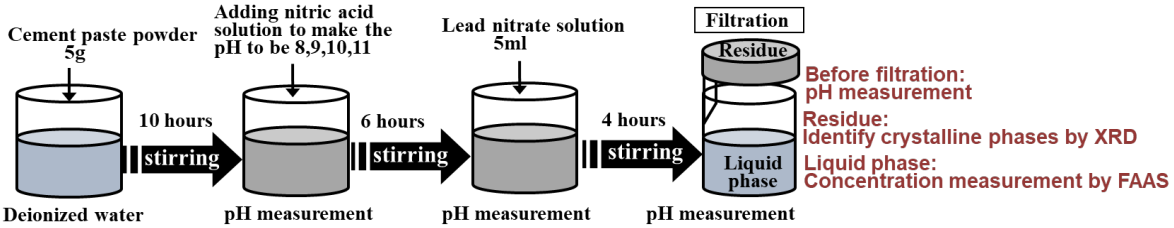

Figure 3.9 Adsorption test (pH adjustment by nitric acid solution).

3.2.1.2 Adsorption test of Pb by synthetic CSH

Two types of synthesized CSH with Ca/Si ratios of 0.83 and 1.40 were used for the experiment. Since the CSH with a Ca/Si ratio of 1.40 was difficult to synthesize, we purchased it from Taiheiyo Cement Corporation. Hereafter, the two types of CSH are described as CSH0.83 and CSH1.40, respectively.

The CSH0.83 was made from $Ca(OH)_2$, SiO_2, and deionized water as its raw materials. Turbid fluid with a water to powder ratio of 30 was stirred at 70 rpm at the chosen 0.83 Ca/Si ratio. A hydrothermal reaction was performed at 50°C for 24 h to synthesize the CSH. After synthesis, the mixed solution was filtered with membrane filters, and drying was carried out by vacuum degassing. Table 3.5 shows the materials and synthesis conditions used for the synthesis of CSH0.83.

Table 3.5 Materials and synthesis conditions for CSH0.83.

Synthesized phase	Ca/Si	Materials(g)			Temperature (°C)	Time (hr)
		$Ca(OH)_2$	SiO_2	H_2O		
CSH gel	0.83	17.40	12	882	50	24

Fig. 3.10 shows the XRD results of synthesized CSH. The figure shows a diffraction diagram resembling that of relevant previous studies[153,154]. This observation demonstrated that the CSH0.83 had been synthesized. That outcome was also confirmed by the thermogravimeter/differential thermal analyzer (TG-DTA; DTG-60H, Shimadzu Corporation, see Fig. 3.11), which demonstrated that there was no unreacted $Ca(OH)_2$. The Ca/Si atomic ratio was also confirmed by EDX.

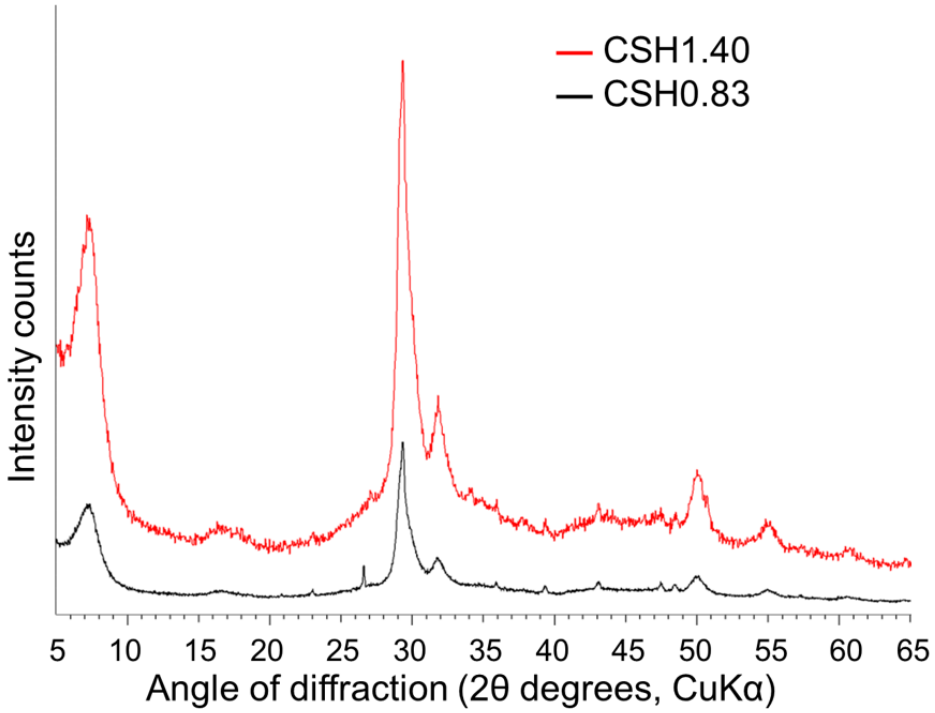

Figure 3.10 Results of XRD for CSH.

Figure 3.11 TG-DTA apparatus.

The adsorption tests simulated an environment in which structures are exposed to various chloride solutions such as those used for deicing, and seawater. Fig. 3.12 shows the procedure of the adsorption tests. Many studies have reported on the effects of carbonation on the microstructure of cement paste and the properties of CSH[122,155,156]. To prevent carbonation of the samples, the materials were fabricated and the adsorption experiments were conducted with minimal exposure to air. The adsorption tests were carried out in a 30 mL beaker which was kept airtight. Firstly, hydrated cement paste powder was added to deionized water (liquid-solid ratio: 20 mL/g), then the mixed solution was stirred for 10 h in a closed container. After that, the mixed solution was filtered with membrane filters. Secondly, NaCl, KCl, $MgCl_2$, $CaCl_2$, and $Ca(NO_3)_2$ solutions were added to the filtrate of the cement paste with a concentration of 10 mass % and then stirred for 1 h. Hereafter, the mixed solutions are referred to as NaClPM, KClPM, $MgCl_2$PM, $CaCl_2$PM, and $Ca(NO_3)_2$PM, respectively. The filtrate of the cement paste (hereafter, referred to as “pore solution”) was retained for reference. Thirdly, 1 mL of $Pb(NO_3)_2$ solution with a known concentration of Pb ions and 1 g of synthesized CSH ground to a powder with grains smaller than 75μm in size were jointly added to the mixed solutions and then stirred for 6 h.

In this test, the concentrations of Pb ions were 0.4, 10, 16, and 25 g/L. Finally, the mixtures were filtered with membrane filters, and the liquid phases were used to determine the concentration of heavy metal ions by FAAS. The degree of Pb adsorption was also calculated by Eq. (3.1). The residues were used to investigate the Ca/Si ratios by EDX. Before filtration, the pH values of these mixed solutions were measured.

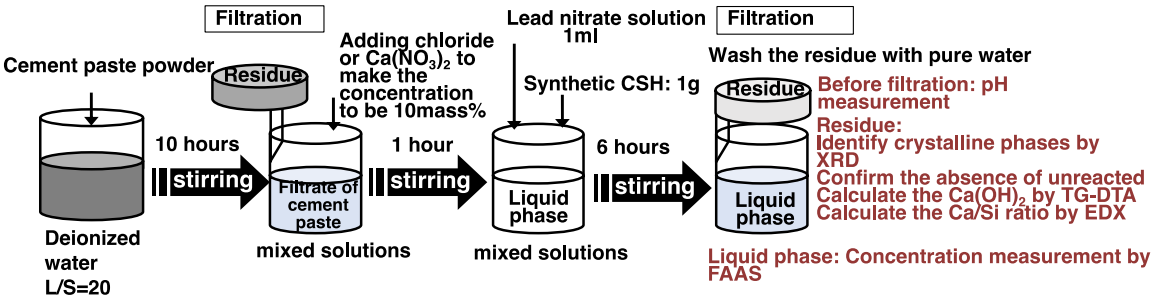

Figure 3.12 Adsorption test of Pb by synthesis of CSH.

3.2.2 XRD analysis

Following the adsorption tests, the crystalline phases of the synthesized CSH samples were identified by XRD to investigate their alteration and the form of the adsorbed Pb. The test was performed at a Bragg angle (2 theta) ranging from 5° to 65° using a Cu Kα X-ray source. The data was analyzed using the EVA software tool.

3.2.3 EDX analysis

Spectroscopic analysis of the synthesized CSH samples, which had been exposed to various solutions, was conducted using EDX with a JEOL JSM-6010PLUS, as shown in Fig. 3.13. This technique was employed to determine the Ca/Si ratios in the CSH. Prior to analysis, the synthesized CSH particle size was adjusted to below 75μm, and the samples were preserved in a vacuum desiccator to prevent any atmospheric interference.

For non-conductive materials, such as these CSH samples, it is standard practice to coat the samples with a conductive material before spectroscopic measurements. This coating enhances the quality of the obtained images by facilitating the emission of secondary electrons. Gold, known for its excellent conductivity, is often used for this purpose. However, for superior resolution, platinum is preferred. In this study, the samples were coated with platinum.

The EDX analysis involved selecting individual point spectra from several neighbouring points within local areas approximately 200 × 200 μm in size. For each specimen, two such areas were chosen, with a total of five points analyzed per area. The spectroscopic examination was conducted at an accelerated voltage of 15 kV to ensure optimal resolution and accuracy in measuring the Ca/Si ratios.

Figure. 3.13 EDX apparatus.

CHAPTER 4. EFFECTS OF CHLORIDE SOLUTIONS ON HEAVY METAL LEACHING FROM MORTARS

This chapter discusses how chloride-based salts affect the immobilization and leaching of Cu, Zn, and Pb from cement hydrates and analyzes the associated internal changes in crystalline phase. Tank leaching tests totaling 625 days were conducted. The effect of various chloride-based salts on the pore volume of mortar was analyzed on day 64 of contact with chlorides. Meanwhile, at the end of the tank leaching test on day 625 (i.e., the last day of immersion), internal changes associated with crystallization following exposure to various chlorides were analyzed using XRD.

4.1 Effect of the types of solutions on the leaching of HMs

The cumulative leachate quantities of HMs obtained from mortar specimens immersed in deionized water and the chloride solutions for 625 days are shown in Figs. 4.1 to 4.8. Fig. 4.6 and Fig. 4.8 show the same results as Fig. 4.5 and Fig. 4.7, respectively, but the results for the solutions other than the $CaCl_2$ solution are magnified. The data shown in these figures represent the cumulative mass of each HMs in the leachate, which is calculated per unit mass of the mortar specimen (mg/kg). This value is plotted as a function of the square root of the leaching time ($day^{1/2}$).

The results for Cu, Zn, and Pb all show that the largest leachate quantity was observed in the case of the $CaCl_2$ solution, while the quantity was the smallest in the case of the deionized water. Considering the types of cations of the chloride solutions, the largest leachate quantities can be seen in the case of Ca^{2+}, followed by K^+, Na^+, and Mg^{2+}, regardless of the water/cement ratio. The cases of the NaCl and KCl solutions, which show

very closely similar results, may be treated as equivalent.

In addition, from Fig. 4.5 and Fig. 4.7 it is found that the cumulative leachate quantity of Pb ions from the specimen immersed in the $CaCl_2$ solution is more than six times as large as that in the other solutions. Similarly, the amount of Cu and Zn leached from the specimens immersed in the $CaCl_2$ solution was significantly higher than the other chloride solutions (see Figs. 4.1 to 4.4). It is evident that the $CaCl_2$ solution creates a different leaching environment for Pb ions from the immersed specimens, as opposed to those in the other chloride solutions. These results are consistent with a previous study[30]. In addition, Miura et al.[157] have reported that the quantities of chloride permeating concrete were larger in the case of $CaCl_2$ solution than for NaCl solution, and that the permeated chloride reacts with the hydrates and even dissolves them. This is most likely the reason for the significant increase in Cu, Zn, and Pb leaching when in contact with $CaCl_2$ solution.

Since the horizontal axis in Figs. 4.1 to 4.8 corresponds to the square root of the actual number of days of leaching, the leachate quantity should increase linearly on the graphs if the migration of HMs ions out of the mortars is entirely governed by diffusion. Regarding the leaching of Cu, Zn and Pb, the findings depicted in Figs. 4.1 to 4.8 demonstrated that regardless of the water-cement ratio of the mortars and chloride contact solutions types being investigated, each release curve consistently exhibited two distinct linear parts. Both segments indicated a linear relationship between the cumulative release, and the square root of time. This is similar to the findings of Song et al[140]. and Cinquepalmi et al.[141]. van der Sloot et al.[32] reported the cumulative release curve may exhibit a plateau due to the depletion of a constituent controlled by diffusion (see Fig. 2.20). The plateau represents the slowing or cessation of the release rate of a given diffusion control component as it is exhausted over time. For long-term leaching, if partial or complete depletion of the diffusive component leads to the appearance of a plateau, in a plot where the horizontal axis is the square root of time, this may be indicated by a marked change in the slope of the curve, e.g., a shift from an initially steeper

slope to a gentler slope. This implies that, at this stage, while diffusion control remains the predominant factor, the pace of heavy metal dispersion may decelerate owing to the decrease in mobile heavy metal entities. While the overarching process continues to be governed by diffusion mechanisms, the particular characteristics of diffusion may undergo alterations. The plateau of the leaching curve in heavy metal leaching experiments is usually caused by the depletion of the "leaching capacity" of the heavy metal. Leaching capacity is commonly used to describe the maximum amount of a substance that can be dissolved from a solid substrate (e.g., soil, cementitious materials, etc.) and released into the environment under specific conditions. The results of this experiment demonstrates that the presence of chloride enhances the leaching capacity of Cu, Zn, and Pb in mortar. Furthermore, despite the identical quantity of Cu, Zn, and Pb added per unit mass of the cement paste, the leaching capacity of Cu and Zn is markedly lower than that of Pb, differing by more than an order of magnitude.

Furthermore, it was observed that from the 100th day, the effective diffusion coefficient for the chloride solutions (except $CaCl_2$ solutions) was almost the same as that for the deionized water. It seems that the dominant factor governing the leaching of Cu, Zn, and Pb from the specimens immersed in chloride solutions becomes the same as that in the deionized water after 100 days, while differing for the first 100 days. However, in the case of mortar specimens in contact with $CaCl_2$, despite the increased diffusion coefficients attributed to the influence of $CaCl_2$, leading to a faster leaching rate, even after reaching the plateau phase where the diffusion coefficient decreases, the leaching rate of Cu, Zn, and Pb remains higher compared to other solutions. This phenomenon indicates that while the diffusion process slows down upon reaching the saturation point, it still facilitates a relatively more rapid release of HMs in the presence of $CaCl_2$ than in other solutions. Furthermore, after 400 days, for the mortar samples in contact with a 10 mass% $CaCl_2$ solution, the leaching rates of Cu, Zn, and Pb began to accelerate again. Here, the leaching of Cu, Zn, and Pb may not be caused by

the solution itself, but rather by the chemical erosion of the hardened cement, leading to mortar deterioration and thus higher leaching. When assessing the long-term effects of contact with chloride solutions on the immobilization of HMs, the type and concentration of different chlorides and their chemical erosion effects on hardened cement should be considered.

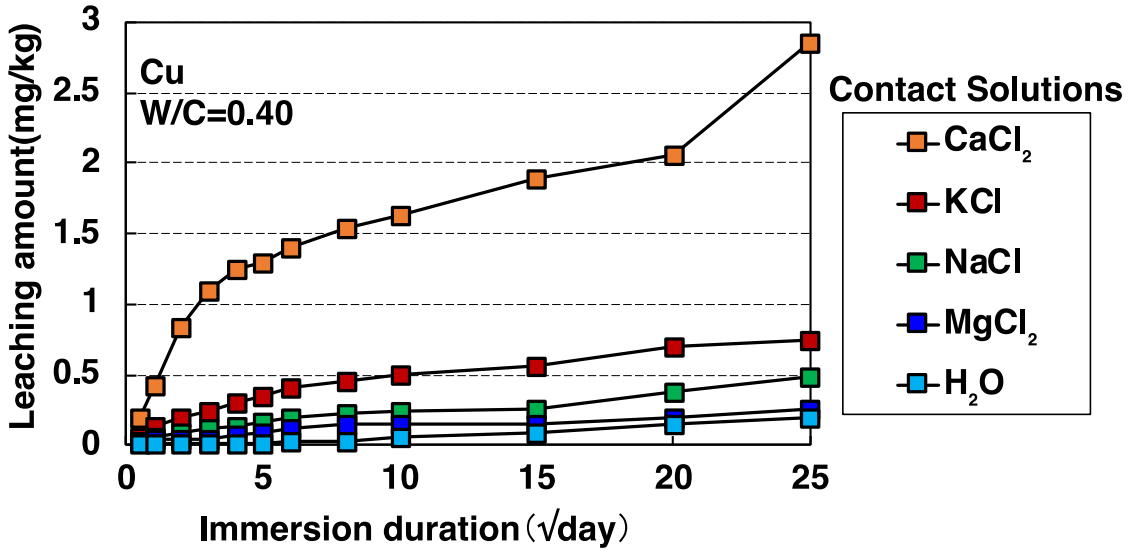

Figure 4.1. Cumulative leachate quantity of Cu from mortars (W/C = 0.40) immersed in different contact solutions for 625 days.

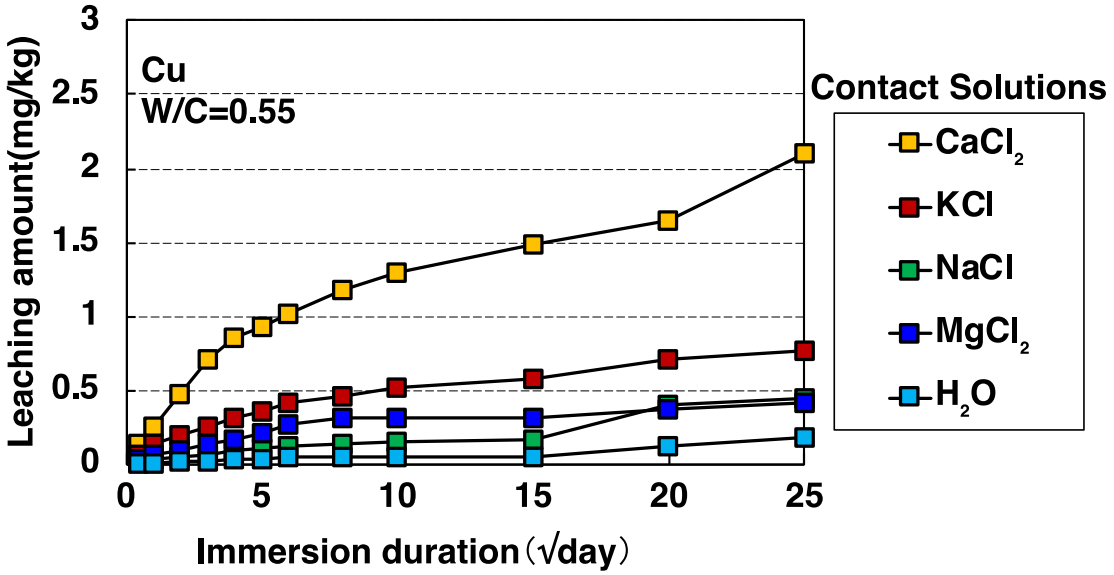

Figure 4.2 Cumulative leachate quantity of Cu from mortars (W/C = 0.55) immersed in different contact solutions for 625 days.

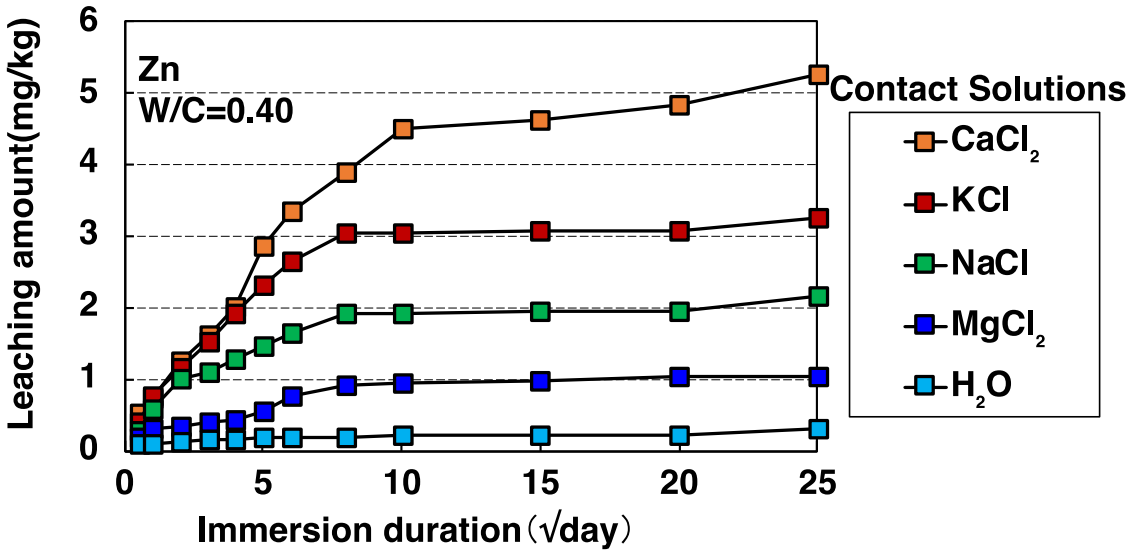

Figure 4.3 Cumulative leachate quantity of Zn from mortars (W/C = 0.40) immersed in different contact solutions for 625 days.

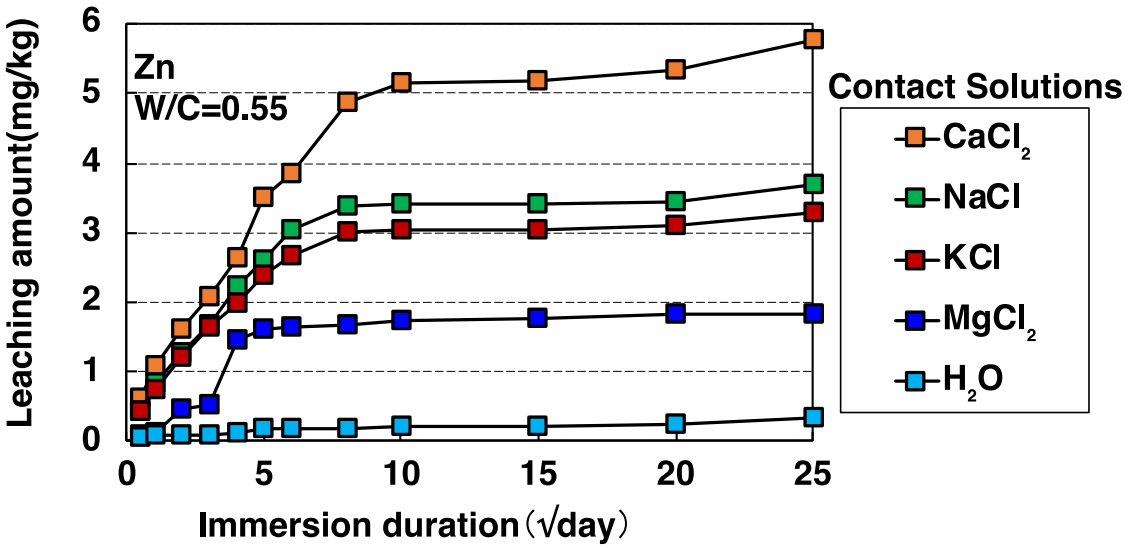

Figure 4.4 Cumulative leachate quantity of Zn from mortars (W/C = 0.55) immersed in different contact solutions for 625 days.

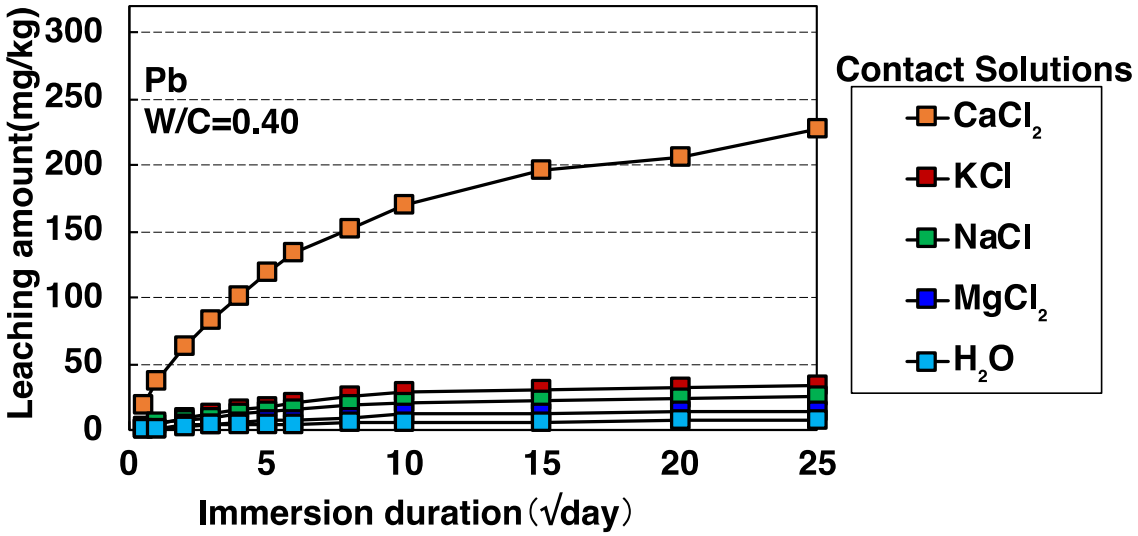

Figure 4.5 Cumulative leachate quantity of Pb from mortars (W/C = 0.40) immersed in different contact solutions for 625 days.

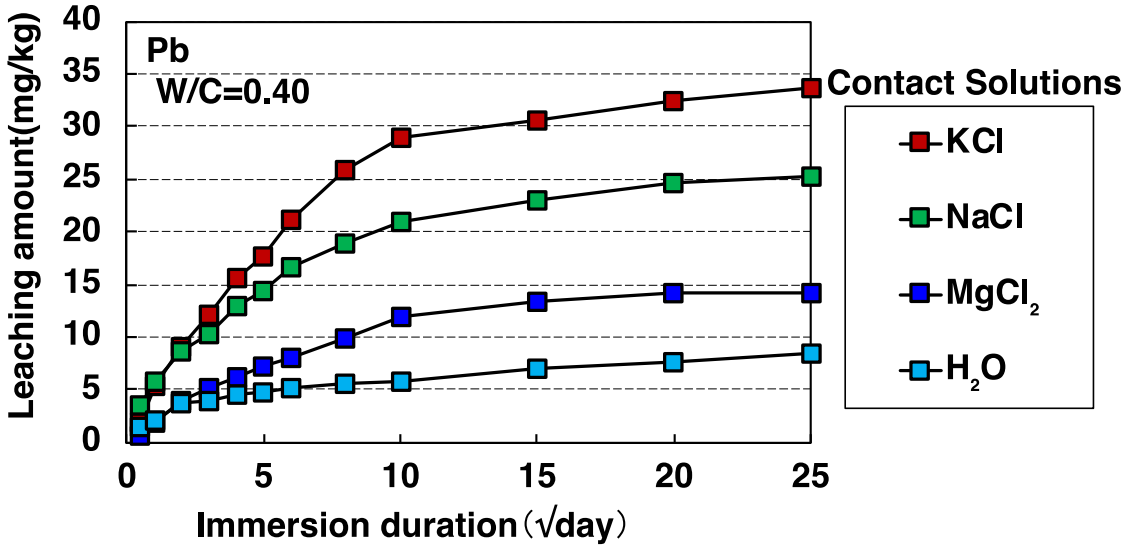

Figure 4.6 Cumulative leachate quantity of Pb from mortars (W/C = 0.40) immersed in different contact solutions (except $CaCl_2$ solution) for 625 days.

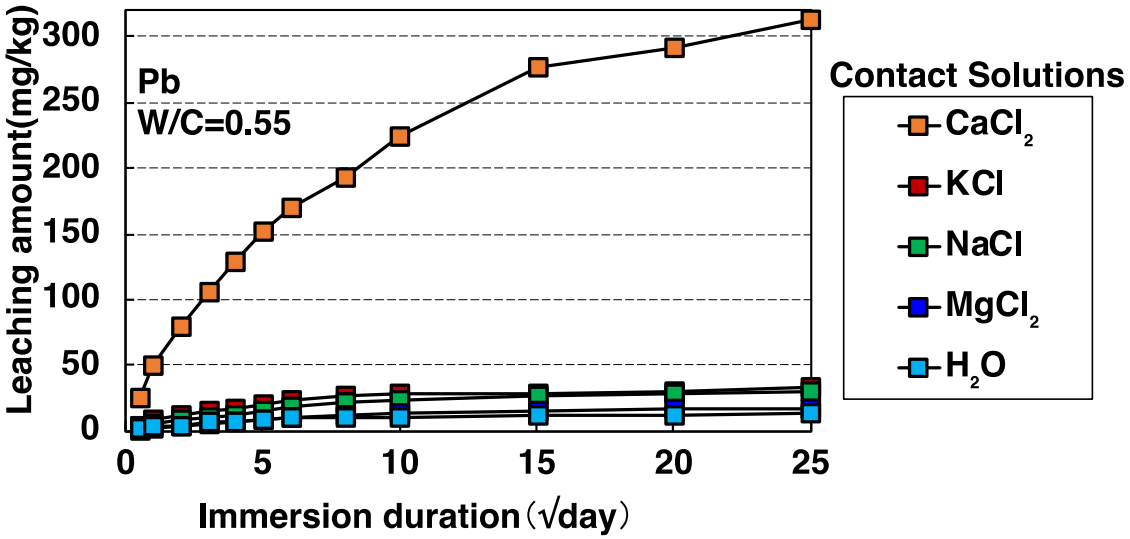

Figure 4.7 Cumulative leachate quantity of Pb from mortars (W/C = 0.55) immersed in different contact solutions for 625 days.

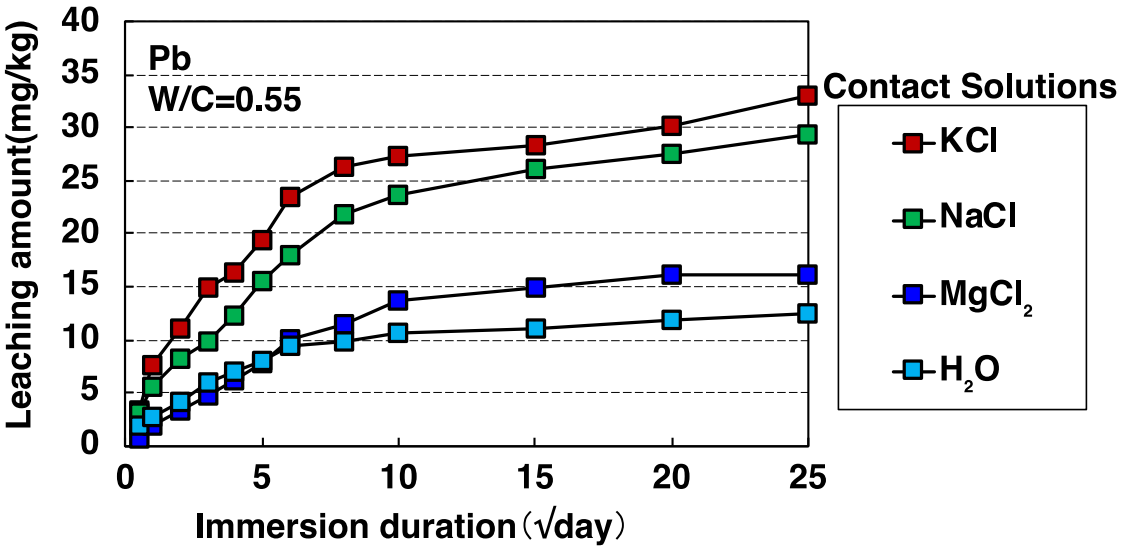

Figure 4.8 Cumulative leachate quantity of Pb from mortars (W/C = 0.55) immersed in different contact solutions (except $CaCl_2$ solution) for 625 days.

4.2 Effect of chlorides on pore size distribution

The MIP was conducted to assess the impact of chlorides, as well as Cu, Zn, and Pb, on the pore structure of mortar specimens. As a result of the aforementioned tank leaching test, the leaching of Pb is consistently significantly higher than that of Cu and Zn, regardless of the type of chloride solution or deionized water used. Alford et al.[158] reported that the addition of high

concentrations of $Pb(NO_3)_2$ led to the formation of large amounts of gel, which in turn caused deleterious cracks in the cement pastes. Figs. 4.9 to 4.11 displays the pore size distribution measurements of the initial sample at 28 days of age. In this study, the addition of Pb (1% of Pb, by mass relative to the cement mass), in contrast to Cu and Zn (1% of Cu and Zn, by mass relative to the cement mass), did not result in a significant difference in the quantity of fine pores within the cement paste. This observation confirms that the high leaching rates of Pb are not due to a change in pore structure caused by the addition of $Pb(NO_3)_2$.

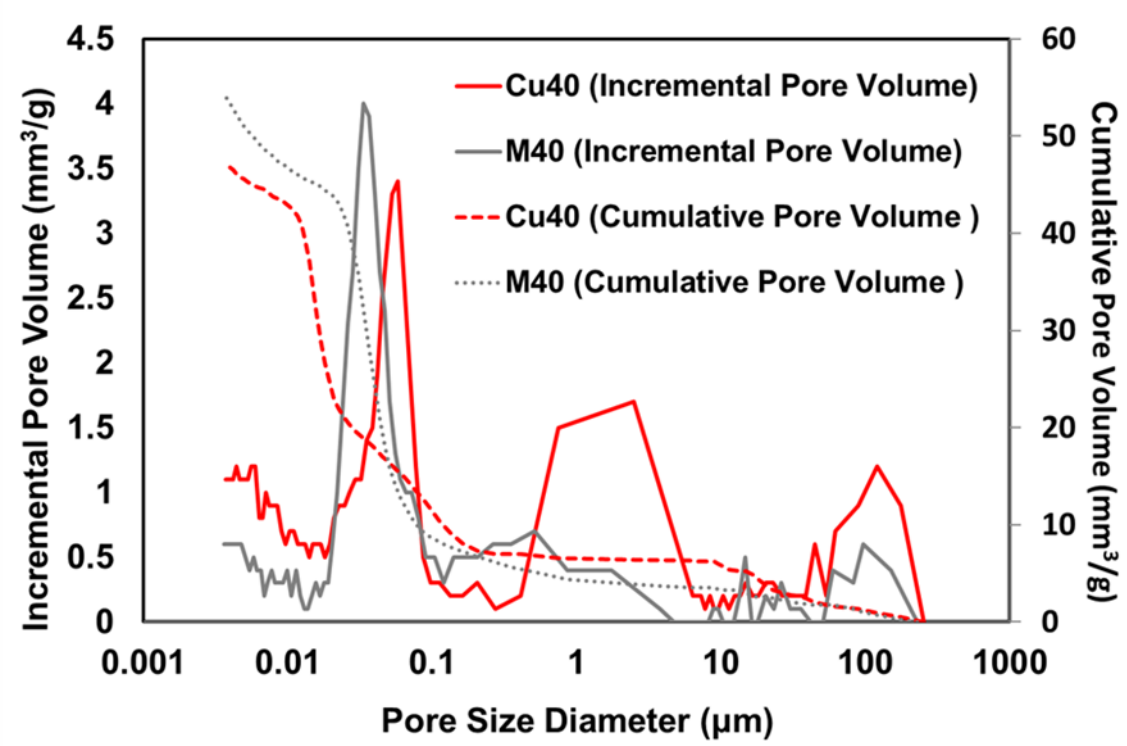

Figure 4.9 Pore size distribution measurements of the initial sample at 28 days of age (containing Cu, W/C = 0.40).

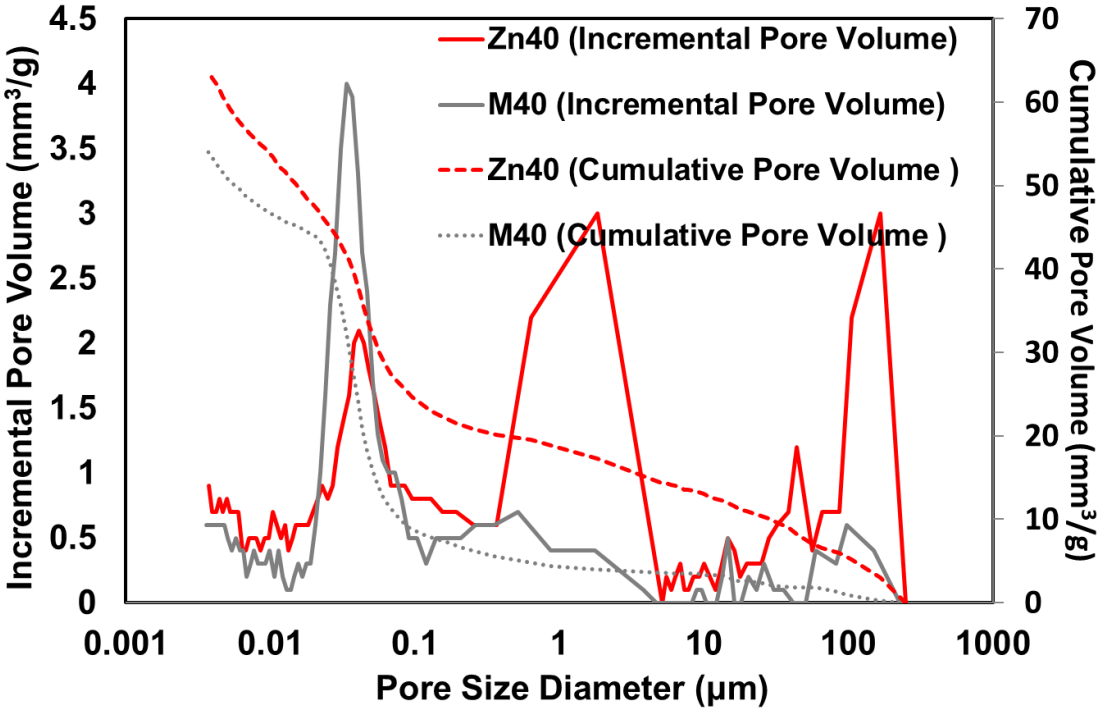

Figure 4.10 Pore size distribution measurements of the initial sample at 28 days of age (containing Zn, W/C = 0.40).

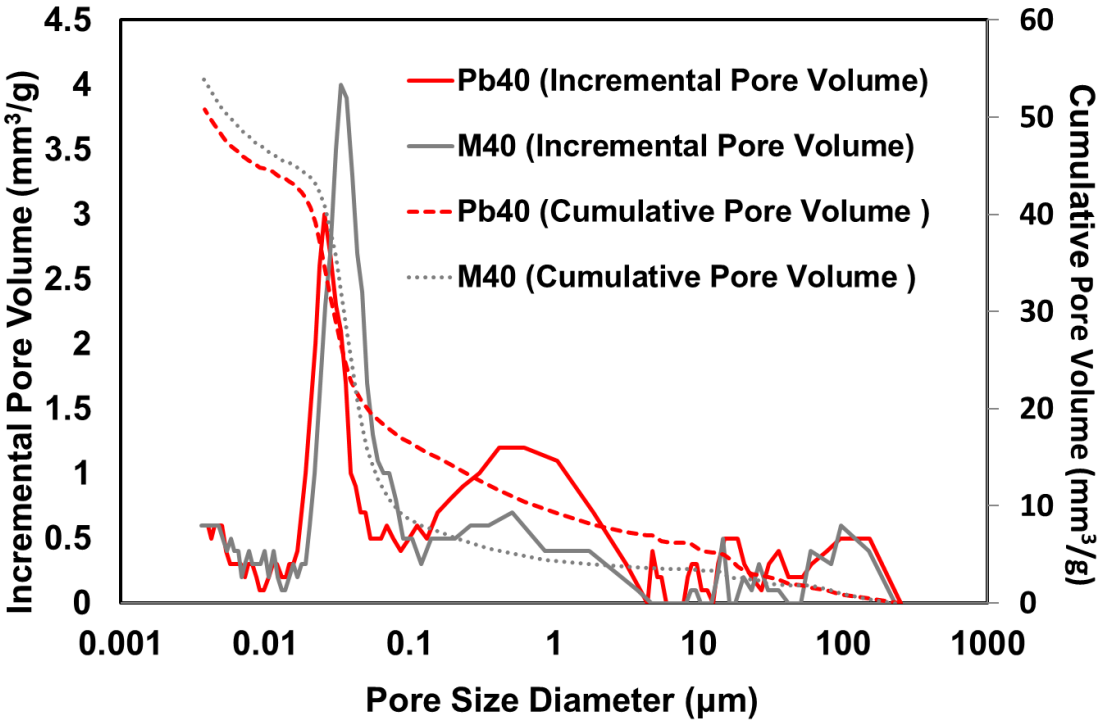

Figure 4.11 Pore size distribution measurements of the initial sample at 28 days of age (containing Pb, W/C = 0.40).

The pore volumes of the mortar specimens before immersion and after immersion for

64 days are shown in Fig. 4.12. The regular differences that could be evaluated in the pore volume in the specimens immersed in the solutions could not be observed for each water/cement ratio. These results mean that the large leachate quantity for the $CaCl_2$ solution was not attributable to alterations in pore structure. The change in pore volume due to chloride solution is not the dominant factor affecting the Pb leaching. The pore size distribution measurement results are provided in the appendix.

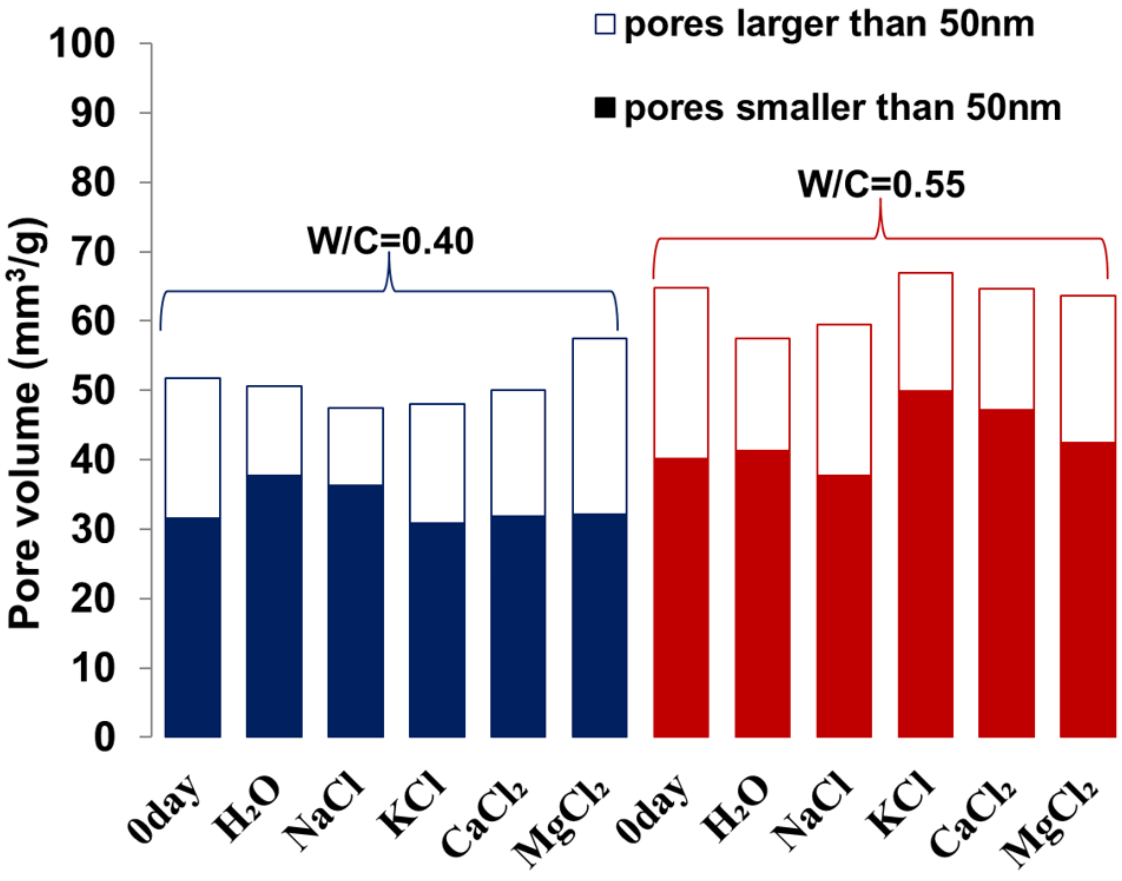

Figure 4.12 Pore volumes of specimens immersed in each solution for 64 days ('0 day' shows the result before immersion.).

4.3 Results of XRD analysis

XRD qualitative analyses of Cu, Zn, and Pb for the central area of the mortar specimens immersed for 625 days showed no changes in crystalline phases over the duration of the tank leaching tests, although the peak intensities of alite and larnite were reduced. The XRD

patterns for samples collected from the surface areas of the mortar specimens containing Pb are shown in Fig. 4.13, both before tank leaching and after 625 days of tank leaching. In all specimens in contact with the chloride solutions, diffraction peaks of Friedel's salt were observed, a finding also reported in previous studies[159,160]. Peaks of Friedel's salt were also observed in the samples containing Cu and Zn. In addition, in the cases of the deionized water, almost no changes were observed in the chemical composition (crystal phase) of the hydrates in the mortar specimens containing Cu, Zn, and Pb, except that portlandite was leached.

Moreover, as shown in Fig. 4.14, in the case of the $MgCl_2$ solution, brucite peaks were detected in the samples containing Cu, Zn, and Pb; on the other hand, portlandite peaks were not observed. Konno et al.[161] reported that when hardened cement paste was immersed in $MgCl_2$ solution, it would become completely covered with a brucite crystal layer[161,162]. Therefore, it can be said that as shown in Eq. (4.1) the portlandite in the specimens was almost entirely decomposed to form brucite which reduced the pH value to around 9.

Furthermore, based on the qualitative analysis results from XRD in this study, it was not possible to unequivocally identify any compounds of Cu, Zn, or Pb within the cementitious body. This indicates that the distribution of heavy metal compounds is not uniform, or they exist in an amorphous state, as very fine particles, or in complex structures within the cement matrix (e.g., compounded with other compounds in the cement matrix), thus preventing accurate identification by XRD.

$$Ca(OH)_2 + MgCl_2 \rightarrow Mg(OH)_2 + CaCl_2 \qquad (4.1)$$

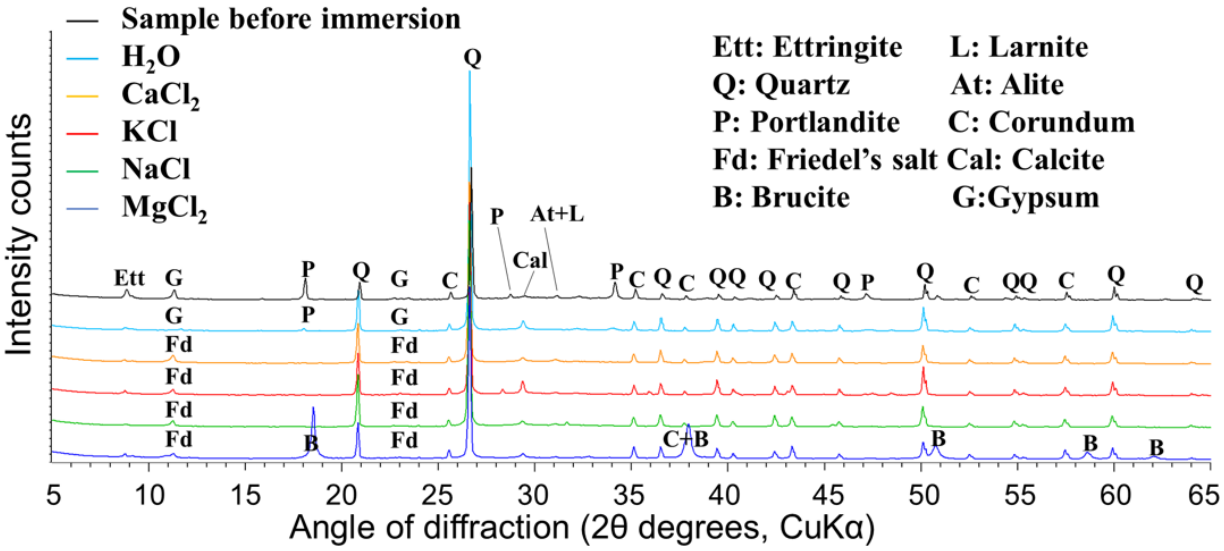

Figure 4.13 XRD patterns of samples collected from the surface of mortar specimens containing Pb before tank leaching and after 625 days of tank leaching (Corundum was intentionally added in the samples.).

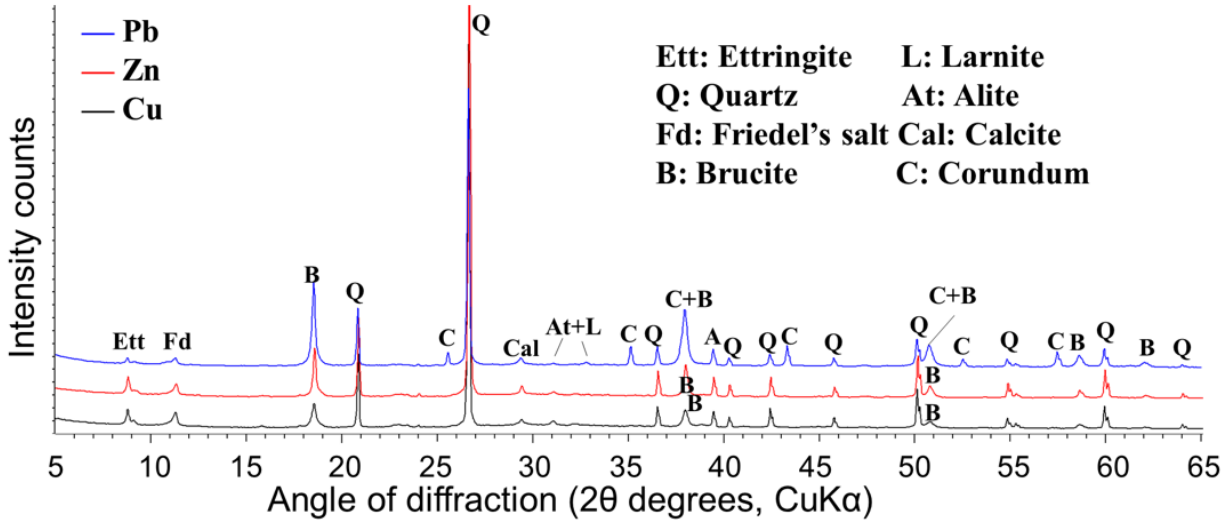

Figure 4.14 XRD patterns of samples collected from the surface of mortar specimens containing Cu, Zn and Pb in $MgCl_2$ solutions (Corundum was intentionally added in the sample containing Pb.).

4.4 Effect of the water/cement ratio and pH on the leaching of the HMs

The leaching ratio, which is defined as a ratio of the cumulative leachate quantity to the Cu, Zn, and Pb content in the specimen, is shown in Fig. 4.15, Fig. 4.16, and Fig. 4.17, respectively. The leaching ratio of the mortar specimens with a water/cement ratio of 0.40 is lower than for

those with a water/cement ratio of 0.55 in every case except for the case in which the mortar specimens containing Cu are immersed in $CaCl_2$ solutions. Considering that the total pore volume is larger in the mortar specimens with a water/cement ratio of 0.55 than in those with a water/cement ratio of 0.40 (see Fig. 4.12), it is thought that a larger total pore volume tends to result in a higher leaching ratio, other things being equal.

The values shown on top of the bars in Fig. 4.15, Fig. 4.16, and Fig. 4.17 are the pH values of the solutions on the 625th day in the tank leaching tests. As shown in these figures, a low leaching ratio for HMs, in other words, a high fixation capacity for HMs, is observable in the $MgCl_2$ solution. Zn and Pb are amphoteric in nature and their theoretical least solubility appears at pH values of around 9.2 and 9.8, respectively[163], a figure which is comparable to the alkalinity of the $MgCl_2$ solution, as opposed to the others which are more harshly caustic. Although Cu is not amphoteric, its solubility is also least at a pH value of around 9.4. The poor solubility of Cu under alkaline conditions therefore also leads to a lowest leaching ratio at a pH that is comparable to those for Zn and Pb.

Li et al.[31,52] have reported that the leaching of HMs in s/s materials can be considered as a pH-dependent and corresponding heavy metal hydroxide solubility-controlled process. Moreover, it has also been stated that the pH value of the system influences the leaching, fixation, and speciation of HMs in hardened cement[36,164,165]. Therefore, the relatively low leachate quantities of Zn, Cu, and Pb in the $MgCl_2$ solution may be related to the relatively low solubility of these HMs at pH values of around 8.8 (Cu, Zn) and 9.0 (Pb).

Although previous studies have demonstrated that concentrated $MgCl_2$-based deicers deteriorate concrete more severely than deicers based on $CaCl_2$ or NaCl[166,167], the results of this study showed that the risk of leaching of Cu, Zn and Pb caused by 10 mass% $MgCl_2$ solution was the lowest as compared to 10 mass% $CaCl_2$ solution, 10 mass% NaCl solution, and10 mass% KCl solution. Whatever the reason or reasons, including pH-dependent effects, this finding is empirically robust.

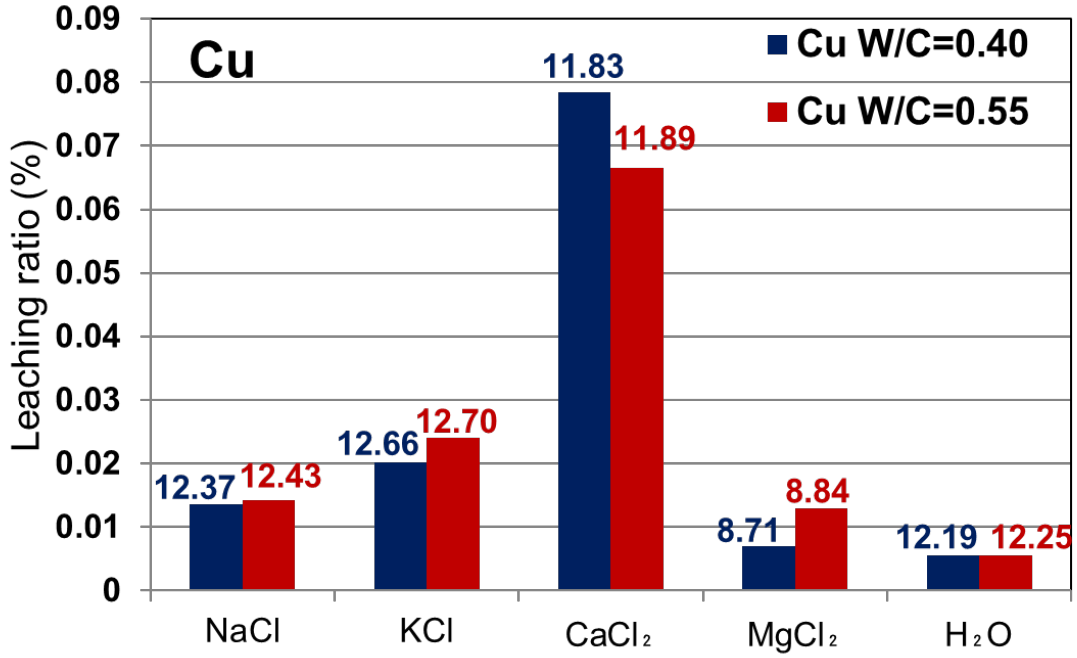

Figure 4.15 Leaching ratio of Cu for mortars immersed in each solution for 625 days (The value on the bar represents the pH value of the solution.).

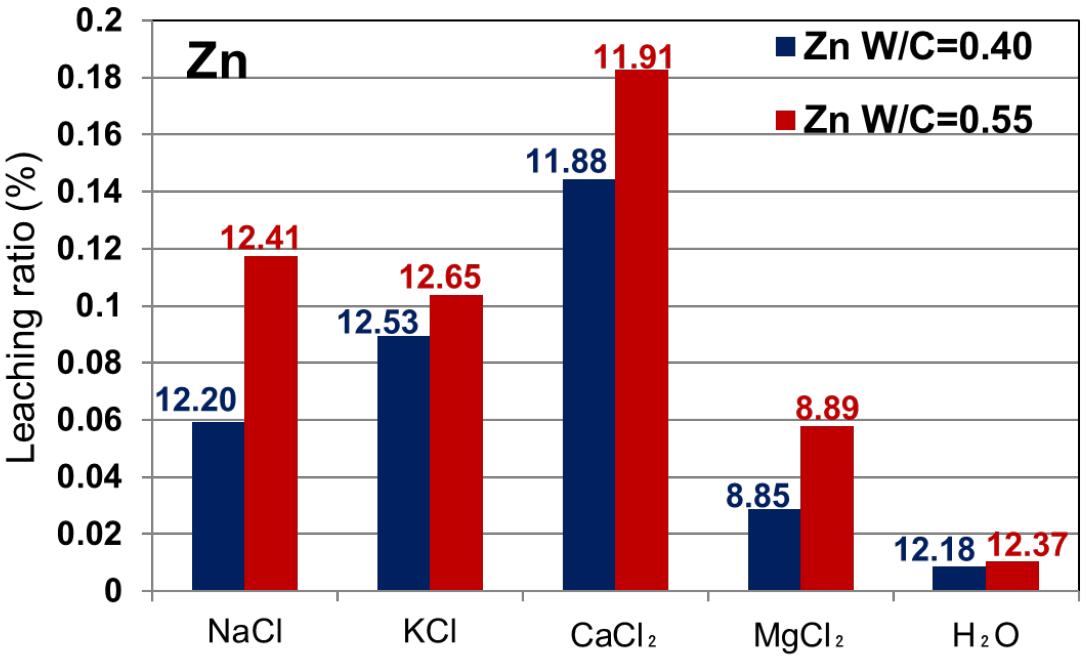

Figure 4.16 Leaching ratio of Zn for mortars immersed in each solution for 625 days (The value on the bar represents the pH value of the solution.).

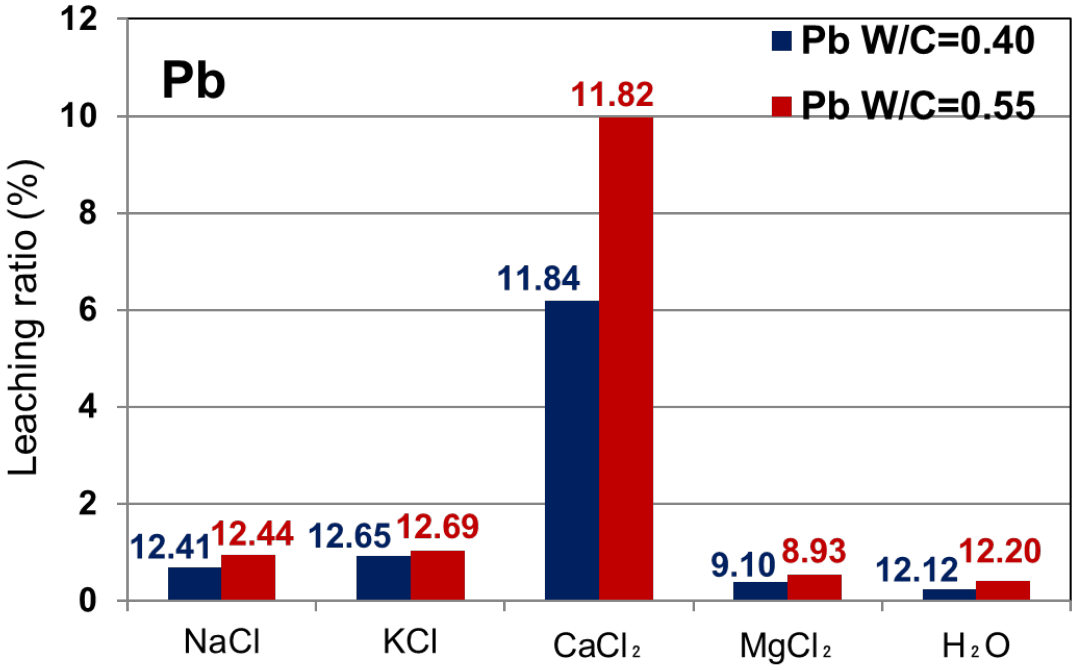

Figure 4.17 Leaching ratio of Pb for mortars immersed in each solution for 625 days (The value on the bar represents the pH value of the solution.).

4.5 Results of EPMA

For the elements of Ca and Si, each element's mass content was converted to the oxide content after the EPMA. The distribution of Pb, CaO, and Cl contents in mortar samples immersed in H_2O, KCl, and $CaCl_2$ solutions for 625 days was analyzed using surface analysis with EPMA scanning and is depicted in Figs. 4.18 to 4.20. Figs. 4.21 to 4.23 present the average content distribution curves for Pb, CaO, Pb/CaO, and Cl in these solutions. In all samples, a decrease in the content of CaO near the immersed surface is observed, suggesting that calcium leaching occurred.

Figs. 4.19(d), 4.20(d), and 4.23 illustrate that, near the immersed surface, the bound chloride content is notably higher in the presence of $CaCl_2$ as compared to KCl. However, in the case of KCl, a higher concentration of chloride is observed to penetrate deeper into the interior regions. Delagrave et al.[168–170] reported a strong effect of the associated cations on the chloride binding capacity in cement-based material, and the characteristics of the

associated cations may have a major impact on the likelihood of chloride ions entering the adsorption sites. $CaCl_2$ and $MgCl_2$ solutions showed a significant increase in Cl binding capacity compared to NaCl and KCl solutions. Cl supplied by NaCl and KCl is more diffusible than Cl supplied by $CaCl_2$[168,171,172]. In the case of KCl solutions, the weaker binding capacity of chloride ions relative to $CaCl_2$ may have resulted in higher internal penetration of chloride ions. This may explain the lower leaching of Pb in KCl solution compared with $CaCl_2$.

Figs. 4.21 and 4.22 show that after 625 days of immersion, the overall Pb and CaO levels in the test area, except near the immersed surface (0-1 mm area), are lower in the case of $CaCl_2$ than in the case of KCl and H_2O. Moreover, the ratio of Pb to CaO content was at the same level in all samples. The results suggest that the higher level of Pb leaching in the case of $CaCl_2$ is most likely due to calcium dissolution caused by $CaCl_2$.

(a) Pb

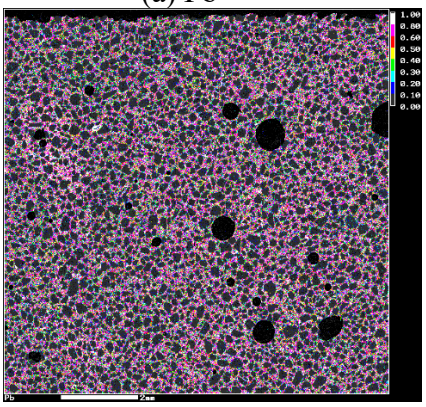

(b) CaO

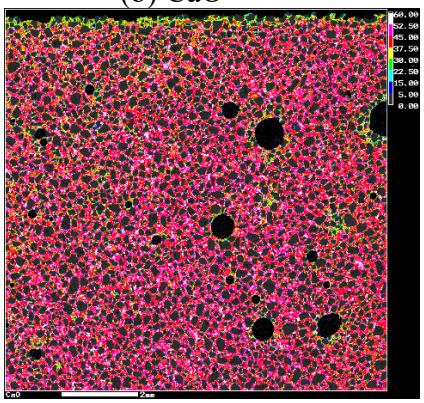

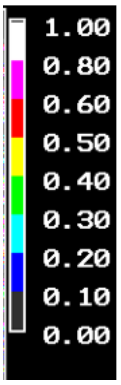

(c) SiO_2

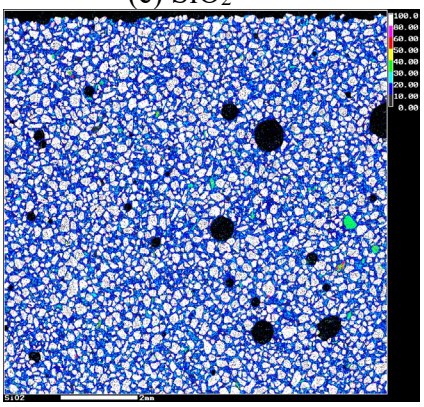

(The upper side of the image represents the immersion surface, and the color bar indicates mass%).

Figure 4.18 Distribution of Pb, CaO and SiO_2 content in mortar immersed in H_2O (For the elements of Ca and Si, each element's mass content was converted to the oxide content after the EPMA.).

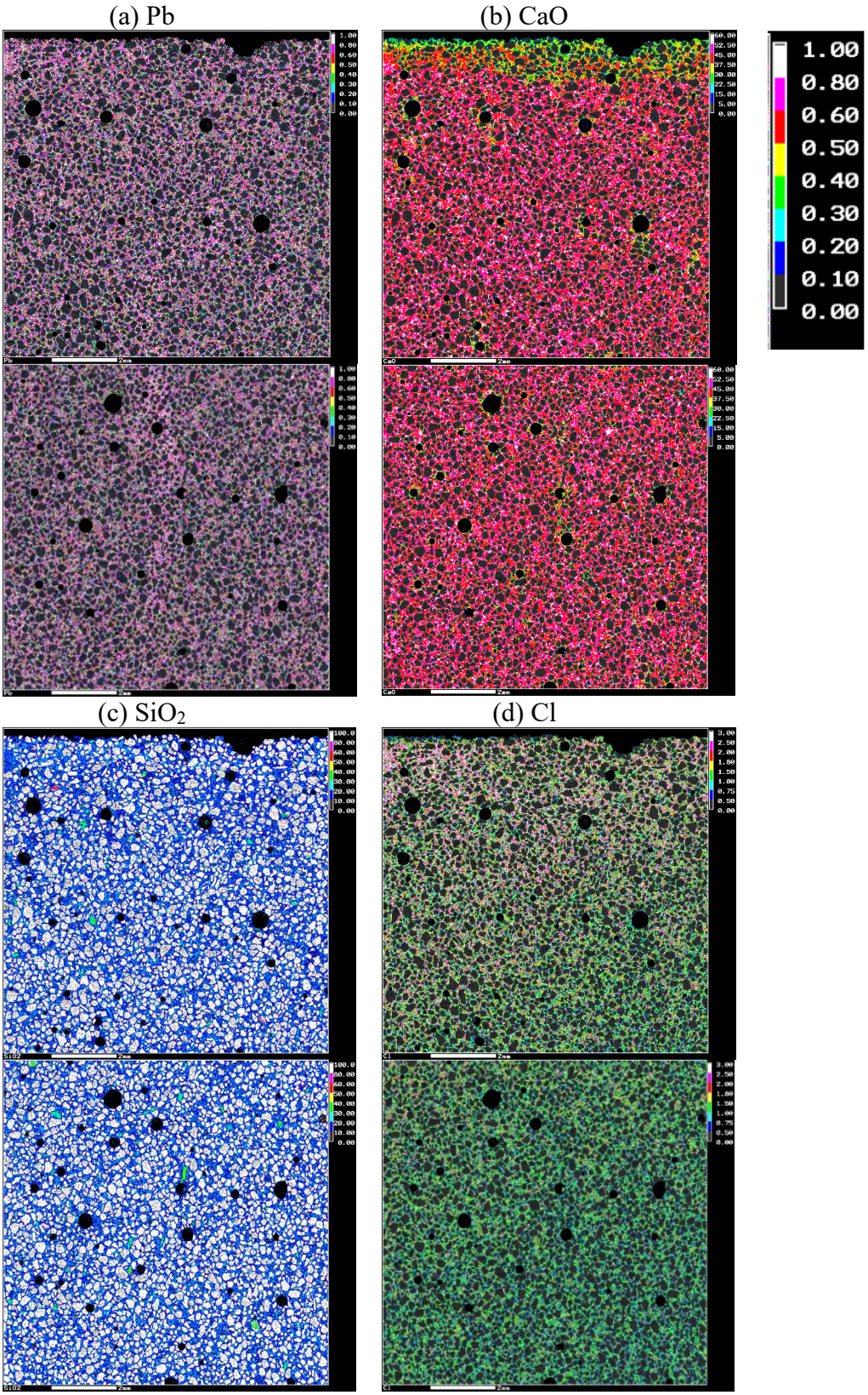

(The upper side of the image represents the immersion surface, and the color bar indicates mass%).

Figure 4.19 Distribution of Pb, CaO, SiO_2 and Cl content in mortar immersed in KCl (For the elements of Ca and Si, each element's mass content was converted to the oxide content after the EPMA.).

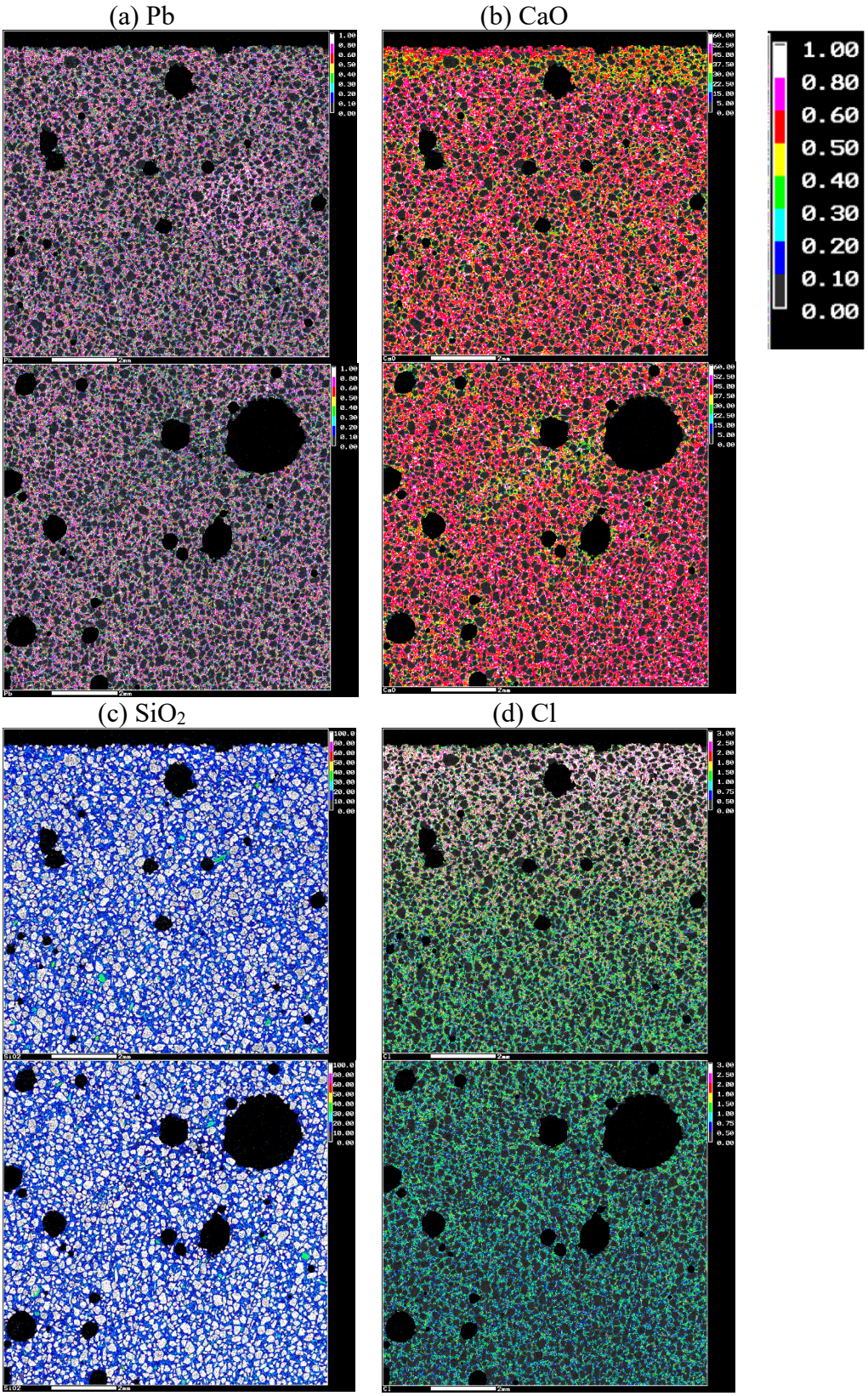

(The upper side of the image represents the immersion surface, and the color bar indicates mass%).

Figure 4.20 Distribution of Pb, CaO, SiO_2 and Cl content in mortar immersed in $CaCl_2$ (For the elements of Ca and Si, each element's mass content was converted to the oxide content after the EPMA.).

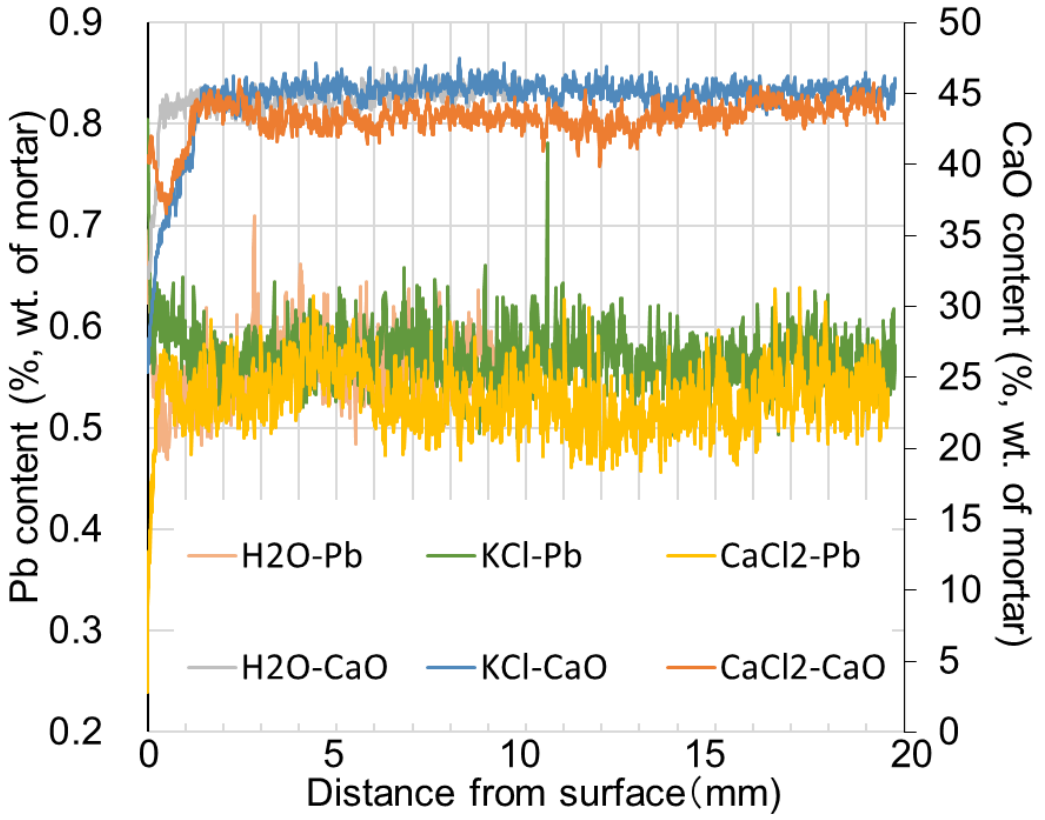

Figure 4.21 Average content distribution curves of Pb and CaO on mortar immersed in H_2O, KCl and $CaCl_2$ for 625 days.

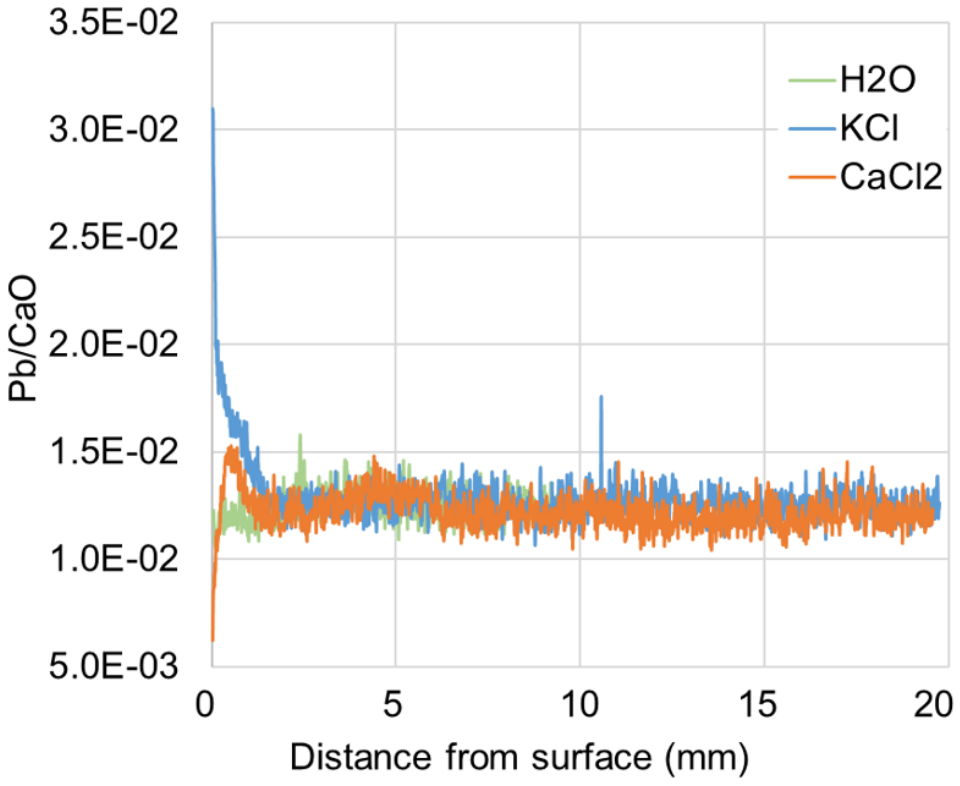

Figure 4.22 The ratio of Pb content to CaO content.

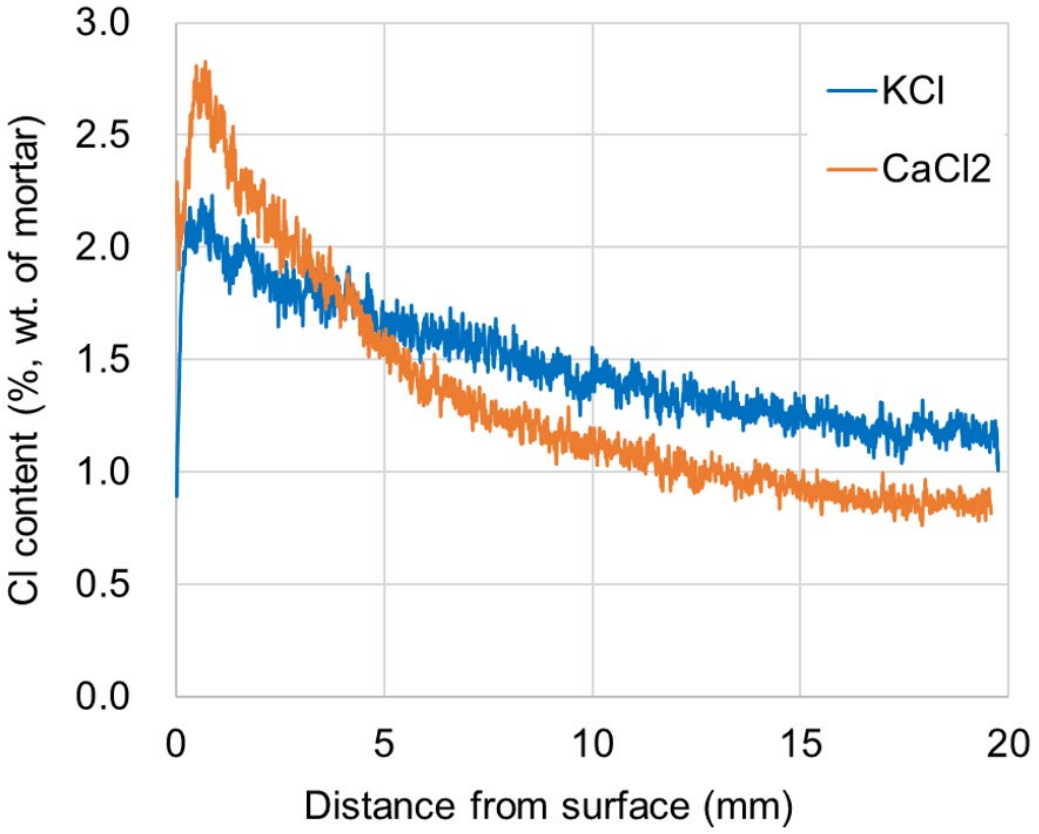

Figure 4.23 Average content distribution curves of Cl on mortar immersed in KCl and $CaCl_2$.

4.6 Summary

In this chapter, tank leaching tests in several chloride solutions were conducted to investigate the leaching characteristics of Cu, Zn, and Pb in mortars when the mortars were in contact with chloride solutions. The experimental results have yielded the following conclusions:

1. The leaching of Cu, Zn, and Pb is most significant with $CaCl_2$ solution.
2. In the case of the $MgCl_2$ solution, most portlandite in the specimens was decomposed to form brucite which reduced the pH value to around 9. This fact caused lower leachate quantities of Zn, Cu, and Pb.
3. The leachate quantity of Pb from the specimens immersed in the $CaCl_2$ solution is more than six times as large as that in the other solutions. The leachate quantity was the

smallest in the case of the deionized water.

4. Correlations between changes in pore volume and Pb leaching were not observed for the specimens immersed in each chloride solution for 64 days at the same water/cement ratio.

5. Compared with the specimens with a water/cement ratio of 0.55, the specimens with a water/cement ratio of 0.40 had a lower total pore volume, resulting in lower leachate quantities of HMs.

6. Based on the qualitative analysis results from XRD in this study, it was impossible to determine definitively the forms of Cu, Zn and Pb compounds that exist in the mortars.

7. According to the EPMA results in this study, in the case of KCl solutions, the weaker binding capacity of chloride ions relative to $CaCl_2$ may explain the lower leaching of Pb in KCl solution compared with $CaCl_2$.

CHAPTER 5. EFFECTS OF CHLORIDE SOLUTIONS ON THE ADSORPTION AND DESORPTION PROPERTIES OF LEAD IN HARDENED CEMENT AND CSH

This chapter focuses on adsorption in cement hydrates as one of the factors affecting heavy metal leaching. It investigates the Pb adsorption characteristics of hardened cement under various chloride environments and pH values through adsorption experiments. Additionally, the chapter examines the effect of different chlorides on the Ca/Si ratio of synthesized CSH.

5.1 Effect of chloride solutions on adsorption/desorption characteristics of Pb in cement paste

5.1.1 Results of adsorption test

In a previous study[173], when the contact solution was deionized water, the adsorption of Pb on cement paste could be regressed to a Freundlich-type adsorption isotherm. In general, the Freundlich type adsorption isotherm is expressed by the adsorption isotherm shown in Eq. (5.1)[174]. The range of values for n, spanning from 0 to 1, 1 to 2, and 2 to 10, corresponds to poor, moderate, and good adsorption capacities, respectively[175,176].

$$V = K_F P^{1/n} \quad (5.1)$$

Where,

V: adsorption capacity at equilibrium (mg per gram of adsorbent sample).

P: equilibrium concentration of Pb (ppm).

K_F, n: Freundlich adsorption constants.

"1/n" is the affinity between the adsorbent and the adsorbate, and "K_F" represents adsorption capacity in addition to affinity[177].

Figs. 5.1 and 5.2 show the adsorption isotherms for each chloride solution, as well as for deionized water. Considering the type of cations in chloride solutions, the adsorption capacity for Ca^{2+} ions is the highest, followed by K^+, Na^+, and Mg^{2+}. Integrating this observation with the results of the tank leaching test for Pb, it is discernible that a lower adsorption of Pb on cement paste correlates with a higher leaching amount obtained after contact with chloride solutions.

The adsorption isotherms for deionized water obtained in this study are in close agreement with those of previous studies[30,173]. In the cement paste, Pb adsorption was found to conform to a Freundlich-type adsorption isotherm, as represented by Eq. (5.1), for each contact solution tested. The parameters of the Freundlich adsorption isotherm for each solution case are shown in Table 5.1. This implies that Pb is likely adsorbed onto the surface of cement hydrates in a manner similar to that in deionized water, across all the solutions used in this experiment. Analysis of Table 5.1 reveals that the adsorption capacity of cement paste for Pb is influenced by its contact with various chloride salts. Specifically, after contact with NaCl and KCl, the cement paste exhibits an enhanced adsorption capacity for Pb compared to its pre-contact state, yet it still maintains moderate adsorption capacities. In contrast, contact with $MgCl_2$ results in good adsorption capacities. However, exposure to LiCl and $CaCl_2$ reduces the cement paste's Pb adsorption capacity. Notably, after contact with $CaCl_2$, the adsorption amount is significantly lower compared to other cases, and the adsorption capacity is categorized as poor, whereas the interaction with LiCl maintains the Pb adsorption capacity at moderate levels, consistent with its pre-contact state.

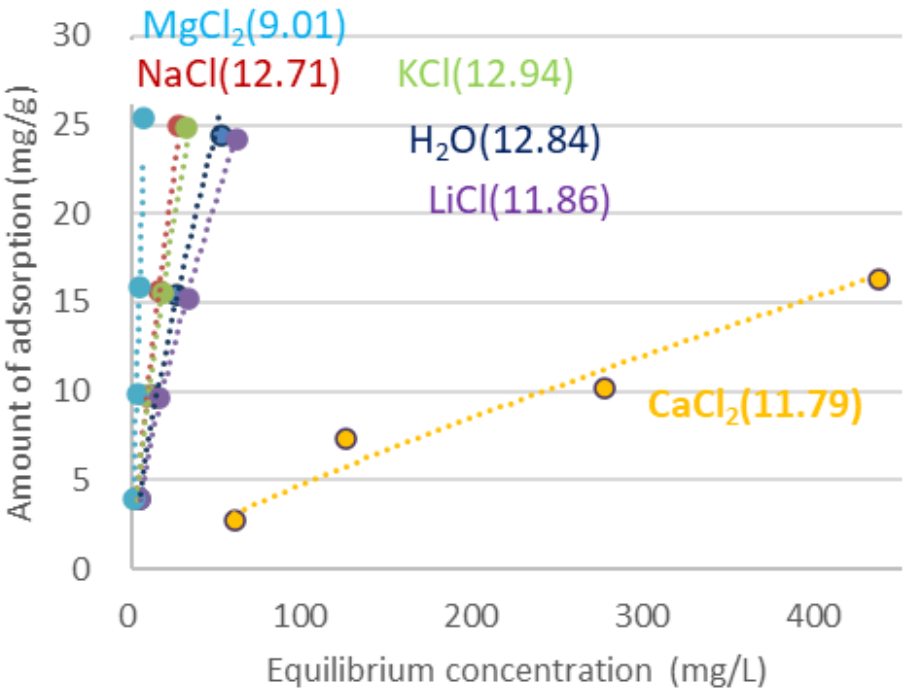

Figure 5.1 Effects of types of solutions on adsorption isothermal curves.

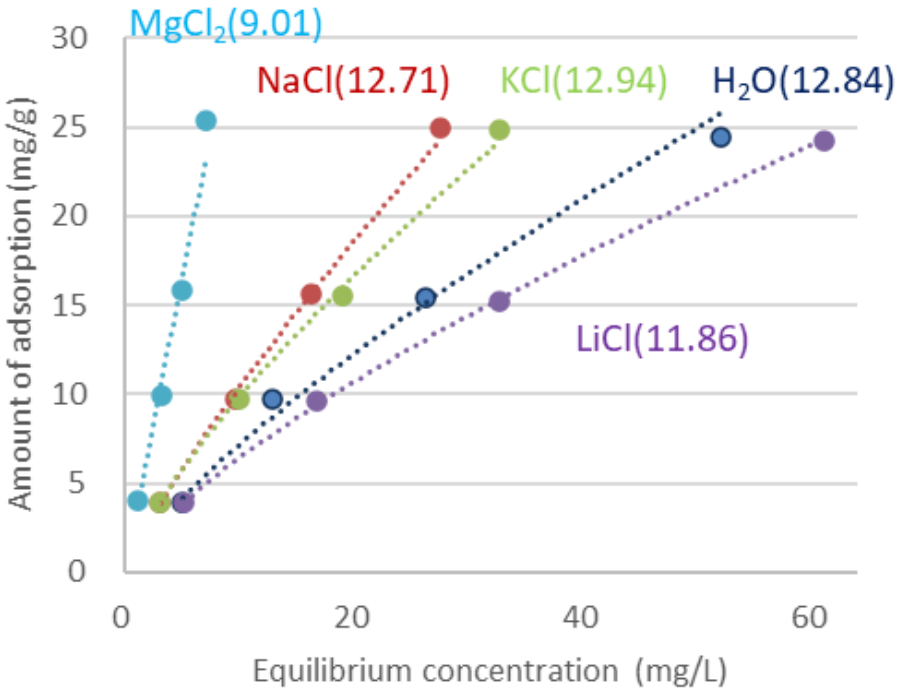

Figure 5.2 Effects of types of solutions on adsorption isothermal curves (except $CaCl_2$ solution).

Table 5.1 Freundlich adsorption isotherm parameters.

Parameter	Pore solution	NaCl	KCl	$CaCl_2$	LiCl	$MgCl_2$
K_F	1.20	1.72	1.52	0.74	1.18	3.51
n	1.29	1.27	1.20	1.02	1.36	1.03
R^2	0.99	1.00	1.00	0.96	1.00	0.99

The average pH values of the solutions shown in parentheses in Figs. 5.1 and 5.2 indicate that they approach the neutral side when in contact with $MgCl_2$ solution. The increased adsorption of Pb with the decrease in pH value is a behavior observed in alkaline environments, such as those found within cement matrices. It has been reported that under alkaline conditions, Pb forms insoluble compounds, such as hydroxides, which are then immobilized within the cement matrix[178,179]. The solubility of Pb hydroxides varies with pH; as the pH decreases from 13 to 10, the solubility of Pb hydroxides decreases (see Fig.2.4). This suggests that with the lowering of pH, Pb increasingly forms insoluble compounds, leading to stronger fixation within the cement matrix and an increase in adsorption amounts. and in the case of the $MgCl_2$ solution, the decrease in pH may be one of the main reasons for the increase in the amount of adsorption. Furthermore, it was noted that with $CaCl_2$, there was a significant reduction in pH to 11.79, compared to the pH values of 12.71 or higher in other contact solutions. This decrease closely resembles the effect observed with LiCl, which had a pH of 11.86. These findings suggest that the reduction in pH is not the main factor leading to the notably decreased adsorption capacity in the case of $CaCl_2$.

According to Miura et al.[157], in the case of $CaCl_2$ solution, the amount of chloride permeation into concrete is greater than that of other solvents, and the permeated chloride reacts with or dissolves hydrates. This suggests that one reason why $CaCl_2$ solution adsorbed less Pb than other chloride solutions (other than $MgCl_2$ solution) is that $CaCl_2$ solution promoted calcium dissolution from the cement paste, and the change in hydrates

due to $CaCl_2$ solution reduced the adsorption capacity.

5.1.2 Results of XRD analysis

The XRD analysis results of the residue with the highest adsorption are shown in Fig. 5.3. Friedel's salt diffraction peaks were observed in the sample in contact with chloride solution. This was consistent with many previous studies. It is hypothesized that a specific reaction takes place when cement paste, which has adsorbed Pb ions, interacts with a solution of either alkali metal chloride or calcium chloride, as shown in Eqs. (5.2) and (5.3). However, the XRD analysis conducted in the current investigation did not reveal the presence of any crystalline Pb-compounds.

$$\text{Pb-compounds} + 2\text{MCl} \rightarrow PbCl_2 + 2\text{M-compounds (M:}Na^+, K^+ \text{ or } Li^+) \quad (5.2)$$

$$\text{Pb-compounds} + CaCl_2 \rightarrow PbCl_2 + \text{Ca-compounds} \quad (5.3)$$

In the case of $MgCl_2$ solution, the brucite peak was detected, while the portlandite peak was much smaller than in the other solutions. Konno et al.[161] have reported that when cement paste is immersed in a $MgCl_2$ solution, the surface of the specimen becomes completely covered with a layer of $Mg(OH)_2$ crystals within just 3 hours. This suggests that in this study, portlandite was almost entirely decomposed into brucite. Mundell et al.[163] also reported that Pb is an amphoteric metal with its theoretical minimum solubility occurring at pH 8.5. They noted that the dissolution rate of Pb increases as the pH moves away from this value. Therefore, one reason for the increased adsorption of Pb in the $MgCl_2$ solution is that the pH is about 9 due to the consumption of $Ca(OH)_2$, which is in the region of the lowest pH for the leaching rate.

In the case of $CaCl_2$ solution, hydrates changes were mentioned in the previous

section as a factor in the decrease in adsorption capacity for Pb, but XRD analysis did not identify any significant differences from the other solutions.

In the case of NaCl, KCl, and LiCl solutions, the composition of the hydrates hardly changed, and therefore, the adsorption capacity of each solution for Pb did not seem to change much.

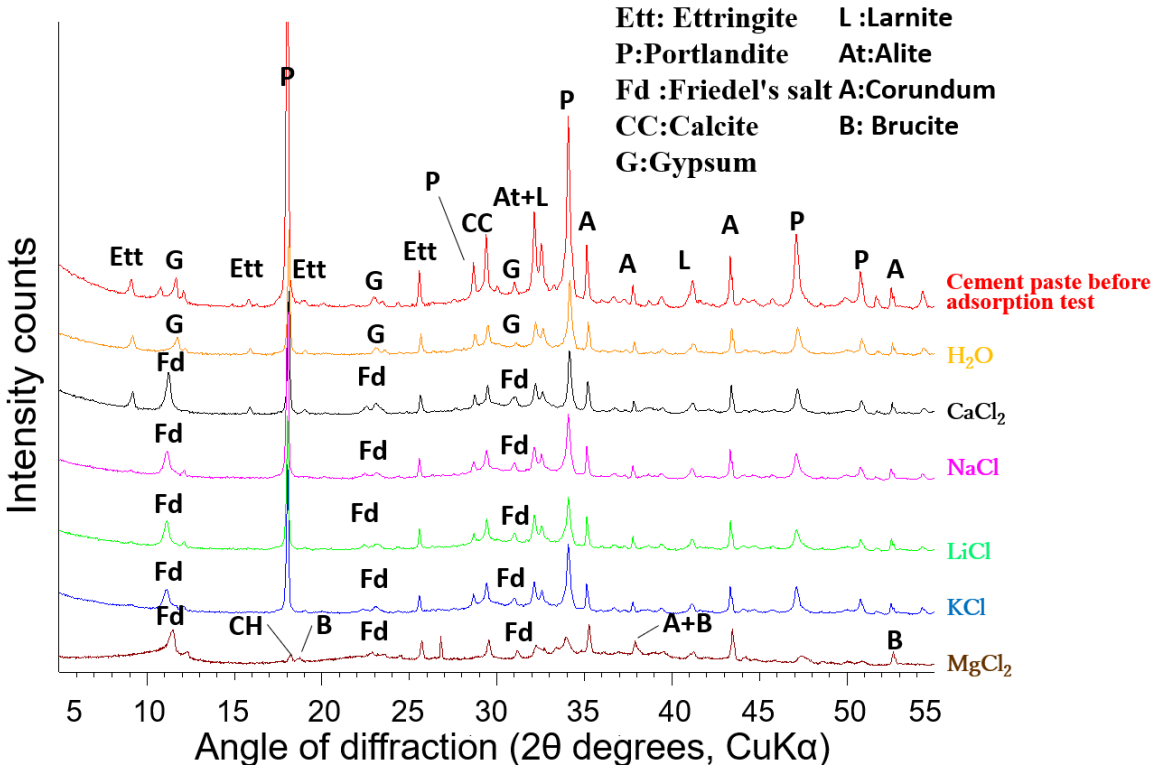

Figure 5.3 XRD pattern of samples before and after the adsorption tests (using 25000 mg/L of Pb nitrate solution).

5.1.3 Comparison of the effect of chloride solution on adsorption/desorption characteristics of Pb

In a previous study of our laboratory, Kawai et al.[30] conducted two main tests on cement paste. First, they carried out Pb adsorption tests using deionized water, to see how well the cement paste could adsorb Pb. Then, they performed Pb desorption tests on the cement paste that had adsorbed Pb, using various chloride solutions. After the desorption tests, the quantity of Pb remaining adsorbed on the cement paste was determined by subtracting the

amount desorbed from the initial adsorption quantity. This calculation allowed the researchers to establish the relationship between the remaining adsorbed Pb and the equilibrium concentration during the desorption tests. Figures 5.4 and 5.5 show the relationships between the equilibrium concentration of Pb ions and the amount of Pb adsorbed in various contact solutions. They include data on the remaining adsorbed Pb after desorption tests (Kawai's results[30]) and the adsorption isotherms of Pb (the equilibrium concentration of Pb ions and the amount of Pb adsorbed following the adsorption tests, as reported in section 5.1.1 of this study). The experiments utilized NaCl, KCl, LiCl, and $CaCl_2$ as contact solutions. Taking the logarithm of both sides of Eq. (5.1) results in a linear equation as represented by Eq. (5.4). The slope of this linear equation corresponds to 1/n, where n is the adsorption constant. The shape of the adsorption isotherm depends on n.

$$\log V = \log K_F + 1/n \log C \tag{5.4}$$

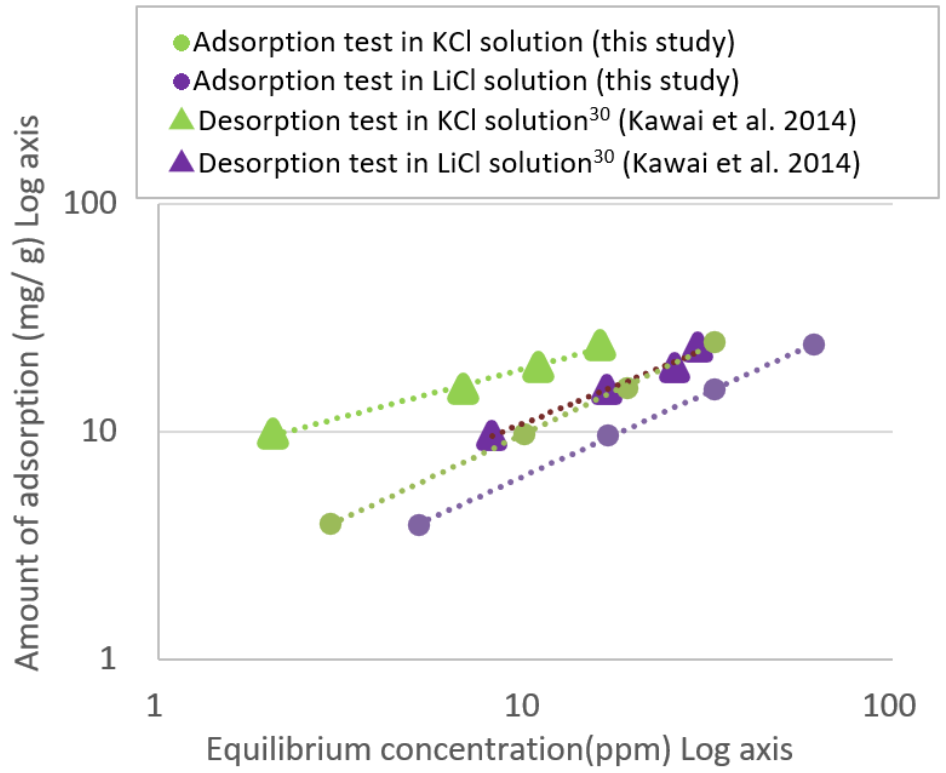

Figure 5.4 Relationship between equilibrium concentration and adsorption amount of Pb for adsorption and for desorption test in KCl and LiCl solutions.

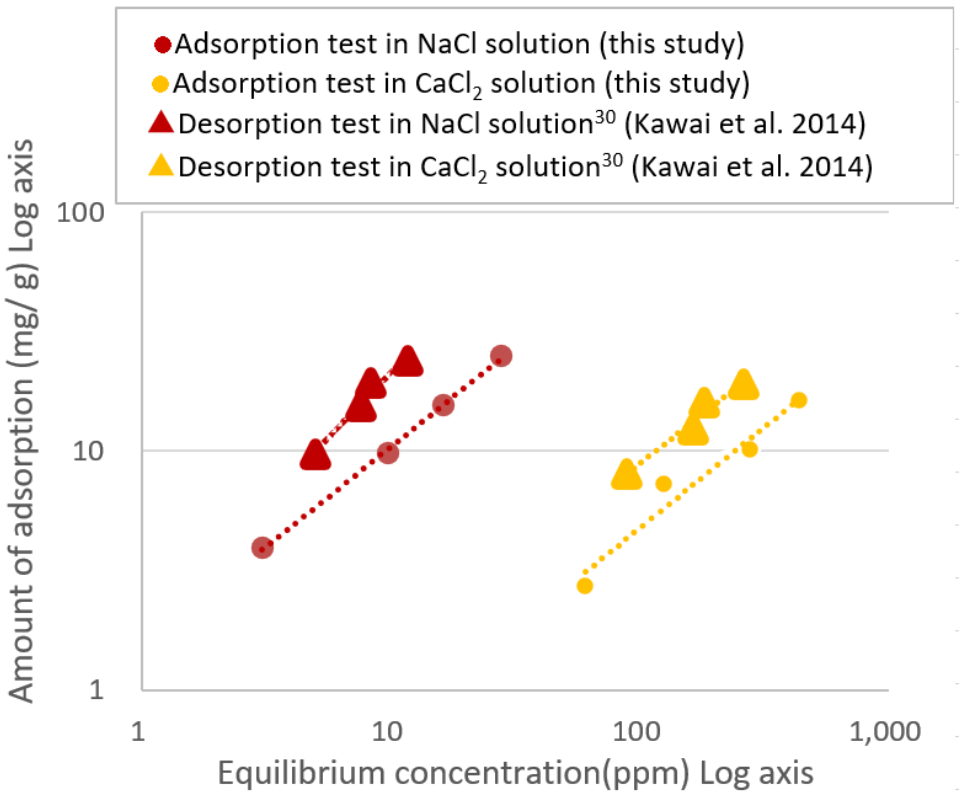

Figure 5.5 Relationship between equilibrium concentration and adsorption amount of Pb for adsorption and for desorption test in NaCl and $CaCl_2$ solutions.

Since the slopes of the approximate lines are almost equal between the results of this study and those of the previous studies, it can be assumed that there is no difference in the affinity of Pb adsorption sites between the two studies. However, regardless of the type of solution, the results obtained from the previous study tended to show higher adsorption capacity than those obtained from the present study. This implies that when cement paste is exposed to chloride solutions such as NaCl or $CaCl_2$ before the adsorption of Pb (during the adsorption test), the number of adsorption sites decreases. However, it is believed that these sites remain available for adsorption even when the cement paste is exposed to chloride solutions like NaCl or $CaCl_2$ after the adsorption of Pb (during the desorption test). The adsorption sites here are assumed to be cement hydrates, but since compounds related to Pb could not be identified by XRD, the adsorption properties of individual hydrates could not be considered. In the case of desorption tests, the cement is stirred for a longer period of time than in adsorption tests, and it is possible that differences in the progress of hydration reactions, such as hydration of unhydrated cement, may be related to differences in the amount of adsorption, but this is not clear at present and should be investigated in the future.

5.2 Effect of pH of contact solution on adsorption properties

To further elucidate the impact of pH changes caused by chlorides on the adsorption of Pb, we conducted adsorption tests of Pb in environments with varying pH values. This approach is intended to provide a deeper understanding of how pH fluctuations influence Pb's adsorption behavior.

5.2.1 Results of adsorption test

The results of adsorption tests conducted using two different pH adjustment methods are

presented in Figs. 5.6 and 5.7. The results at pH 12.64 were referenced from prior study[180] conducted by our research lab. The pH values shown in the figure were measured just before the addition of the heavy metal solution. The adsorption of Pb at all tested pH levels can be categorized under the Freundlich adsorption isotherm model, as represented by Eq. (5.1).

Furthermore, we conducted a comparative analysis between the results of pH value changes on Pb adsorption and the effects of various chloride salts on Pb adsorption. We discovered that although a pH range from 12 to neutral typically promotes high adsorption levels of Pb, the introduction of chlorides such as NaCl, KCl, $CaCl_2$, and LiCl led to a decrease in Pb adsorption, presenting considerable variability, even though $CaCl_2$、LiCl、$MgCl_2$ reduced the pH to the optimal range for Pb adsorption. This outcome indicates that factors beyond the pH value, such as the specific nature and concentration of coexisting ions, are critical in regulating Pb adsorption in cement-based materials. The unique characteristics of chloride ions might affect the surface properties of the cement matrix, thereby altering adsorption kinetics. This also raises the question of potential competition for adsorption sites by these coexisting ions or the formation of less adsorbable Pb compounds.

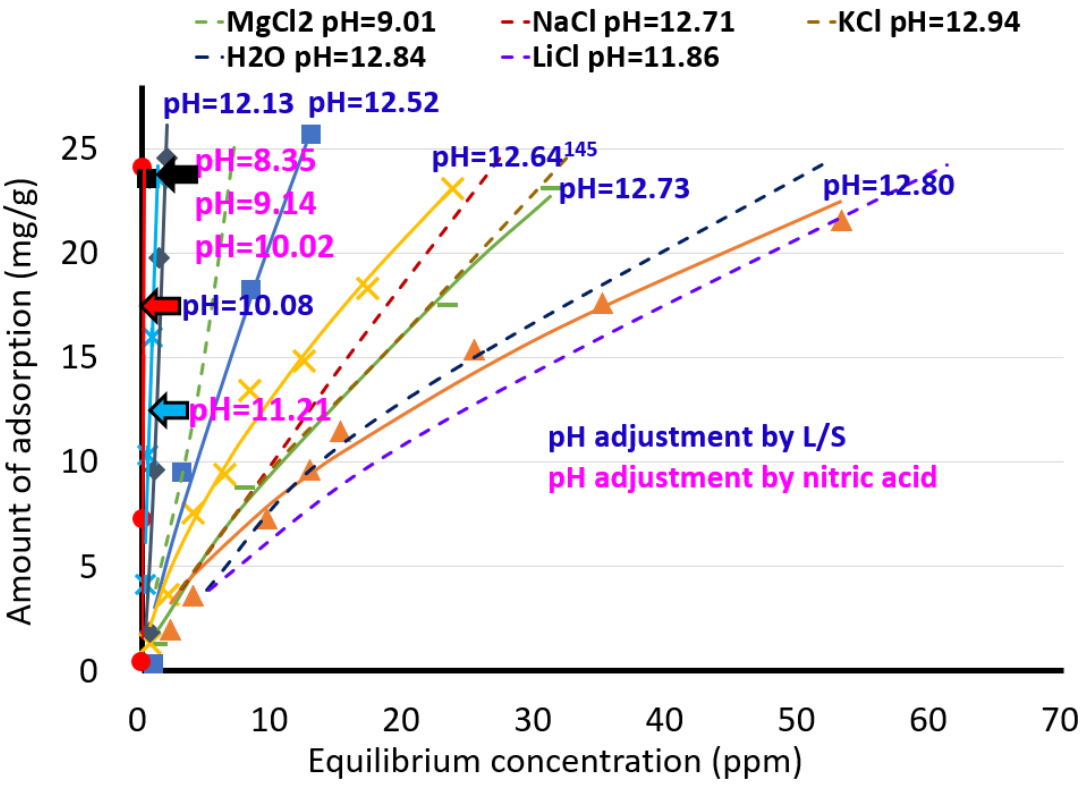

Figure 5.6 Effects of pH of contact solutions on adsorption isothermal curves (solid line indicates pH adjustment results).

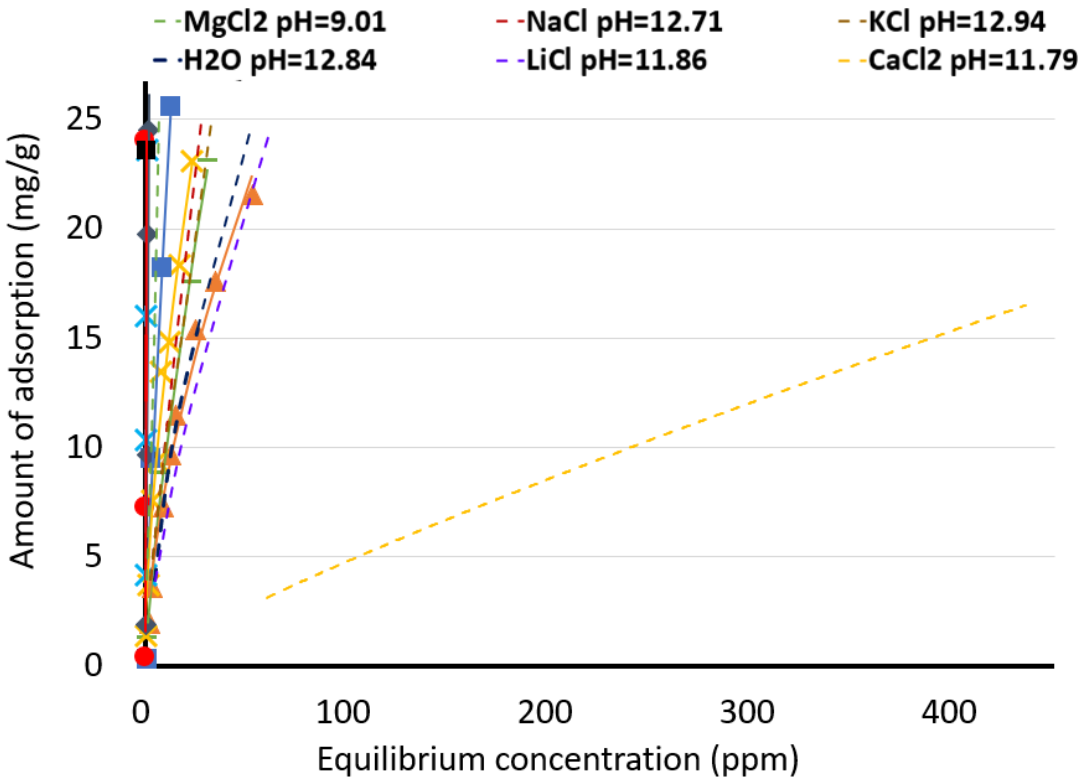

Figure 5.7 Effects of pH of contact solutions on adsorption isothermal curves with increased $CaCl_2$ concentration (solid line indicates pH adjustment results).

5.2.2 Results of XRD analysis

Fig. 5.8 presents the analysis results of the residue adjusted using a nitric acid solution for pH. Compared to the pre-adsorption cement paste, a reduction in portlandite, ettringite, alite, and larnite was confirmed. XRD analysis was conducted on residues with the highest adsorption amounts, which were adjusted in pH according to L/S ratios, specifically at 50 mL/g and 20 mL/g. However, the average pH values for each were 12.73 and 12.80, respectively, with a minimal pH variation of 0.07, resulting in similar peaks and indicating no significant compound differences due to pH change. Regarding the Pb compounds presumed to be present in the post-adsorption test residues, although some similar peaks were present across all analyses, they were mostly partial matches and did not suffice for identification.

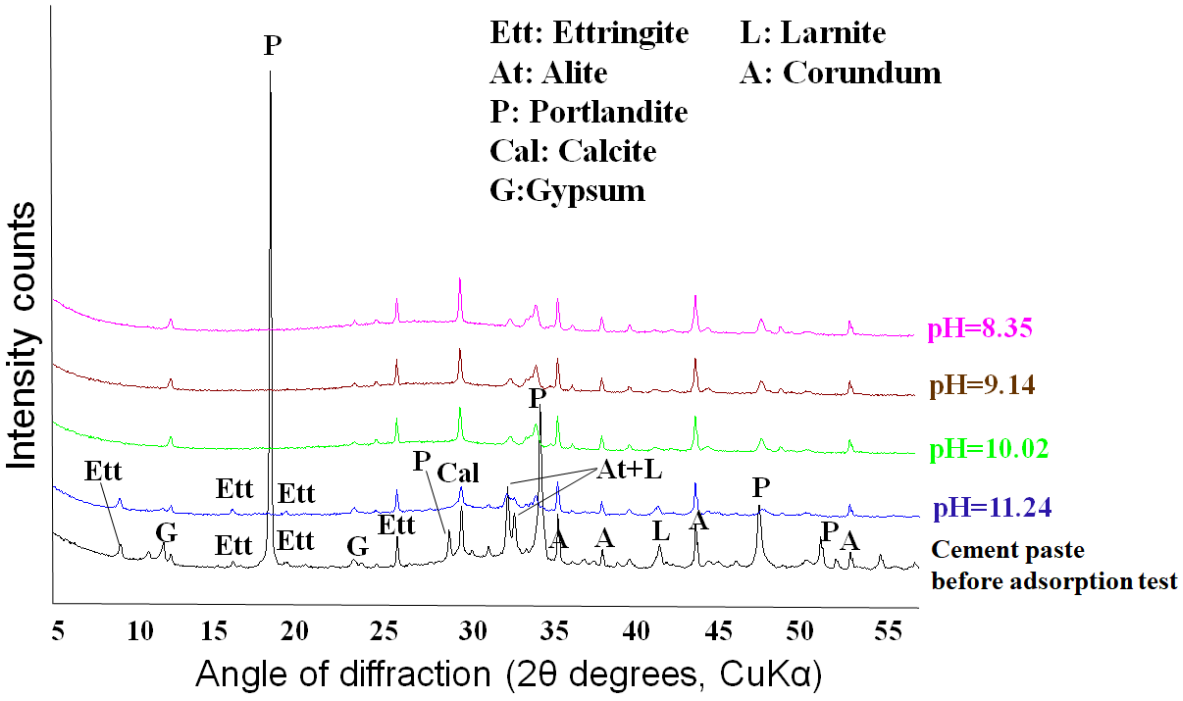

Figure 5.8 XRD pattern of samples before and after the adsorption tests (pH adjustment by nitric acid solution).

5.3 Effect of the contact solutions on the adsorption characteristics of Pb in CSH

5.3.1 Adsorption test results

Adsorption isotherms allow the analysis of a material's adsorption capacity. This study employs two common models, Freundlich and Langmuir, shown in Eqs. (5.1) and Eq. (5.5)[181], respectively.

$$V = K_L Q_{max} P/(1 + K_L P) \quad (5.5)$$

Where,

K_L:Langmuir adsorption coefficient (L/mg).

Q_{max}: the maximum adsorption capacity of adsorbent sample (mg/g).

Table 5.2 summarizes the simulated parameters for these models. The R^2 value of the Freundlich model was higher than that of the Langmuir model (except for the result of CSH1.40 after contact with NaCl solution.), as observed. Moreover, the results of CSH0.83 exposed to $CaCl_2$ solution could not be simulated by the Langmuir model. It appeared that the Freundlich model fits the experimental data better. Throughout the adsorption process, research revealed that multilayer surface adsorption occurred at heterogeneous surfaces. Guo et al.[182] have also reported Freundlich adsorption isotherms in adsorption experiments with CSH.

Table 5.2 Langmuir and Freundlich adsorption isotherm parameters.

Parameter			Pore solution	NaCl	KCl	$CaCl_2$	$Ca(NO_3)_2$
Langmuir	CSH0.83	K_L (L/mg)	0.088	0.044	0.036	-	0.014
		Q_{max} (mg/g)	48.08	41.15	55.87	-	153.85
		R^2	0.78	0.52	0.86	-	0.21
	CSH1.40	K_L (L/mg)	0.034	0.026	0.011	0.0054	0.031
		Q_{max} (mg/g)	32.36	34.13	57.14	13.44	19.53
		R^2	0.98	0.99	0.80	0.95	0.75
Freundlich	CSH0.83	K_F	4.19	2.56	1.79	0.74	2.08
		n	0.96	1.06	1.12	1.02	1.04
		R^2	0.98	0.98	1.00	0.99	1.00
	CSH1.40	K_F	0.64	0.82	0.57	0.13	0.15
		n	1.092	1.211	1.062	1.419	1.330
		R^2	0.96	0.98	0.98	0.98	1.00

-: Cannot be simulated with Langmuir

The adsorption isothermal curves of Pb ions for CSH in contact with different solutions are shown in Figs. 5.9 to 5.12. For $MgCl_2$PM the Pb concentration was found to be undetectable at the 10^{-2} ppm level. As shown in Figs. 5.9 to 5.12, the results for NaClPM, KClPM, and pore solution displayed very similar adsorption quantities for Pb. In addition, regardless of the Ca/Si ratio of the CSH, the equilibrium concentration of Pb in the mixed solution of $CaCl_2$PM was the highest. In other words, the CSH exposed to $CaCl_2$PM had the lowest adsorption capacity for Pb. Evidently, the adsorption properties of Pb in CSH for the $CaCl_2$ solution were different from those for other contact solutions. This accords with the behavior of cement pastes exposed to a similar range of solutions in this study (see Figs. 5.1 and 5.2). When this result was combined with the results of the tank leaching tests, it was found that the lower the adsorbability of Pb on CSH, the greater the leachate quantities obtained by contact with the chloride solutions.

Comparing the results for the CSH0.83 with the results for the cement paste (W/C=0.40) as shown in Figs. 5.9 and 5.10, it is evident that the adsorption capacity of CSH0.83 is larger than that of the cement paste and that CSH0.83 has a stronger affinity for Pb than cement paste (W/C=0.40). Comparing the results for CSH1.40 and CSH0.83,

CSH0.83 adsorbs more Pb than CSH1.40 for either contact solution. This is because the lower the calcium-silica ratio, the greater the specific surface area.

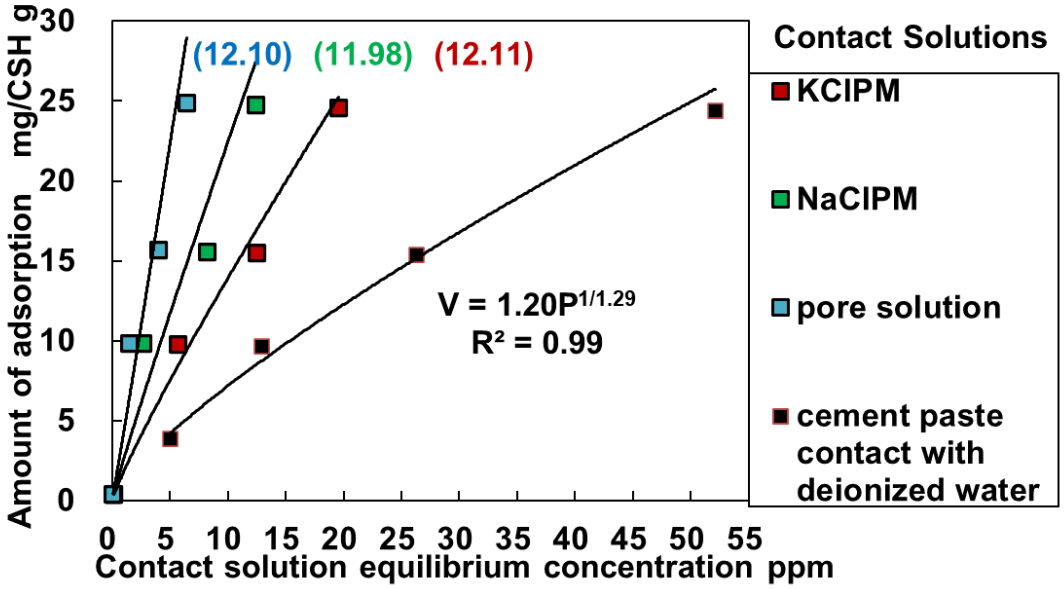

Figure 5.9 Adsorption isothermal curves of Pb on CSH0.83 in pore solution, NaCl, KCl solutions, and on cement paste in deionized water (average pH value in parentheses).

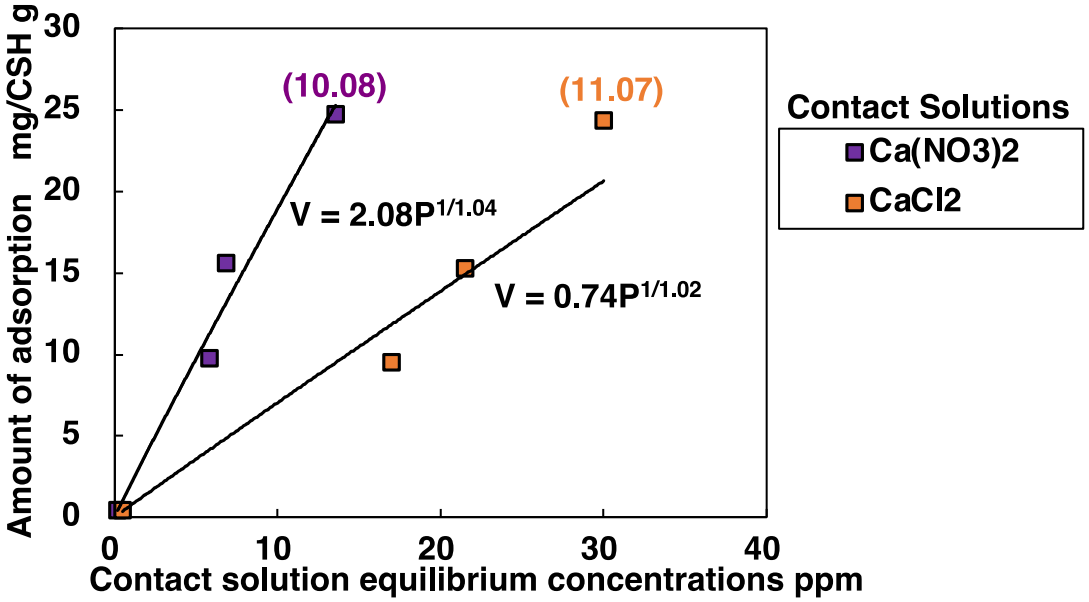

Figure 5.10 Adsorption isothermal curves of Pb on CSH0.83 in $CaCl_2$ and $Ca(NO_3)_2$ solutions (average pH value in parentheses).

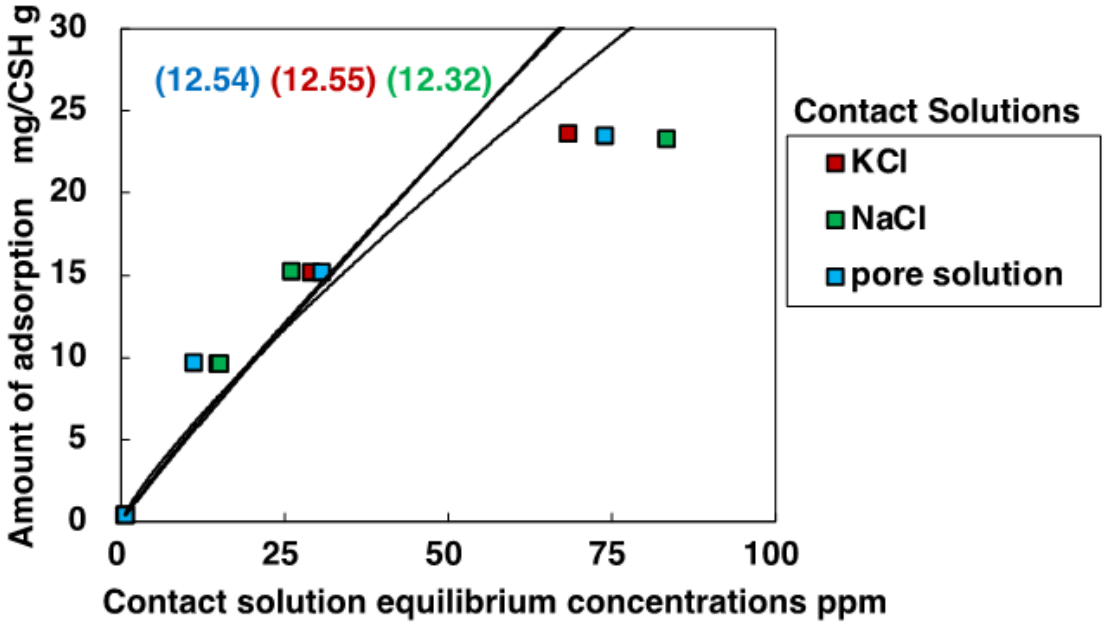

Figure 5.11 Adsorption isothermal curves of Pb on CSH1.40 in pore solution, NaCl and KCl solutions (average pH value in parentheses).

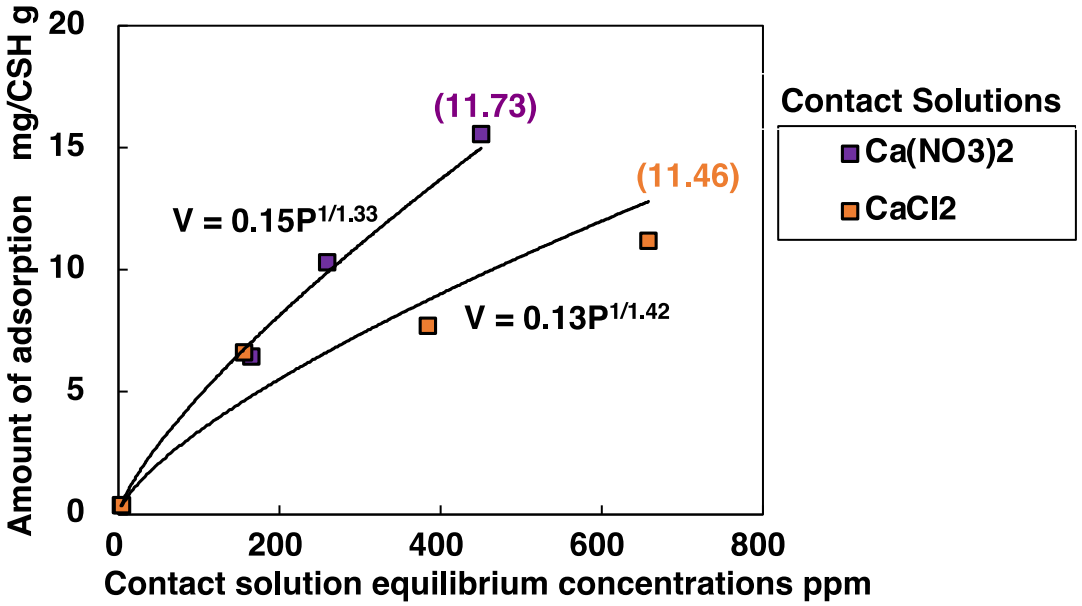

Figure 5.12 Adsorption isothermal curves of Pb on CSH1.40 in $CaCl_2$ and $Ca(NO_3)_2$ solutions (average pH value in parentheses).

According to previous studies[183,184], as shown in Eq. (5.6), dissociation of silanol sites (SiOH) due to high solution pH yields a negatively charged surface. Ions in the pore solution are prone to interact strongly with silanol sites in ways that lead to adsorption. Therefore, alkaline cations may be able to bind onto the CSH surface as shown in Eq. (5.7).

Several studies indicate that the Ca^{2+} cations are potential-determining ions for the CSH surface, with the ability to reverse CSH surface charge[183,185]. It is also reported that the zeta potential of CSH with the addition of NaCl was similar to that of CSH without the addition of NaCl (pure CSH), and no changes due to adsorbed ions were observed[183]. Meanwhile, Plusquellec et al.[186,187] reported that the change in zeta potential was much lower for KCl additions even at concentrations many times higher than the $CaCl_2$ concentration compared to higher $CaCl_2$ additions leading to higher zeta potential. This change is not sufficient to cause a charge reversal.

$$\equiv SiOH + OH^- \Leftrightarrow \equiv SiO^- + H_2O \quad (5.6)$$

$$\equiv SiOH + Ca^{2+} \Leftrightarrow \equiv SiOCa^+ + H^+ \quad (5.7)$$

Moreover, in the case of Ca^{2+}, as shown in Figs. 5.10 and 5.12, due to the reaction shown in Eq. (5.7), the pH value is lower than that in other cases. The reaction produces H^+ which dissolves the hydroxide precipitates of HMs. This also leads to a rise in the equilibrium concentration of Pb in the $CaCl_2$PM solution.

5.3.2 XRD analysis Results

The results of the XRD analyses for the residues obtained from the samples showing the highest Pb adsorption quantities are shown in Fig. 5.13. Save for $MgCl_2$PM, the samples in contact with the chloride solutions showed little chemical alteration of the hydrate. The (002) reflection of the CSH occurring at $2\theta(CuK\alpha)=7.0°\sim 9.0°$ enables the basal spacing between silicate layers in the CSH structure to be determined[188]. In the case of the $MgCl_2$PM, this peak becomes indistinct, indicating that the CSH becomes lower crystallinity. This is in agreement with the conclusion by Tang et al.[154] that even

minor initial Mg^{2+} input decreases the crystallinity of CSH. Additionally, brucite peaks were detected after contact with $MgCl_2$PM. This finding is consistent with the lower crystallinity of CSH and confirms the conclusion by Tang et al.[189]. Shao et al.[190] have already reported that brucite can thus be used as a promising mineral for HMs immobilization. Therefore, the increase in the Pb adsorption can also be attributed to the formation of brucite which reduced the pH value to around 8.66. Although Zhao et al.[191] confirmed the identity of the adsorbed heavy metal phases (e.g., $Ni_3Si_2O_5(OH)_4$ and Ni_2SiO_4 of the Ni-CSH group, etc.) from the XRD patterns of CSH, confirming the identity of heavy metal phases from XRD patterns can be challenging due to the similarity in diffraction peaks among many phase compositions[192]. Here, we were not able to confirm the crystalline phase of the Pb compounds in any samples.

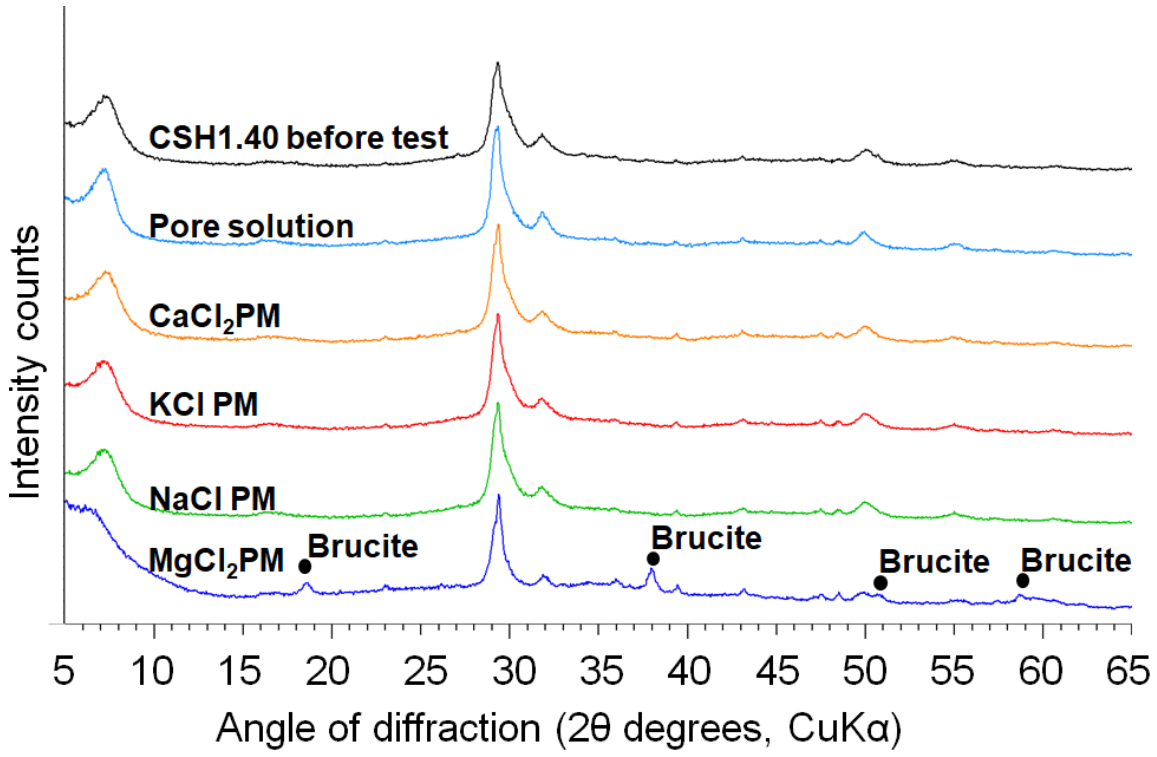

Figure 5.13 XRD pattern of CSH1.40 before and after the adsorption tests (25 g/L of Pb nitrate solution).

5.3.3 EDX analysis-CSH0.83 results

As shown in Fig. 5.14, individual point spectra were selected from several neighboring points within a local area of the order of 200×200 μm. A total of five individual spot spectra grouped into two such areas were recorded. The Ca/Si atomic ratios calculated from the spectra of each of these spots are shown in Fig. 5.15. The bars on the histogram in Fig. 5.15 represent the Ca/Si results for the five individual point spectra of each sample, tested five times to exclude the effect of errors. As shown in Fig. 5.15, in all cases other than $MgCl_2$PM, it was confirmed that the Ca/Si ratio increased.

When CSH was in contact with NaClPM and KClPM, only very low levels of sodium and potassium were detected on the CSH residues by EDX, although the concentrations of both sodium and potassium in the chloride contact solutions were more than twice the concentrations of calcium in the case of the $CaCl_2$PM. In addition, NaClPM, KClPM, and pore solution showed a very close Ca/Si ratio but in the case of $MgCl_2$PM the Ca/Si ratio was the smallest. This corresponded well with the result of Pb adsorption. Therefore, compared with the pore solution, in the case of NaClPM and KClPM, it seems that the adsorption capacity of Pb on cement pastes in each contact solution does not change markedly.

In the cases of $CaCl_2$PM and $Ca(NO_3)_2$PM, the increase in the Ca/Si mole ratio is slightly larger than that in the cases of NaClPM and KClPM. The higher Ca/Si mole ratio and calcium contents indicate that $CaCl_2$ plays a beneficial role in retaining Ca^{2+} in CSH. The increase in the Ca/Si ratio also caused a decrease in the adsorption sites for Pb, which was probably due to Ca occupying the adsorption sites[193]. This may lead to a reduction in the adsorbability of Pb in the cases of $CaCl_2$PM and $Ca(NO_3)_2$PM. Additionally, in the case of $MgCl_2$PM, the Ca/Si mole ratio showed an evident decrease. This can be explained by the fact that in the process of CSH decalcification as shown in Eq. (5.8), $MgCl_2$ can react with the cementitious CSH and convert it to non-cementitious magnesium silicate

hydrate (MSH)[162,194]. This may in turn lead to an increase in the adsorbability of Pb.

$$CSH + MgCl_2 \rightarrow MSH + CaCl_2 \quad (5.8)$$

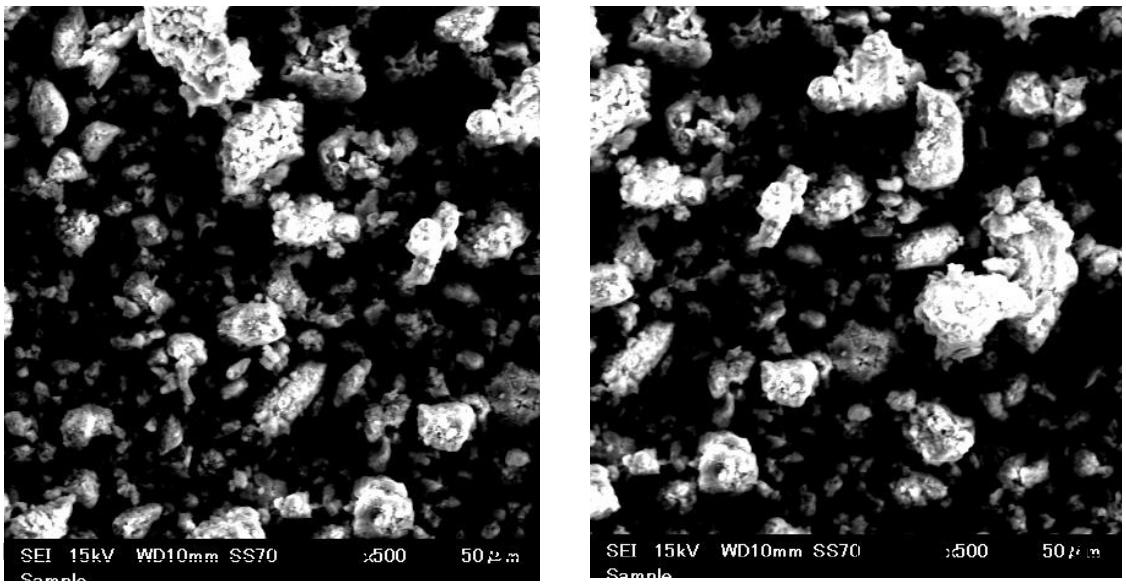

Figure 5.14 SEM micrograph of two sites from which EDX analyses were taken on CSH0.83.

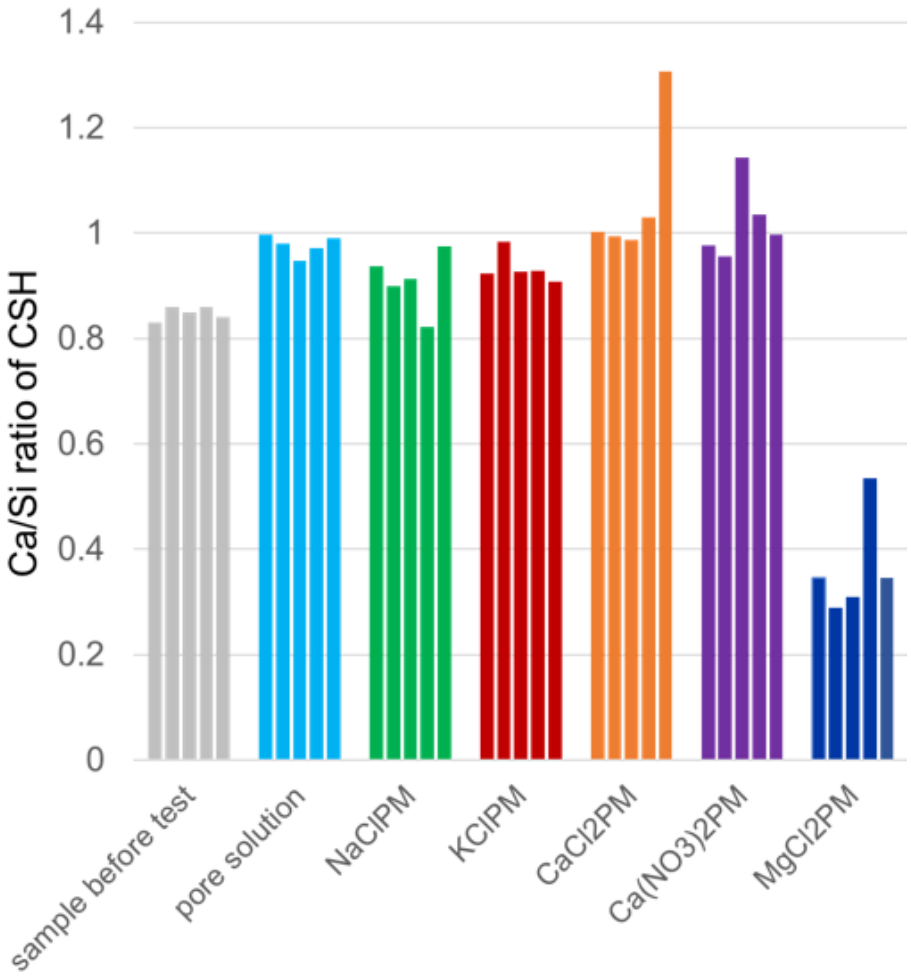

Figure 5.15 Ca/Si mole ratios of CSH0.83 before and after the adsorption tests (The bars represent the Ca/Si results for the five individual point spectra.).

5.4 Summary

In this study, adsorption tests in several chloride solutions and in $Ca(NO_3)_2$ solution were conducted to investigate the adsorption characteristics of Pb in CSH when in contact with chloride solutions and $Ca(NO_3)_2$ solution. In addition, Pb adsorption tests were conducted in several chloride solutions and different pH environments to analyze the effects of NaCl, KCl, $MgCl_2$ and $CaCl_2$ on the adsorption characteristics of Pb in cement paste. From the above-mentioned experimental results, the following conclusion can be drawn:

1. When chloride solutions were used as the contact solution for Pb adsorption tests

on cement pastes, the highest adsorption was observed with $MgCl_2$ solution, followed by NaCl, KCl, deionized water, and LiCl solutions. Notably, the adsorption was significantly lower with $CaCl_2$ solution.

2. When cement paste is exposed to chloride solutions such as NaCl or $CaCl_2$ before the adsorption of Pb, the number of adsorption sites decreases. However, it is believed that these sites remain available for adsorption even when the cement paste is exposed to chloride solutions like NaCl or $CaCl_2$ after the adsorption of Pb.

3. In Pb adsorption tests conducted by varying the pH of the solution in contact with cement paste, it was observed that regardless of the pH adjustment method, the amount of adsorption tended to increase as the pH of the solution decreased from around 13 to 10. However, this trend was not observed in the presence of chlorides.

4. For varying the pH of the solution in contact with the cement paste, including the use of chloride solutions, Pb adsorption in the range of this study approximates the Freundlich adsorption isotherm.

5. When nitric acid was used to adjust the pH in Pb adsorption tests, the residue showed a decrease in portlandite, ettringite, alite, and larnite compared to residues where the pH was adjusted using the L/S method. Additionally, when Pb adsorption tests were conducted using chloride solution as the contact solution, portlandite almost converted to brucite in the case of $MgCl_2$ solution. However, no definitive identification of Pb compounds was achieved in any of the experiments.

6. Pb adsorption by CSH was greatest in the case of $MgCl_2$PM, while NaClPM, KClPM, and pore solution showed closely similar adsorption quantities for Pb. It was found that the lower the adsorption capacity of Pb on CSH, the larger the leachate quantities in contact with these solutions.

7. Regardless of the Ca/Si ratio of CSH, the contact solution equilibrium concentration of Pb is the highest in the case of $CaCl_2$PM. This finding is an important

reason for the highest rate of Pb leaching in the field where $CaCl_2$ solutions are used in contact with mortar.

8. The higher Ca/Si mole ratio and calcium contents realized after the contact of CSH with $CaCl_2$ indicate that $CaCl_2$ plays a beneficial role in retaining Ca^{2+} in CSH.

CHAPTER 6. GENERAL CONCLUSIONS AND RECOMMENDATIONS

6.1 Conclusion

This study conducted tank leaching tests in various chloride solutions to investigate the long-term leaching behavior of Cu, Zn and Pb in mortar when they come into contact with chloride solutions. Additionally, adsorption experiments were performed in several chloride solutions and $Ca(NO_3)_2$ solutions to analyze the adsorption characteristics of Pb when CSH (calcium silicate hydrate) is exposed to these solutions. Furthermore, Pb adsorption tests were conducted in various chloride solutions and in environments of different pH values, to study the effects of NaCl, KCl, $MgCl_2$, and $CaCl_2$ on the adsorption characteristics of Pb in cement paste. Based on the experimental results obtained from this study, the following conclusions are drawn:

Effect of various chloride solutions on the long-term leaching behavior of Cu, Zn, and Pb in mortar

1. The leaching rate of Pb is consistently significantly higher than that of Cu and Zn, regardless of the type of chloride solution or deionized water used.
2. The leaching of Cu, Zn, and Pb is most significant with $CaCl_2$ solution.
3. In the case of the $MgCl_2$ solution, most portlandite in the specimens was decomposed to form brucite which reduced the pH value to around 9. This fact caused lower leachate quantities of Zn, Cu, and Pb.
4. The leachate quantity of Pb from the specimens immersed in the $CaCl_2$ solution is more than six times as large as that in the other solutions. The leachate quantity was the smallest in the case of the deionized water.
5. Correlations between changes in pore volume and Pb leaching were not observed for the

specimens immersed in each chloride solution for 64 days at the same water/cement ratio.

6. Compared with the specimens with a water/cement ratio of 0.55, the specimens with a water/cement ratio of 0.40 had a lower total pore volume, resulting in lower leachate quantities of HMs.
7. Based on the qualitative analysis results from XRD in this study, it was impossible to determine definitively the forms of Cu, Zn and Pb compounds that exist in the mortars.
8. According to the EPMA results in this study, in the case of KCl solutions, the weaker binding capacity of chloride ions relative to $CaCl_2$ may explain the lower leaching of Pb in KCl solution compared with $CaCl_2$.

Effect of various chloride solutions on the adsorption and desorption properties of cement paste for Pb

1. When chloride solutions were used as the contact solution for Pb adsorption tests on cement pastes, the highest adsorption was observed in the case of $MgCl_2$ solution, followed by NaCl, KCl, deionized water, and LiCl solutions. Notably, in the case of $CaCl_2$ solution, the adsorption of Pb was significantly lower, which is one of the main reasons for the significantly higher Pb leaching observed.
2. When cement paste is exposed to chloride solutions such as NaCl or $CaCl_2$ before the adsorption of Pb, the number of adsorption sites decreases. However, it is believed that these sites remain available for adsorption even when the cement paste is exposed to chloride solutions like NaCl or $CaCl_2$ after the adsorption of Pb.
3. In Pb adsorption tests conducted by varying the pH of the solution in contact with cement paste, it was observed that regardless of the pH adjustment method, the amount of adsorption tended to increase as the pH of the solution decreased from around 13 to 10. However, this trend was not observed in the presence of chlorides.
4. For varying the pH of the solution in contact with the cement paste, including the use

of chloride solutions, Pb adsorption in the range of this study approximates the Freundlich adsorption isotherm.

5. When nitric acid was used to adjust the pH in Pb adsorption tests, the residue showed a decrease in portlandite, ettringite, alite, and larnite compared to residues where the pH was adjusted using the L/S method. Additionally, when Pb adsorption tests were conducted using chloride solution as the contact solution, portlandite almost converted to brucite in the case of $MgCl_2$ solution. However, no definitive identification of Pb compounds was achieved in any of the experiments.

Effect of various chloride solutions on the adsorption properties of CSH for Pb

1. $CaCl_2$ plays a beneficial role in maintaining Ca^{2+} in CSH, which leads to a decrease in Pb adsorption sites.
2. Pb adsorption by CSH was greatest in the case of $MgCl_2$PM, while NaClPM, KClPM, and pore solution showed closely similar adsorption quantities for Pb. It was found that the lower the adsorption capacity of Pb on CSH, the larger the leachate quantities in contact with these solutions.
3. Regardless of the Ca/Si ratio of CSH, the contact solution equilibrium concentration of Pb is the highest in the case of $CaCl_2$PM. This finding is an important reason for the highest Pb leaching rates when using $CaCl_2$ solutions in contact with the mortar.

6.2 Recommendations for future works

Based on the conclusions of the present study and previous researches, the following recommendations can be made for future work:

1. This study only considered a 10% chloride solution concentration in experiments, not covering a wider concentration range. Therefore, future research should test various

concentrations of chloride solutions to more comprehensively understand the impact of concentration on heavy metal leaching and adsorption.

2. The present study did not identify the chemical forms of HMs. High-resolution transmission electron microscopy (HRTEM) could be used in future studies to examine the crystal structure, pore distribution, and nano-level phase changes in cement-made materials. This would allow for the analysis of the location and distribution of heavy metal ions within these materials and their interactions with the microstructure. If we find certain microstructures that immobilize HMs better, we could enhance material immobilization capabilities by changing raw materials or manufacturing processes to promote these structures.
3. The range of HMs considered in this study was limited to copper, zinc, and lead, excluding other potential contaminants. Future studies should diversify the types of HMs, exploring the leaching and adsorption behaviors of others like cadmium, selenium, hexavalent chromium, and arsenic in cement-based materials.
4. While this study mainly focused on the influence of chloride solutions, future research could also simulate more complex environmental factors, such as the effects of acid rain and seawater environments on heavy metal leaching and adsorption.
5. The experimental conditions of this study were limited, mainly conducted under indoor conditions with only 625 days of leaching observation. Hence, field application research should be conducted for long-term testing in natural environments to verify the reliability and applicability of the indoor experimental results.
6. The CSH synthesis approach in this study, which utilized a specific method and Ca/Si ratio, may only partially reflect the characteristics of CSH in reality. Therefore, it is recommended to explore various CSH synthesis approaches and investigate the impact of different Ca/Si ratios on the adsorption of HMs.
7. The study material was limited to cement paste in this study. Future research could

expand to a broader range of cementitious materials, particularly those emerging as sustainable alternatives to traditional cement, such as geopolymer, magnesium-based cement, and lime-fly ash mixtures. This would help us understand how different compositions interact with HMs and the environment.

8. Developing predictive models based on this study's results could help forecast heavy metal behavior in various chloride environments. These models are crucial for planning safer construction methods and material development.
9. Future research could also explore remediation and reduction strategies, investigating methods to resist or mitigate the leaching of HMs in cement-based materials due to chlorides.

References

1. Co, A. R. P., Yong Han Ahn, HanmiGlobal & Ltd. *Sustainable Buildings and Infrastructure: Paths to the Future*. (Routledge, 2012). doi:10.4324/9780203130841.
2. Monteiro, P. J. M., Miller, S. A. & Horvath, A. Towards sustainable concrete. *Nat. Mater.* **16**, 698–699 (2017).
3. Griffiths, S. *et al.* Decarbonizing the cement and concrete industry: A systematic review of socio-technical systems, technological innovations, and policy options. *Renew. Sustain. Energy Rev.* **180**, 113291 (2023).
4. Andrew, R. M. Global CO2 emissions from cement production. *Earth Syst. Sci. Data* **10**, 195–217 (2018).
5. Cao, Z., Masanet, E., Tiwari, A. & Akolawala, S. Decarbonizing Concrete: Deep decarbonization pathways for the cement and concrete cycle in the United States, India, and China. *Ind. Sustain. Anal. Lab-Clim. Found.* (2021).
6. U.S. cement production volume 2010-2022. *Statista* https://www.statista.com/statistics/219343/cement-production-worldwide/.
7. Bhagath Singh, G. V. P. & Subramaniam, K. V. L. Quantitative XRD Analysis of Binary Blends of Siliceous Fly Ash and Hydrated Cement. *J. Mater. Civ. Eng.* **28**, 04016042 (2016).
8. Mocharla, I. R., Selvam, R., Govindaraj, V. & Muthu, M. Performance and life-cycle assessment of high-volume fly ash concrete mixes containing steel slag sand. *Constr. Build. Mater.* **341**, 127814 (2022).
9. Zhang, S., Ghouleh, Z., He, Z., Hu, L. & Shao, Y. Use of municipal solid waste incineration bottom ash as a supplementary cementitious material in dry-cast concrete. *Constr. Build. Mater.* **266**, 120890 (2021).
10. He, P., Yu, J., Xue, L. & Han, X. Influence of ion chelator on pore structure, water transport and crack-healing properties of cement pastes incorporating high-volume fly ash and blast-furnace slag. *J.*

Build. Eng. **55**, 104696 (2022).

11. Rashad, A. M. An investigation of high-volume fly ash concrete blended with slag subjected to elevated temperatures. *J. Clean. Prod.* **93**, 47–55 (2015).

12. Thomas, M. & Bremner, T. Performance of lightweight aggregate concrete containing slag after 25years in a harsh marine environment. *Cem. Concr. Res.* **42**, 358–364 (2012).

13. Fang, K., Wang, D., Zhao, J. & Zhang, M. Utilization of ladle furnace slag as cement partial replacement: Influences on the hydration and hardening properties of cement. *Constr. Build. Mater.* **299**, 124265 (2021).

14. Hilton, B. *et al.* The functional and environmental performance of mixed cathode ray tubes and recycled glass as partial replacement for cement in concrete. *Resour. Conserv. Recycl.* **151**, 104451 (2019).

15. Chandru, U., Bahurudeen, A. & Senthilkumar, R. Systematic comparison of different recycled fine aggregates from construction and demolition wastes in OPC concrete and PPC concrete. *J. Build. Eng.* **75**, 106768 (2023).

16. Bogas, J. A., de Brito, J. & Ramos, D. Freeze–thaw resistance of concrete produced with fine recycled concrete aggregates. *J. Clean. Prod.* **115**, 294–306 (2016).

17. Cartuxo, F., De Brito, J., Evangelista, L., Jiménez, J. R. & Ledesma, E. F. Rheological behaviour of concrete made with fine recycled concrete aggregates–Influence of the superplasticizer. *Constr. Build. Mater.* **89**, 36–47 (2015).

18. Mardani-Aghabaglou, A., Tuyan, M. & Ramyar, K. Mechanical and durability performance of concrete incorporating fine recycled concrete and glass aggregates. *Mater. Struct.* **48**, 2629–2640 (2015).

19. Huang, J. *et al.* Recovery of lead and chlorine via thermal co-treatment of municipal solid waste incineration fly ash and lead-rich waste cathode-ray tubes: Analysis of chlorination volatilization mechanism. *J. Hazard. Mater.* **462**, 132752 (2024).

20. Gao, X. *et al.* Performance of fly ash-based geopolymer mortars with waste cathode ray tubes

glass fine aggregate: A comparative study with cement mortars. *Constr. Build. Mater.* **344**, 128243 (2022).

21. Jang, J. G., Ahn, Y. B., Souri, H. & Lee, H. K. A novel eco-friendly porous concrete fabricated with coal ash and geopolymeric binder: Heavy metal leaching characteristics and compressive strength. *Constr. Build. Mater.* **79**, 173–181 (2015).

22. Guzmán-Carrillo, H. R. *et al.* Encapsulation of toxic heavy metals from waste CRT using calcined kaolin base-geopolymer. *Mater. Chem. Phys.* **257**, 123745 (2021).

23. Gollmann, M. A. C., da Silva, M. M., Masuero, Â. B. & dos Santos, J. H. Z. Stabilization and solidification of Pb in cement matrices. *J. Hazard. Mater.* **179**, 507–514 (2010).

24. Ouhadi, V. R., Yong, R. N. & Deiranlou, M. Enhancement of cement-based solidification/stabilization of a lead-contaminated smectite clay. *J. Hazard. Mater.* **403**, 123969 (2021).

25. Poon, C. S., Peters, C. J., Perry, R., Barnes, P. & Barker, A. P. Mechanisms of metal stabilization by cement based fixation processes. *Sci. Total Environ.* **41**, 55–71 (1985).

26. Zhang, J. *et al.* Comparison of the fixation effects of heavy metals by cement rotary kiln co-processing and cement based solidification/stabilization. *J. Hazard. Mater.* **165**, 1179–1185 (2009).

27. Fan, C., Wang, B., Ai, H., Qi, Y. & Liu, Z. A comparative study on solidification/stabilization characteristics of coal fly ash-based geopolymer and Portland cement on heavy metals in MSWI fly ash. *J. Clean. Prod.* **319**, 128790 (2021).

28. Belebchouche, C., Moussaceb, K., Tahakourt, A. & Aït-Mokhtar, A. Parameters controlling the release of hazardous waste (Ni2+, Pb2+ and Cr3+) solidified/stabilized by cement-CEM I. *Mater. Struct.* **48**, 2323–2338 (2015).

29. Moussaceb, K., Ait-Mokhtar, A. & Merabet, D. Influence of leaching conditions on the release kinetics of lead, chromium and nickel from solidified/stabilized cementitious materials. *Environ. Technol.* **33**, 2681–2690 (2012).

30. Kawai, K., Hayashi, A., Kikuchi, H. & Yokoyama, S. Desorption properties of heavy metals

from cement hydrates in various chloride solutions. *Constr. Build. Mater.* **67**, 55–60 (2014).

31. Ledesma, E. F. *et al.* The role of pH on leaching of heavy metals and chlorides from electric arc furnace dust in cement-based mortars. *Constr. Build. Mater.* **183**, 365–375 (2018).

32. Van der Sloot, H. A. & Dijkstra, J. J. Development of horizontally standardized leaching tests for construction materials: a material based or release based approach?: Identical leaching mechanisms for different materials. (ECN, 2004).

33. Hartwich, P. & Vollpracht, A. Influence of leachate composition on the leaching behaviour of concrete. *Cem. Concr. Res.* **100**, 423–434 (2017).

34. Zha, X. *et al.* Effect of supercritical carbonation on the strength and heavy metal retention of cement-solidified fly ash. *Cem. Concr. Res.* **120**, 36–45 (2019).

35. Metalssi, O. O., Aït-Mokhtar, A. & Ruot, B. Influence of cellulose ether on hydration and carbonation kinetics of mortars. *Cem. Concr. Compos.* **49**, 20–25 (2014).

36. Van Gerven, T., Van Baelen, D., Dutré, V. & Vandecasteele, C. Influence of carbonation and carbonation methods on leaching of metals from mortars. *Cem. Concr. Res.* **34**, 149–156 (2004).

37. Gjørv, O. E. *Durability Design of Concrete Structures in Severe Environments*. (CRC Press, 2014). doi:10.4324/9781482265903.

38. Bozkurt, S., Moreno, L. & Neretnieks, I. Long-term processes in waste deposits. *Sci. Total Environ.* **250**, 101–121 (2000).

39. Jaishankar, M., Tseten, T., Anbalagan, N., Mathew, B. B. & Beeregowda, K. N. Toxicity, mechanism and health effects of some heavy metals. *Interdiscip. Toxicol.* **7**, 60–72 (2014).

40. Nriagu, J. O. A history of global metal pollution. *Science* **272**, 223–223 (1996).

41. Li, Y., Zhang, H., Shao, L., Zhou, X. & He, P. Impact of municipal solid waste incineration on heavy metals in the surrounding soils by multivariate analysis and lead isotope analysis. *J. Environ. Sci.* **82**, 47–56 (2019).

42. Goldhaber, S. B. Trace element risk assessment: essentiality vs. toxicity. *Regul. Toxicol. Pharmacol.* **38**, 232–242 (2003).

43. G. Georgopoulos, A. R., M. J. Yonone-Lioy, R. E. Opiekun, P. J. Lioy, P. Environmental Copper: Its Dynamics and Human Exposure Issues. *J. Toxicol. Environ. Health Part B* **4**, 341–394 (2001).

44. Żukowska, J. & Biziuk, M. Methodological evaluation of method for dietary heavy metal intake. *J. Food Sci.* **73**, R21–R29 (2008).

45. Malviya, R. & Chaudhary, R. Leaching behavior and immobilization of heavy metals in solidified/stabilized products. *J. Hazard. Mater.* **137**, 207–217 (2006).

46. Delagrave, A., Pigeon, M., Marchand, J. & Revertégat, É. Influence of chloride ions and pH level on the durability of high performance cement pastes (Part II). *Cem. Concr. Res.* **26**, 749–760 (1996).

47. Marchand, J., Bentz, D. P., Samson, E. & Maltais, Y. Influence of calcium hydroxide dissolution on the transport properties of hydrated cement systems. *Mater. Sci. Concr. Spec. Vol. Calcium Hydroxide Concr.* 113–29 (2001).

48. Vollpracht, A. & Brameshuber, W. Binding and leaching of trace elements in Portland cement pastes. *Cem. Concr. Res.* **79**, 76–92 (2016).

49. Current Status and Issues Related to Trace Element Leaching from Concrete. *Jpn. Soc. Civ. Eng.* (2003).

50. He, R. *et al.* Copper slag: The leaching behavior of heavy metals and its applicability as a supplementary cementitious material. *J. Environ. Chem. Eng.* **9**, 105132 (2021).

51. Sun, X. & Yi, Y. Utilization of incineration bottom ash, waste marine clay, and ground granulated blast-furnace slag as a construction material. *Resour. Conserv. Recycl.* **182**, 106292 (2022).

52. Li, X. D., Poon, C. S., Sun, H., Lo, I. M. C. & Kirk, D. W. Heavy metal speciation and leaching behaviors in cement based solidified/stabilized waste materials. *J. Hazard. Mater.* **82**, 215–230 (2001).

53. Sdiri, A., Higashi, T., Jamoussi, F. & Bouaziz, S. Effects of impurities on the removal of heavy metals by natural limestones in aqueous systems. *J. Environ. Manage.* **93**, 245–253 (2012).

54. Tsakiridis, P. E., Papadimitriou, G. D., Tsivilis, S. & Koroneos, C. Utilization of steel slag for Portland cement clinker production. *J. Hazard. Mater.* **152**, 805–811 (2008).

55. Gencel, O., Karadag, O., Oren, O. H. & Bilir, T. Steel slag and its applications in cement and concrete technology: A review. *Constr. Build. Mater.* **283**, 122783 (2021).

56. Chatterjee, A. & Sui, T. Alternative fuels – Effects on clinker process and properties. *Cem. Concr. Res.* **123**, 105777 (2019).

57. Achternbosch, M. *et al.* Heavy metals in cement and concrete resulting from the co-incineration of wastes in cement kilns with regard to the legitimacy of waste utilisation. *Karlsr. Forschungszentrum Karlsr. GmbH* (2003).

58. Zeng, Q., Liu, X., Zhang, Z., Wei, C. & Xu, C. (Charles). Synergistic utilization of blast furnace slag with other industrial solid wastes in cement and concrete industry: Synergistic mechanisms, applications, and challenges. *Green Energy Resour.* **1**, 100012 (2023).

59. Siddique, R. & Bennacer, R. Use of iron and steel industry by-product (GGBS) in cement paste and mortar. *Resour. Conserv. Recycl.* **69**, 29–34 (2012).

60. Thomas, M. D. A. *Optimizing the use of fly ash in concrete*. vol. 5420 (Portland Cement Association Skokie, IL, USA, 2007).

61. Pratt, P. L. The use of fly ash in concrete-A European view. *MRS Online Proc. Libr. OPL* **178**, 177 (1989).

62. Sushil, S. & Batra, V. S. Analysis of fly ash heavy metal content and disposal in three thermal power plants in India. *Fuel* **85**, 2676–2679 (2006).

63. Fernandez-Turiel, J. L., De Carvalho, W., Cabañas, M., Querol, X. & Lopez-Soler, A. Mobility of heavy metals from coal fly ash. *Environ. Geol.* **23**, 264–270 (1994).

64. Llorens, J. F., Fernandez-Turiel, J. L. & Querol, X. The fate of trace elements in a large coal-fired power plant. *Environ. Geol.* **40**, 409–416 (2001).

65. Liao, H.-C. & Jiang, S.-J. Determination of cadmium, mercury and lead in coal fly ash by slurry sampling electrothermal vaporization inductively coupled plasma mass spectrometry. *Spectrochim.*

Acta Part B At. Spectrosc. **54**, 1233–1242 (1999).

66. Fytianos, K., Tsaniklidi, B. & Voudrias, E. Leachability of heavy metals in Greek fly ash from coal combustion. *Environ. Int.* **24**, 477–486 (1998).

67. Noor, T. *et al.* Chapter 14 - Types, sources and management of urban wastes. in *Urban Ecology* (eds. Verma, P., Singh, P., Singh, R. & Raghubanshi, A. S.) 239–263 (2020).

68. Serre, B. M. & McCarthy, L. H. Municipal solid waste management: Production, management, and environmental effects. in *Encyclopedia of Soils in the Environment (Second Edition)* (eds. Goss, M. J. & Oliver, M.) 321–332 (Academic Press, 2023).

69. Solid Waste Management. *World Bank* https://www.worldbank.org/en/topic/urbandevelopment/brief/solid-waste-management.

70. Kaza, S., Yao, L., Bhada-Tata, P. & Van Woerden, F. *What a waste 2.0: a global snapshot of solid waste management to 2050*. (World Bank Publications, 2018).

71. Lam, C. H. K., Ip, A. W. M., Barford, J. P. & McKay, G. Use of Incineration MSW Ash: A Review. *Sustainability* **2**, 1943–1968 (2010).

72. Tillman, D. A. Incineration of municipal and hazardous solid wastes. (2012).

73. Silva, R. V., de Brito, J., Lynn, C. J. & Dhir, R. K. Use of municipal solid waste incineration bottom ashes in alkali-activated materials, ceramics and granular applications: A review. *Waste Manag.* **68**, 207–220 (2017).

74. Chandler, A. J. *et al.* Municipal solid waste incinerator residues. (1997).

75. Hjelmar, O. Disposal strategies for municipal solid waste incineration residues. *J. Hazard. Mater.* **47**, 345–368 (1996).

76. Glasser, F. P. Fundamental aspects of cement solidification and stabilisation. *J. Hazard. Mater.* **52**, 151–170 (1997).

77. Gutsalenko, T. Solidification/Stabilization of harbor sediments using GGBS-based hydraulic binders. (Université Paris-Saclay, 2020).

78. Trussel, S. S. & Spence, R. D. A review of stabilisation/solidification interferes. *Waste Manag.*

14, 507–519 (1994).

79. Murat, M. & Sorrentino, F. Effect of large additions of Cd, Pb, Cr, Zn, to cement raw meal on the composition and the properties of the clinker and the cement. *Cem. Concr. Res.* **26**, 377–385 (1996).

80. Ortego, J. D., Jackson, S., Yu, G.-S., McWhinney, H. & Cocke, D. L. Solidification of hazardous substances-a TGA and FTIR study of Portland cement containing metal nitrates. *J. Environ. Sci. Health Part A* **24**, 589–602 (1989).

81. Taylor, H. F. Proposed structure for calcium silicate hydrate gel. *J. Am. Ceram. Soc.* **69**, 464–467 (1986).

82. Richardson, I. G. & Groves, G. W. Models for the composition and structure of calcium silicate hydrate (C-S-H) gel in hardened tricalcium silicate pastes. *Cem. Concr. Res.* **22**, 1001–1010 (1992).

83. Taylor, H. F. *Cement chemistry*. vol. 2 (Thomas Telford London, 1997).

84. Bonaccorsi, E., Merlino, S. & Kampf, A. R. The crystal structure of tobermorite 14 Å (plombierite), a C–S–H phase. *J. Am. Ceram. Soc.* **88**, 505–512 (2005).

85. Hong, S.-Y. & Glasser, F. P. Alkali sorption by C-S-H and C-A-S-H gels: Part II. Role of alumina. *Cem. Concr. Res.* **32**, 1101–1111 (2002).

86. Zain, A. M., Shaaban, M. G. & Mahmud, H. Immobilization of petroleum sludge incorporating portland cement and rice husk ash. *Int. J. Chem. Eng. Appl.* **1**, 234 (2010).

87. Chen, Q. Y., Tyrer, M., Hills, C. D., Yang, X. M. & Carey, P. Immobilisation of heavy metal in cement-based solidification/stabilisation: A review. *Waste Manag.* **29**, 390–403 (2009).

88. Tits, J., Wieland, E., Dobler, J.-P. & Kunz, D. The Uptake of Strontium by Calcium Silicate Hydrates under High pH Conditions: An Experimental Approach to Distinguish Adsorption from Co-precipitation Processes. *MRS Online Proc. Libr.* **807**, 1–6 (2003).

89. Mancini, A. *et al.* Fe(II) interaction with cement phases: Method development, wet chemical studies and X-ray absorption spectroscopy. *J. Colloid Interface Sci.* **588**, 692–704 (2021).

90. Ziegler, F., Gieré, R. & Johnson, C. A. Sorption mechanisms of zinc to calcium silicate hydrate:

sorption and microscopic investigations. *Environ. Sci. Technol.* **35**, 4556–4561 (2001).

91. Evans, N. D. M. Binding mechanisms of radionuclides to cement. *Cem. Concr. Res.* **38**, 543–553 (2008).

92. Tommaseo, C. E. & Kersten, M. Aqueous solubility diagrams for cementitious waste stabilization systems. 3. Mechanism of zinc immobilizaton by calcium silicate hydrate. *Environ. Sci. Technol.* **36**, 2919–2925 (2002).

93. Lin, C.-K., Chen, J.-N. & Lin, C.-C. An NMR, XRD and EDS study of solidification/stabilization of chromium with Portland cement and C3S. *J. Hazard. Mater.* **56**, 21–34 (1997).

94. Ivey, D. G. *et al.* Electron microscopy of heavy metal waste in cement matrices. *J. Mater. Sci.* **25**, 5055–5062 (1990).

95. Baldermann, A. *et al.* Uptake of aqueous heavy metal ions (Co2+, Cu2+ and Zn2+) by calcium-aluminium-silicate-hydrate gels. *Cem. Concr. Res.* **147**, 106521 (2021).

96. Baldermann, A. *et al.* Removal of heavy metals (Co, Cr, and Zn) during calcium–aluminium–silicate–hydrate and trioctahedral smectite formation. *J. Mater. Sci.* **54**, 9331–9351 (2019).

97. Qiao, G. *et al.* Molecular insights into migration of heavy metal ion in calcium silicate hydrate (CSH) surface and intra-CSH (Ca/Si = 1.3). *Constr. Build. Mater.* **365**, 130097 (2023).

98. Conner, J. R. & Hoeffner, S. L. The history of stabilization/solidification technology. *Crit. Rev. Environ. Sci. Technol.* **28**, 325–396 (1998).

99. Chen, Q. Y., Tyrer, M., Hills, C. D., Yang, X. M. & Carey, P. Physicochemical Treatment Processes. *Waste Manag.* **29**, 390–403 (2009).

100. Lange, L. C., Hills, C. D. & Poole, A. B. The effect of accelerated carbonation on the properties of cement-solidified waste forms. *Waste Manag.* **16**, 757–763 (1996).

101. Murakami S. pH and Solubility of Metal Ions - Water Purification Forum - Science and Technology. *Infomation from Ube City, Japan* http://water-solutions.jp/tech_basic-2/neutralizing/ph_metal-ion-solubility/.

102. Brown Jr, G. E., Foster, A. L. & Ostergren, J. D. Mineral surfaces and bioavailability of heavy metals: a molecular-scale perspective. *Proc. Natl. Acad. Sci.* **96**, 3388–3395 (1999).

103. Wang, L. K., Vaccari, D. A., Li, Y. & Shammas, N. K. Chemical precipitation. in *Physicochemical treatment processes* 141–197 (Springer, 2005).

104. Komarneni, S., Breval, E., Roy, D. M. & Roy, R. Reactions of some calcium silicates with metal cations. *Cem. Concr. Res.* **18**, 204–220 (1988).

105. Prince, W., Edwards-Lajnef, M. & Aïtcin, P.-C. Interaction between ettringite and a polynaphthalene sulfonate superplasticizer in a cementitious paste. *Cem. Concr. Res.* **32**, 79–85 (2002).

106. Fan, C., Wang, B. & Xu, Y. Solidification/stabilization and immobilization mechanism of Pb(II) and Zn(II) in ettringite. *Cem. Concr. Res.* **174**, 107350 (2023).

107. Cody, A. M., Lee, H., Cody, R. D. & Spry, P. G. The effects of chemical environment on the nucleation, growth, and stability of ettringite [Ca3Al(OH)6]2(SO4)3·26H2O. *Cem. Concr. Res.* **34**, 869–881 (2004).

108. Gijbels, K. *et al.* Radiological and leaching assessment of an ettringite-based mortar from ladle slag and phosphogypsum. *Cem. Concr. Res.* **128**, 105954 (2020).

109. Chrysochoou, M. & Dermatas, D. Evaluation of ettringite and hydrocalumite formation for heavy metal immobilization: Literature review and experimental study. *J. Hazard. Mater.* **136**, 20–33 (2006).

110. Poellmann, H., Auer, St., Kuzel, H.-J. & Wenda, R. Solid solution of ettringites: Part II: Incorporation of B(OH)4− and CrO42− in 3CaO·Al2O3·3CaSO4·32H2O. *Cem. Concr. Res.* **23**, 422–430 (1993).

111. Barnett, S. J., Macphee, D. E., Lachowski, E. E. & Crammond, N. J. XRD, EDX and IR analysis of solid solutions between thaumasite and ettringite. *Cem. Concr. Res.* **32**, 719–730 (2002).

112. McCarthy, G. J., Hassett, D. J. & Bender, J. A. Synthesis, crystal chemistry and stability of ettringite, a material with potential applications in hazardous waste immobilization. *MRS Online Proc.*

Libr. OPL **245**, 129 (1991).

113. Lin, T. T., Lin, C. F., Wei, W. C. J. & Lo, S. L. Mechanisms of metal stabilization in cementitious matrix: interaction of tricalcium aluminate and copper oxide/hydroxide. *Environ. Sci. Technol.* **27**, 1312–1318 (1993).

114. Diamond, S. Delayed ettringite formation — Processes and problems. *Cem. Concr. Compos.* **18**, 205–215 (1996).

115. Klemm, W. A. & Bhatty, J. I. *Fixation of heavy metals as oxyanion-substituted ettringites*. (Portland Cement Association, 2002).

116. Bonen, D. & Sarkar, S. L. The effects of simulated environmental attack on immobilization of heavy metals doped in cement-based materials. *J. Hazard. Mater.* **40**, 321–335 (1995).

117. Zhang, Z. *et al.* Solidification/stabilization and risk assessment of heavy metals in municipal solid waste incineration fly ash: A review. *Sci. Total Environ.* **892**, 164451 (2023).

118. Ashraf, W. Carbonation of cement-based materials: Challenges and opportunities. *Constr. Build. Mater.* **120**, 558–570 (2016).

119. Šavija, B. & Luković, M. Carbonation of cement paste: Understanding, challenges, and opportunities. *Constr. Build. Mater.* **117**, 285–301 (2016).

120. Johannesson, B. & Utgenannt, P. Microstructural changes caused by carbonation of cement mortar. *Cem. Concr. Res.* **31**, 925–931 (2001).

121. Young, J. F., Berger, R. L. & Breese, J. Accelerated curing of compacted calcium silicate mortars on exposure to CO2. *J. Am. Ceram. Soc.* **57**, 394–397 (1974).

122. Suzuki, K., Nishikawa, T. & Ito, S. Formation and carbonation of C-S-H in water. *Cem. Concr. Res.* **15**, 213–224 (1985).

123. Hartmann, T., Paviet-Hartmann, P., Rubin, J. B., Fitzsimmons, M. R. & Sickafus, K. E. The effect of supercritical carbon dioxide treatment on the leachability and structure of cemented radioactive waste-forms. *Waste Manag.* **19**, 355–361 (1999).

124. Macias, A., Kindness, A. & Glasser, F. P. Impact of carbon dioxide on the immobilization

potential of cemented wastes: Chromium. *Cem. Concr. Res.* **27**, 215–225 (1997).

125. Shafique, M. S. B., Walton, J. C., Gutierrez, N., Smith, R. W. & Tarquin, A. J. Influence of Carbonation on Leaching of Cementitious Wasteforms. *J. Environ. Eng.* **124**, 463–467 (1998).

126. Alba, N., Vázquez, E., Gassó, S. & Baldasano, J. M. Stabilization/solidification of MSW incineration residues from facilities with different air pollution control systems. Durability of matrices versus carbonation. *Waste Manag.* **21**, 313–323 (2001).

127. Sanchez, F., Gervais, C., Garrabrants, A. C., Barna, R. & Kosson, D. S. Leaching of inorganic contaminants from cement-based waste materials as a result of carbonation during intermittent wetting. *Waste Manag.* **22**, 249–260 (2002).

128. Ginneken, L. van, Dutre, V., Adrianses, W. & Weyten, H. Effect of supercritical carbon dioxide treatment on the leaching performance of a cement-stabilised waste-form. in *8th meeting on supercritical fluids* (2002).

129. Valls, S. & Vàzquez, E. Accelerated carbonatation of sewage sludge–cement–sand mortars and its environmental impact. *Cem. Concr. Res.* **31**, 1271–1276 (2001).

130. Müllauer, W., Beddoe, R. E. & Heinz, D. Effect of carbonation, chloride and external sulphates on the leaching behaviour of major and trace elements from concrete. *Cem. Concr. Compos.* **34**, 618–626 (2012).

131. Ebert, B. A. R. & Kirkelund, G. M. Effects of Chlorides and Sulphates on Heavy Metal Leaching from Mortar with Raw and Electrodialytically Treated MSWI Fly Ash. *Waste Biomass Valorization* **13**, 2673–2688 (2022).

132. Quina, M. J., Bordado, J. C. M. & Quinta-Ferreira, R. M. The influence of pH on the leaching behaviour of inorganic components from municipal solid waste APC residues. *Waste Manag.* **29**, 2483–2493 (2009).

133. Liu, Q. *et al.* Heavy metal leaching behaviour and long-term environmental risk assessment of cement-solidified municipal solid waste incineration fly ash in sanitary landfill. *Chemosphere* **300**, 134571 (2022).

134. Zhang, W., Zhao, L., Yuan, Z., Li, D. & Morrison, L. Assessment of the long-term leaching characteristics of cement-slag stabilized/solidified contaminated sediment. *Chemosphere* **267**, 128926 (2021).

135. Du, Y.-J., Wei, M.-L., Reddy, K. R., Liu, Z.-P. & Jin, F. Effect of acid rain pH on leaching behavior of cement stabilized lead-contaminated soil. *J. Hazard. Mater.* **271**, 131–140 (2014).

136. Sebag, M. G., Korzenowski, C., Bernardes, A. M. & Vilela, A. C. Evaluation of environmental compatibility of EAFD using different leaching standards. *J. Hazard. Mater.* **166**, 670–675 (2009).

137. van der Sloot, H. A. Characterization of the leaching behaviour of concrete mortars and of cement–stabilized wastes with different waste loading for long term environmental assessment. *Waste Manag.* **22**, 181–186 (2002).

138. Dell'Orso, M., Mangialardi, T., Paolini, A. E. & Piga, L. Evaluation of the leachability of heavy metals from cement-based materials. *J. Hazard. Mater.* **227–228**, 1–8 (2012).

139. Pang, F., Wei, C., Zhang, Z., Wang, W. & Wang, Z. The migration and immobilization for heavy metal chromium ions in the hydration products of calcium sulfoaluminate cement and their leaching behavior. *J. Clean. Prod.* **365**, 132778 (2022).

140. Song, F., Gu, L., Zhu, N. & Yuan, H. Leaching behavior of heavy metals from sewage sludge solidified by cement-based binders. *Chemosphere* **92**, 344–350 (2013).

141. Cinquepalmi, M. A., Mangialardi, T., Panei, L., Paolini, A. E. & Piga, L. Reuse of cement-solidified municipal incinerator fly ash in cement mortars: Physico-mechanical and leaching characteristics. *J. Hazard. Mater.* **151**, 585–593 (2008).

142. Bone, B. *et al.* Review of scientific literature on the use of stabilisation/solidification for the treatment of contaminated soil, solid waste and sludges (SC980003/SR2). *Environ. Agency Bristol* (2004).

143. ANSI/ANS-16.1-2003 (R2017) - Measurement of the Leachability of Solidified Low-Level Radioactive Wastes by a Short-Term Test Procedure.

144. NEN, N. Leaching characteristics of solid earthy and stony building and waste materials.

Leaching Tests Delft Ned. Norm.-Inst. (1995).

145. Hohberg, I., de Groot, G. J., van der Veen, A. M. H. & Wassing, W. Development of a leaching protocol for concrete. *Waste Manag.* **20**, 177–184 (2000).

146. Batchelor, B. Leach models: Theory and application. *J. Hazard. Mater.* **24**, 255–266 (1990).

147. Kosson, D. S., Kosson, T. T. & Van der Sloot, H. *Evaluation of solidification/stabilization treatment processes for municipal waste combustion residues*. (1993).

148. JIS, R. 5210; Portland Cement. *Jpn. Stand. Assoc. Tokyo Jpn.* (2009).

149. Lu, C.-C., Hsu, M. H. & Lin, Y.-P. Evaluation of heavy metal leachability of incinerating recycled aggregate and solidification/stabilization products for construction reuse using TCLP, multi-final pH and EDTA-mediated TCLP leaching tests. *J. Hazard. Mater.* **368**, 336–344 (2019).

150. Soleimanifar, M., Jayasuriya, A., Adams, M. P. & Rodriguez-Freire, L. Leaching composition and associated microbial community of recycled concrete aggregate (RCA). *J. Hazard. Mater.* **442**, 130048 (2023).

151. Japan Society of Civil Engineers. Test method for leaching of trace elements from hardened concrete, JSCE Standards (JSCE-G 575). (2005).

152. Kawai, K., Miyamoto, Y. & Sakanaka, K. Study on diffusion and adsorption of heavy metals in cement hydrates. *Cem. Sci. Concr. Technol.* **61**, 123–128 (2007).

153. Chen, J. J., Thomas, J. J., Taylor, H. F. W. & Jennings, H. M. Solubility and structure of calcium silicate hydrate. *Cem. Concr. Res.* **34**, 1499–1519 (2004).

154. Li, H. *et al.* Effects of synthetic CSH-tartaric acid nanocomposites on the properties of ordinary Portland cement. *Cem. Concr. Compos.* **129**, 104466 (2022).

155. Lu, B. *et al.* Characteristics of CSH under carbonation and its effects on the hydration and microstructure of cement paste. *Constr. Build. Mater.* **364**, 129952 (2023).

156. Boumaaza, M., Turcry, P., Huet, B. & Aït-Mokhtar, A. Influence of carbonation on the microstructure and the gas diffusivity of hardened cement pastes. *Constr. Build. Mater.* **253**, 119227 (2020).

157. T. Miura, M. Tomon, , MM. Kawamura, H. Seiki & T. Hara. Deterioration of concrete structures by deicing salt in Japan. *Proc. Jpn. Concr. Inst.* **21**, 29–38 (1999).

158. Alford, N. Mcn., Rahman, A. A. & Salih, N. The effect of lead nitrate on the physical properties of cement pastes. *Cem. Concr. Res.* **11**, 235–245 (1981).

159. Talero, R. Synergic effect of Friedel's salt from pozzolan and from OPC co-precipitating in a chloride solution. *Constr. Build. Mater.* **33**, 164–180 (2012).

160. Wilson, W., Gonthier, J. N., Georget, F. & Scrivener, K. L. Insights on chemical and physical chloride binding in blended cement pastes. *Cem. Concr. Res.* **156**, 106747 (2022).

161. Konno, K., Schwotzer, M., KALTENBACH, J. & GERDES, A. Promoting effect of de-icing agent on calcium leaching of hardened cement paste. *Cem. Sci. Concr. Technol.* **69**, 440–447 (2015).

162. Xie, N., Dang, Y. & Shi, X. New insights into how MgCl2 deteriorates Portland cement concrete. *Cem. Concr. Res.* **120**, 244–255 (2019).

163. Mundell, J. A. & Hill, K. R. In place precipitation immobilization: technical and economic assessment at the AY Mcdonald foundry site, Dubuque, Iowa. *Proc. Hazard. Wastes Environ. Emergencies Houst. TX* 177–181 (1984).

164. Halim, C. E., Amal, R., Beydoun, D., Scott, J. A. & Low, G. Implications of the structure of cementitious wastes containing Pb(II), Cd(II), As(V), and Cr(VI) on the leaching of metals. *Cem. Concr. Res.* **34**, 1093–1102 (2004).

165. Heasman, L., van der Sloot, H. A. & Quevauviller, P. *Harmonization of leaching/extraction tests*. (1997).

166. Cody, R. D., CODY, A. M., SPRY, P. G. & GAN, G.-L. Experimental deterioration of highway concrete by chloride deicing salts. *Environ. Eng. Geosci.* **2**, 575–588 (1996).

167. Shi, X., Fay, L., Peterson, M. M., Berry, M. & Mooney, M. A FESEM/EDX investigation into how continuous deicer exposure affects the chemistry of Portland cement concrete. *Constr. Build. Mater.* **25**, 957–966 (2011).

168. Delagrave, A., Marchand, J., Ollivier, J.-P., Julien, S. & Hazrati, K. Chloride binding capacity of

various hydrated cement paste systems. *Adv. Cem. Based Mater.* **6**, 28–35 (1997).

169. Suryavanshi, A. K., Scantlebury, J. D. & Lyon, S. B. Mechanism of Friedel's salt formation in cements rich in tri-calcium aluminate. *Cem. Concr. Res.* **26**, 717–727 (1996).

170. Arya, C., Buenfeld, N. R. & Newman, J. B. Factors influencing chloride-binding in concrete. *Cem. Concr. Res.* **20**, 291–300 (1990).

171. HIsada, M., Ito, S. & Sakai, I. A study on the diffusivity of ions through mortar and the change of cement hydration due to the chemical deterioration process. *Jpn. J. JSCE* 39–50 (2004).

172. De Weerdt, K., Colombo, A., Coppola, L., Justnes, H. & Geiker, M. R. Impact of the associated cation on chloride binding of Portland cement paste. *Cem. Concr. Res.* **68**, 196–202 (2015).

173. Kawai, K., Tano, S., Ishida, T. & Sakanaka, K. A study on mechanism of heavy metal leaching from concrete. *Cem. Sci. Concr. Technol.* **60**, 314–321 (2007).

174. Freundlich, H. Ueber die adsorption in loesungen. *Z Phys Chem* **57**, 385–470 (1907).

175. Brdar, M., Šćiban, M., Takači, A. & Došenović, T. Comparison of two and three parameters adsorption isotherm for Cr(VI) onto Kraft lignin. *Chem. Eng. J.* **183**, 108–111 (2012).

176. Freundlich, H. M. F. Over the adsorption in solution. *J Phys Chem* **57**, 1100–1107 (1906).

177. Han, Y.-L. *et al.* Recovery of gold from industrial wastewater by extracellular proteins obtained from a thermophilic bacterium Tepidimonas fonticaldi AT-A2. *Bioresour. Technol.* **239**, 160–170 (2017).

178. Macphee, D. E. & Glasser, F. P. Immobilization science of cement systems. *MRS Bull.* **18**, 66–71 (1993).

179. Qian, G., Cao, Y., Chui, P. & Tay, J. Utilization of MSWI fly ash for stabilization/solidification of industrial waste sludge. *J. Hazard. Mater.* **129**, 274–281 (2006).

180. Hayashi, A., Kikuchi, H., Takaya, H. & Kawai, K. Migration of Heavy Metals in Cement Hydrates Caused by Carbonation, *Proceeding of the 10th International Conference on Civil and Environmental Engineering*. 237–241.

181. Natarajan, R. *et al.* Adsorption performance of magnetic mesoporous silica microsphere support

toward the remediation of acetaminophen from aqueous solution. *J. Water Process Eng.* **48**, 102835 (2022).

182. Guo, Z. *et al.* Removal mechanisms of phosphate from water by calcium silicate hydrate supported on hydrochar derived from microwave-assisted hydrothermal treatment. *Environ. Technol. Innov.* **28**, 102942 (2022).

183. Bourbatache, K., Millet, O. & Aît-Mokhtar, A. Ionic transfer in charged porous media. Periodic homogenization and parametric study on 2D microstructures. *Int. J. Heat Mass Transf.* **55**, 5979–5991 (2012).

184. Pointeau, I., Reiller, P., Macé, N., Landesman, C. & Coreau, N. Measurement and modeling of the surface potential evolution of hydrated cement pastes as a function of degradation. *J. Colloid Interface Sci.* **300**, 33–44 (2006).

185. Nachbaur, L., Nkinamubanzi, P.-C., Nonat, A. & Mutin, J.-C. Electrokinetic Properties which Control the Coagulation of Silicate Cement Suspensions during Early Age Hydration. *J. Colloid Interface Sci.* **202**, 261–268 (1998).

186. Plusquellec, G., Nonat, A. & Pochard, I. Anion uptake by calcium silicate hydrate. in *32nd Cement and Concrete Science Conference* (2012).

187. Plusquellec, G. & Nonat, A. Interactions between calcium silicate hydrate (C-S-H) and calcium chloride, bromide and nitrate. *Cem. Concr. Res.* **90**, 89–96 (2016).

188. Kanchanason, V. & Plank, J. Role of pH on the structure, composition and morphology of C-S-H–PCE nanocomposites and their effect on early strength development of Portland cement. *Cem. Concr. Res.* **102**, 90–98 (2017).

189. Tang, Y., Schollbach, K., Brouwers, H. J. H. & Chen, W. Effects of soluble magnesium on the structure of calcium silicate hydrate. *Constr. Build. Mater.* **302**, 124402 (2021).

190. Shao, L., Zhou, Y., Chen, J. F., Wu, W. & Lu, S. C. Buffer behavior of brucite in removing copper from acidic solution. *Miner. Eng.* **18**, 639–641 (2005).

191. Zhao, Y., Chen, H. & Yan, Q. Enhanced phosphate removal during the simultaneous adsorption

of phosphate and Ni^{2+} from electroless nickel wastewater by calcium silicate hydrate (CSH). *Environ. Technol. Innov.* **8**, 141–149 (2017).

192. Southam, D. C., Lewis, T. W., McFarlane, A. J., Borrmann, T. & Johnston, J. H. Calcium–phosphorus interactions at a nano-structured silicate surface. *J. Colloid Interface Sci.* **319**, 489–497 (2008).

193. Missana, T., García-Gutiérrez, M., Alonso, U. & Almendros-Ginestá, O. Nickel retention by calcium silicate hydrate phases: Evaluation of the role of the Ca/Si ratio on adsorption and precipitation processes. *Appl. Geochem.* **137**, 105197 (2022).

194. Sutter, L., Peterson, K., Touton, S., Van Dam, T. & Johnston, D. Petrographic evidence of calcium oxychloride formation in mortars exposed to magnesium chloride solution. *Cem. Concr. Res.* **36**, 1533–1541 (2006).

APPENDIX

Pore Size Distribution Measurement Results

Pb W/C=0.4 0d

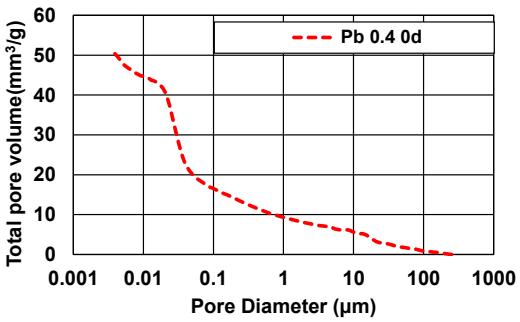

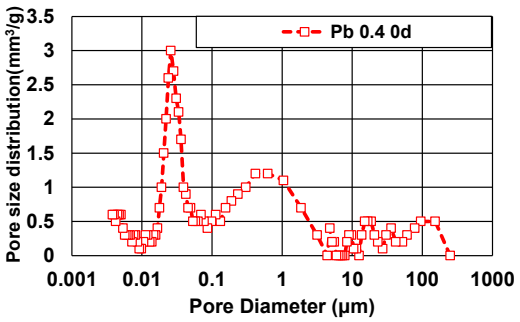

Pb W/C=0.55 0d

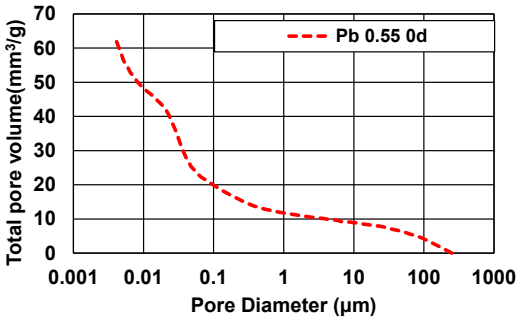

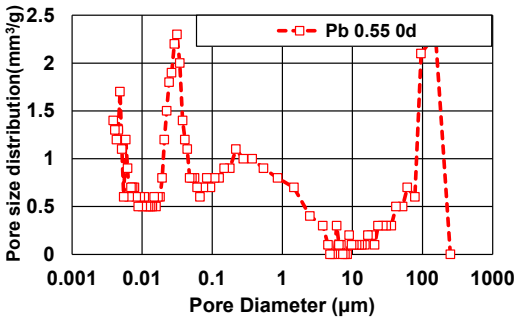

Pb H2O W/C=0.4 64d

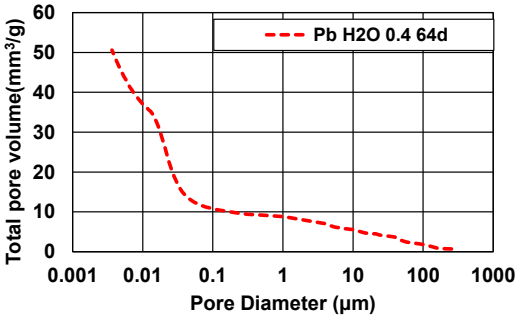

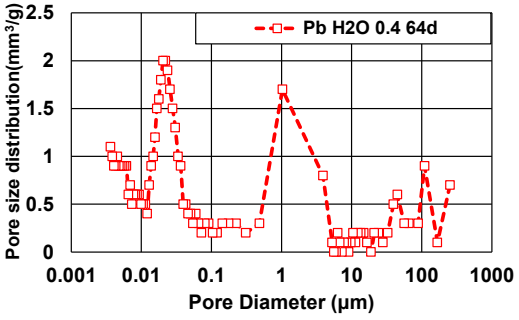

Pb H2O W/C=0.55 64d

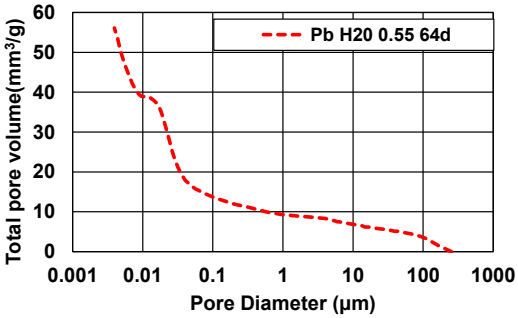

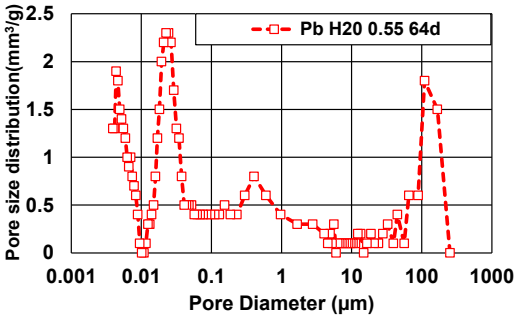

Pb NaCl W/C=0.4 64d

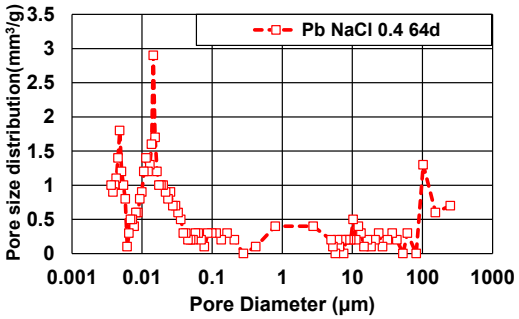

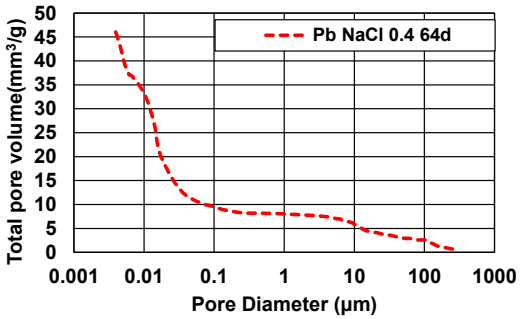

Pb NaCl W/C=0.55 64d

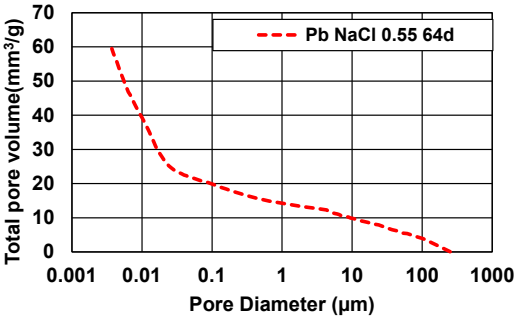

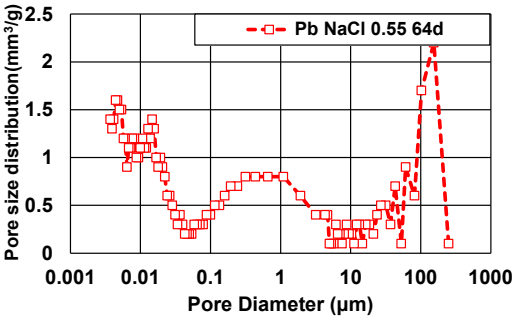

Pb KCl W/C=0.4 64d

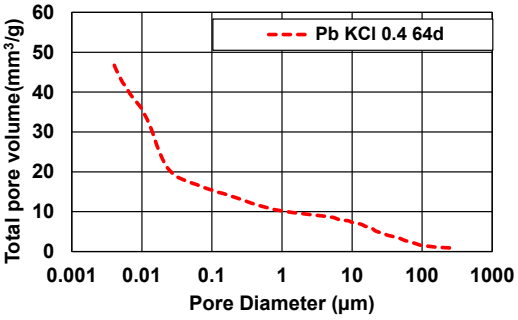

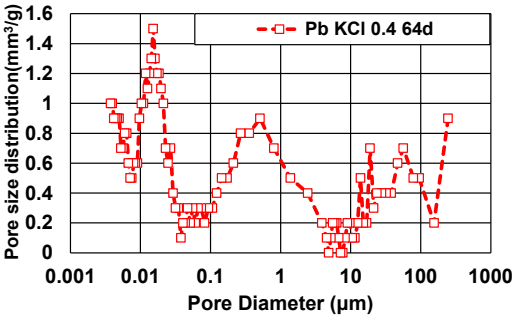

Pb KCl W/C=0.55 64d

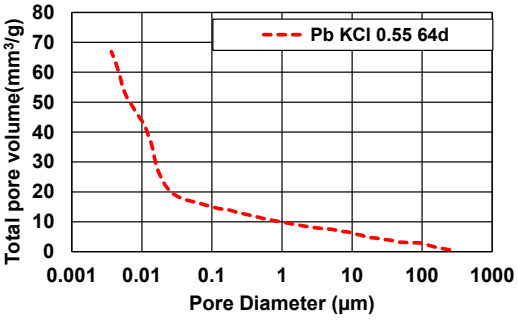

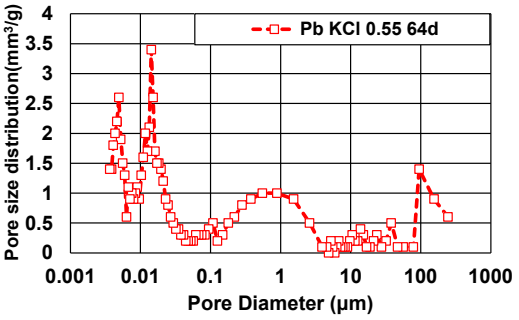

Pb $CaCl_2$ W/C=0.4 64d

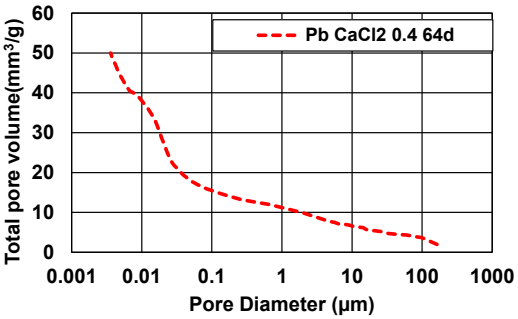

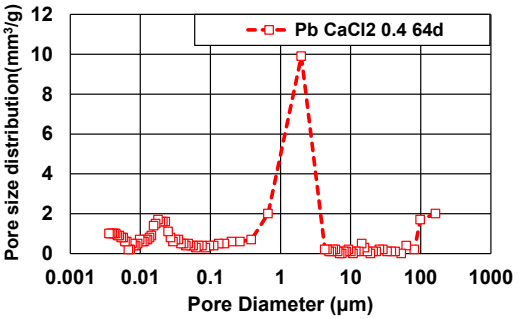

Pb $CaCl_2$ W/C=0.55 64d

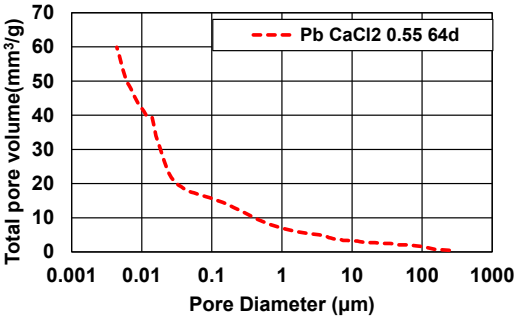

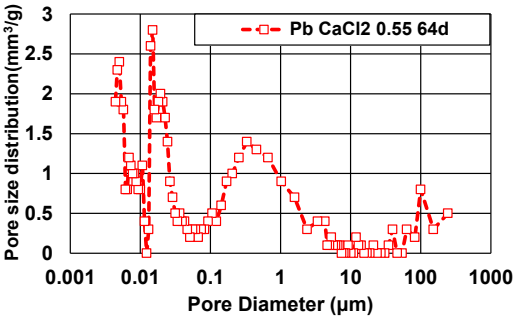

Pb $MgCl_2$ W/C=0.4 64d

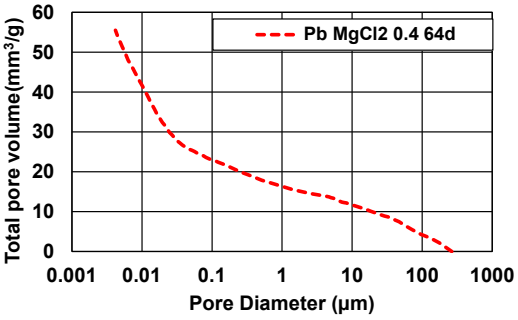

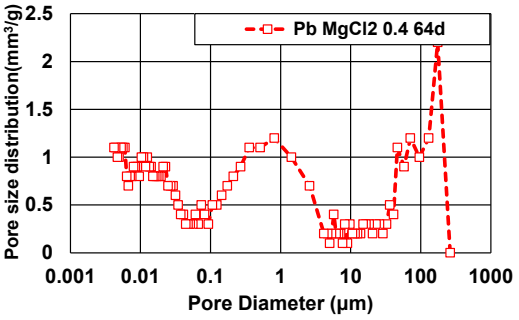

Pb $MgCl_2$ W/C=0.55 64d